UNIVERSITÀ DEL SALENTO

Facoltà di Scienze MM.FF.NN.
Dipartimento di Fisica

Dottorato di Ricerca in Fisica
XXI ciclo

PhD Thesis

Reflectance of Particulate Mixtures of Astrophysical Applications

Tutor: Prof. Sergio Fonti

Candidate: Sarah Montanaro

Anno Accademico 2008 - 2009

Sulla soglia della scienza,
come sulla porta dell'inferno,
si deve porre questo ammonimento:
"Qui si convien lasciare ogni sospetto
Ogni viltá convien che qui sia morta."
Karl Marx,
Per la critica dell'economia politica, 1859.

Contents

List of Figures

List of Tables

Introduction

Mars is one of the most studied objects of the sky. In fact this planet is near the Sun and the Earth and, therefore, it is quite simple to observe it. In addition, its surface shows many characteristics present also on Earth, like mountains, craters, valleys and channels. All such conditions have influenced people with the consequence that the search for signs of life on Mars is one of the greatest purpose during the study of this planet.

Life formation is linked to the presence of liquid water, but Mars, today, is geologically inactive and, consequently, the recycling of fundamental elements for life, such as C, N, O is very limited. However, in the early Mars (about 4 Gy ago), the environment was as warm and wet as in the early Earth, with a dense CO_2 atmosphere, allowing the presence of liquid water. At present Mars shows evidence of transient liquid water, on very small scale in the form of gullies, but these phenomena are sporadic and too small to permit the life formation. Also the presence of some minerals is linked to liquid water. In fact, the formation of evaporite, such as carbonates and sulphates, is possible in presence of liquid water. Actually deposits of such minerals have been found, but their abundance is too low to justify a stable presence of liquid water and, in the past, a warm and wet climate.

For this reason the sky around the Red Planet is full of spacecrafts, which are making a lot of measurements and are sending the results of their observations to the Earth. In particular, an instrument is present on every space mission: the spectrometer.

However, some problems are related to the analysis of the acquired spectra. In fact, all the spectrometers around Mars have a big field of view, and the portion

of surface analyzed is very large. In such scenario it is difficult to hypothesize that the surface spectra acquired are related only to one mineral, but it is more probable that they are related to mixtures of different minerals and rocks.

In addition, the large amount of data, which everyday is sent to the Earth by these instruments, must be analyzed and studied. Many different techniques, for the reduction criteria and analysis, already exist and many others are studied.

My work was born in this scenario. In fact, it was thought for the acquisition of information about each component of a particulate mixture, such as composition, abundance and grain size. Such method must be fast and accurate, and it is necessary to obtain more information in less time.

A theory about the spectral behaviour of mineral mixture, the Hapke Theory of Reflectance (Hapke, 1993), already exists. However such theory was fully demonstrated up to 2.5 μm (Clark, 1983; Johnson et al., 1983), but the spectrometers, presently in orbit around Mars, are performing their measurements in a larger spectral range, for example OMEGA goes from 0.36 to 5.2 μm and PFS from 1 to 45 μm. It seems clear that understanding the behaviour of mixtures above 2.5 μm is fundamental for a correct approach to the measurements.

In this PhD thesis I show only a laboratory study of mineral mixtures and more work must be done to obtain a method applicable to planetary surfaces, because, as it will be shown, many problems have been found during my activity.

The procedure used during this work is very linear, because from one side I have used the mathematical approach, described by Hapke, to predict the spectral behaviour of a mixture, starting from the spectra of the components, while, from the other side, I have measured in laboratory the spectrum of the same mixture, finally comparing the two spectra. As I will show, the mathematical approach is quite difficult, because many parameters must be considered; however, if some of them were proved to be not important, they could be neglected and the theory simplified; so the mathematical approach takes into account some hypotheses aimed to simplify the approach without losing any information and laboratory measurements are necessary to prove such hypotheses.

For this reason, in this work I will focus on the verification of the main hypotheses

and on the problems found, giving an accurate description of the spectral behaviour of a mixture. Finally I will discuss the main results obtained.

In the first chapter I will introduce the object of this work. In particular I will make an introduction to Mars and to the space missions around it, with all their implications. Then I will introduce the importance of the infrared spectral range and the configuration which I have used to perform my measurements: directional hemispherical reflectance, which is related to emissivity. Finally I will introduce the mineral particulate mixtures, which could be defined as intimate, when the particles are mixed homogeneously together, or areal, when the surface is composed of patches each of which of a single pure material.

The principal subject of the second chapter will be the mathematical approach: I will shortly introduce the Radiative Transfer Equation to explain better the Hapke Reflectance Theory. However, the reflectance described by Hapke depends on many variables, such as the abundance, the grain size, the distribution, the optical constants, and so on. Therefore, in order to simplify such theory and use it both in laboratory and in remote sensing spectra, without losing any information, I have made some hypotheses.

In the third chapter, I will describe the experimental procedure, the mineral and the mixtures used for this work and the instruments used.

In the fourth chapter, I will verify the main hypotheses I have made: (1) the particles are all identical and spherical; (2) the scattering is isotropic; (3) the extinction coefficient is equal to unit. Such verification is performed with two types of mixtures, granulometric and compositional, to better understand the influence of every components on the cited hypotheses. In addition I will show how the grain size is fundamental also for the behaviour of the mixtures.

In the fifth chapter, I will show the first result obtained: the extension of the validity of Hapke Theory of Reflectance to the NIR spectral range, up to the principal Christiansen frequency. In addition, I will show some discrepancies found between the theoretical and measured spectra and I will discuss an experiment aimed to explain the reason of such disagreement, probably due to the inhomogeneity in the components distribution.

Finally, in the sixth chapter, I will show that such discrepancy is related to the fact that the radiation does not penetrate into the sample, due to the high absorbing coefficient. Therefore considering a mixture as areal, instead of intimate, is much correct in the MIR region. At the same time I will show that in the NIR range the radiation penetrates into the sample, and, for this reason, considering a mixture as intimate in such spectral range, produces good results. In addition I will use the chi-square function as a test proof of the validity of my approach. Finally, I will describe the main problems related to the areal approximation for a mixture into which the components are not mixed homogeneously; in particular the determination of the portion of surface occupied by each component is not linked to its actual abundance.

Chapter 1

About Mars and its influence on this work

In this chapter I will introduce the object of this PhD thesis, showing how this work has been thought, how the progress of technology has contributed to this subject and the problems correlated with it. I will start with an introduction about Mars and its importance, in Section 1.1, and in Section 1.2 I will briefly describe some of the space missions which are orbiting around it and some of the instruments on board. Starting from some of such instruments, the spectrometers, I will discuss the choice of the spectral range used for this thesis, in Section 1.3. I will continue with an analysis of directional hemispherical reflectance, with its implications, in Section 1.4, and an introduction to mineral particulate mixtures, which are the subject of this work, in Section 1.5. Finally, in Section 1.6, I will shortly summarize this chapter to introduce better the subjects of the following chapters.

1.1 Mars

Mars is the fourth planet from the Sun and it is one of the most studied objects of the Solar System. It is one-tenth of the mass of Earth, its radius is about 3380 Km and its distance from the Sun is 1.52 AU.

The interest about this planet is due to its similarity to the Earth, in fact it is near to the Earth and to the Sun and the observations of its surface show a lot of morphological characteristics present also on Earth, as mountains, craters, valleys

and channels, which could suggest the possibility of the presence of liquid water on its surface. However, the annual average surface temperature is 210 K, with a minimum of 133 K and a maximum of 293 K, the atmospheric pressure is about 7 mbar, and the atmosphere is composed principally of Carbon Dioxide ($C0_2$, 95.32%), with very little Nitrogen (N_2, 2.7%) and Argon (Ar, 1.6%); so, in such conditions, the presence of liquid water on the surface is impossible. In fact it is possible only as sporadic events such as transient liquid water on very small scale in the formation of gullies (Malin and Edgett, 2000), or trapped in a layer of permafrost.

This thin atmosphere does not permit the greenhouse effect, which is important for the thermal equilibrium, but in the past Mars probably had a dense CO_2 atmosphere (Pollack et al., 1987), causing an efficient greenhouse effect. In such conditions Mars was warm and wet and the liquid water was in stable form, such as in rivers and in the sea. The water would have absorbed the CO_2 present in the atmosphere, causing a reduction of greenhouse. As a result the temperature dropped and the water in part evaporated and in part freezed, leaving Mars dry as it is today (Friedmann and Koriem, 1989; McKay and Stoker, 1989; Pollack et al., 1987).

The surface of Mars, shown in Figure 1.1, is mostly covered with dust (regolith), but its actual composition is not well known yet. Understanding the composition and the size of the regolith is, today, one of the major objects of Martian studies. In fact, the knowledge of the mineral composition is important to gather information about the climatological and geological history of Mars. For example, if the volcanos were active, now we should find mafic minerals near them, such as olivine, which were found. It seems clear that finding mineral whose formation is due to the presence of liquid water, such as carbonates and sulphates, would be an important proof that Mars was warm and wet in the past. Such minerals have been just found (Bandfield, 2002; Bibring et al., 2006), but they are not sufficient for proving the presence of long standing bodies of liquid water.

In addition the search for liquid water is linked to the life formation (Westall, 1999), as it will be better explained in Appendix A, which is another attractive subject not only for scientists but also for the general public.

Figure 1.1: Mars surface.

In conclusion Mars is a very interesting object and it is one of the principal destinations of several space missions which have been sent and will be sent to study the planet.

1.2 Space missions

Since 1964, when the first mission, Mariner 4, arrived on Mars, the sky around the red planet is full of spacecrafts.

Mariner 4 took 21 photos of the Mars surface; in addition, it studied the atmosphere and measured a little intrinsic magnetic field.

The following missions which arrived on the planet, Mariner 6 and 7, measured the atmospheric pressure, the surface temperature and the principal component of the atmosphere, the carbon dioxide.

However, the most important missions were Viking 1 and Viking 2, sent in 1975, which were the first missions with two landers on board. The spacecrafts sent on the Earth a lot of photos with a resolution of about ten metres, showing, in addition, changes in the local meteorology. However their scope was to analyze the planetary soil, with the aim of finding the presence of elementary life, but, as it is well known, they did not find it.

Today there are four spacecrafts in orbit around Mars. *Mars Express*, an ESA mission, launched in 2003, shown in Figure 1.2. It has on board several instruments,

Figure 1.2: The Mars Express.

in particular PFS, Planetary Fourier Spectrometer (Formisano et al., 2005), built with the collaboration of the Group of Astrophysics of Lecce. Another important instrument on board of Mars Express, for which the Lecce team had also a role, is OMEGA, Observatoire pour la Minéralogie, l'Eau, les Glaces et l'Activité (Bibring et al., 2005). This instrument is a spectral camera which takes images in three dimensions, where the third dimension is the spectrum between 0.36 and 5.2 μm: its aim is to map the surface composition of Mars. Mars Express has been exploring the atmosphere and surface of Mars from polar orbit since 2003: some of its instruments had measured evidence of recent glacial activity, explosive volcanism, and methane gas.

A successful NASA mission is *Mars Global Surveyor*, launched in 1996. One of the instruments on board is a spectrometer, TES, Thermal Emission Spectrometer (Christensen et al., 2001), which is analyzing the surface. The data which can be obtained by TES are those connected to the temperature, such as the changes of temperature with the day, the thermal inertia (how well the surface transmits heat) and the grain size of the regolith, which can be obtained from the thermal inertia (Spencer, 1990; Aumann and Kieffer, 1973; Edgett and Christensen, 1994; Mellon et

al., 2000). Naturally it is possible to obtain the mineral composition of the surface. In addition the instrument can give information about the atmosphere.

Mars Reconnaissance Orbiter, another NASA mission, was launched in 2005. It has on board a powerful spectral camera, CRISM, Compact Reconnaissance Imaging Spectrometer for Mars (Murchie et al., 2007). CRISM started to work in 2006. Its aim is to obtain the composition of the surface by means of spectra recorded in the visible and infrared spectral range, in particular water-related minerals.

The latest mission which was launched is *Phoenix*, a low-cost mission of NASA. It arrived on the planet in 2008 and it had on board a lander which arrived near the north polar region. Its purpose is to analyze samples of soil and ice to evidence whether the site was ever hospitable for life; in addition it studies the atmosphere obtaining data about the formation, duration and movement of clouds, fog, and dust plumes. The lander was turned off in November 2008, because the Martian polar winter does not permit to its solar panels to produce the required energy.

As already stated, some of the instruments, taken into account in this short review, have seen the involvement of the Astrophysics Group of the University of Salento. The instrument are spectrometers, and the laboratory of the Department has also two spectrometers, which have been used to characterize the space instruments and to take spectra of minerals of interest.

In fact, the group of Lecce is also involved in the construction of MIMA (Martian Infrared Mapper), an infrared spectrometer which will be sent on Mars in 2016 on board of ExoMars, an ESA Mission. As it will be shown in the Appendix B, I am also involved in this project, with the characterization of the instrument. MIMA will be mounted on the rover's mast, shown in Figure 1.3. It will analyze the surface composition in order to search signs of past and present life on Mars, it will try to select the most interesting sites, where to drill and to acquire samples, and it will study the atmosphere in order to take some information about the meteorological conditions and measure gases and aerosols.

In conclusion all these instruments acquire, and send on the Earth, a large amount of data. These data must be analyzed and studied, in order to obtain more information about the planetary characteristics and, for this reason, it is nec-

Figure 1.3: A picture of the rover on board of ExoMars.

essary an accurate study of the reduction and analysis criteria. Many different techniques already exist and many others are currently studied, such in the case of this PhD thesis. In fact the particle size and surface roughness could be obtained using thermal inertia (Spencer, 1990; Aumann and Kieffer, 1973; Edgett and Christensen, 1994; Mellon et al., 2000), the roughness could be obtained also using radar measurements (Evans and Hagfors, 1968), the rock abundance could be obtained using surface temperature measurements (Christensen, 1986), as well as by means of photometric measurements (Hapke, 1981, 1984).

However, some problems related to the analysis of the acquired spectra exist. In fact, all the spectrometers around Mars have a big field of view, and the portion of surface analyzed is very large. In such scenario it is difficult to hypothesize that the surface spectra acquired are related only to one mineral, but it is more probable that they are related to mixtures of different minerals and rocks. My work has been thought in order to understand how to acquire information about each component of a mixture, such as abundance and grain size, from the general spectral behaviour

of a mixture. This work is only a preliminary study, but I hope that a complete method could be obtained in future and be applicable to planetary surface spectra.

1.3 The spectral range

This work originates from the necessity of a fast and reliable study of the spectra recorded by the spectrometers orbiting around Mars and it is based on a comparison between laboratory and calculated reflectance spectra in the NIR (Near Infrared, $2.5 \div 5.0$ μm) and MIR (Medium Infrared, $5.0 \div 25.0$ μm) spectral range.

The choice of this range is due to two reasons. Firstly, because in this range the fundamental vibrational bands, characteristics of each mineral and rocks, are present (Estep-Barnes, 1977). Secondly, because in this work I try to use the Hapke theory, which has been demonstrated, firstly by Clark (1983) and Johnson et al. (1983), to be valid up to 2.5 μm. In addition this spectral range is particularly interesting because the spectral features are influenced by several parameters, depending on the internal characteristics of a mineral, such as the refractive index, as well as external constraints, the grain size, the spatial distribution, etc.

In order to understand better the spectral behaviour of every mineral, it is convenient to divide the spectra into several parts, each of them with a particular spectral feature, e.g. absorption bands, restrahlen bands, transparency features.

However, it is important to mention the *Christiansen frequency* (Conel, 1969), that occurs when $n \cong 1$ and k is small, where n and k are respectively the real and imaginary part of the refractive index. After this frequency k increases and produces the main restrahlen band. The Christiansen frequency is easily recognized because it is a minimum in reflectance, since k is small and there is very little backscattering or absorption, so radiation passes through the sample relatively easily. The principal Christiansen feature is associated to the strongest *restrahlen band*, which is a very strong molecular vibrational band. Both the real and imaginary part of the refractive index are a function of wavelength, so a change of these indices produces a change in the reflectance spectrum (Hunt and Vincent, 1968; Salisbury and Wald, 1991). When k rapidly changes from a very low value, in the absorption range, to a large value

($k > 0.1$), the inversion of the behaviour produces a very strong reflectance band, the restrahlen band, which is located at longer wavelength than the Christiansen frequency.

Another important range occurs between 2.5 μm and the first Christiansen frequency (NIR spectral range): the region of the *absorption features*, basically due to vibrational modes. This region is dominated by volume scattering, because the absorption coefficient is too low ($k \ll 1$) and $n > 1$, so the photons can survive inside the particles and are scattered back to the observer (Salisbury et al., 1992). In addition, the spectral contrast increases with decreasing particle size, because the amount of multiple scattering and first surface reflection increases (Salisbury and Wald, 1991; Mustard and Hays, 1996).

The *restrahlen bands* are strong absorption features, which occur for two different causes: internal modes or external modes (Farmer, 1974; Salisbury et al., 1992). The first occurs when there is a change in bond length or angle, the second when the whole molecule moves as a rigid unit, for example when it translates along an axis or rotates around it. This movement induces a change in the dipole moment, causing an interaction with incident radiation, with a consequent absorption of light. In addition, because of the movement which causes a change in the distribution of the electric charge, not all the frequencies permitted to interact with light are active in the IR. In fact if the molecule is nonsymmetric or has a permanent dipole, the modes will be active in IR, while, on the contrary, in a symmetric molecule without a permanent dipole, the movement does not cause a change in the charge distribution, so the bands will be IR inactive.

Moreover, these bands occur when k is large ($k > 0.1$), so very little energy passes through the grains, and it is all reflected from the sample to the observer, so the interaction is dominated by first surface reflection, producing a maximum in reflectance. This phenomenon is proportional to the particle size. When particle size decreases also the band intensity decreases, and if particles are very small, restrahlen bands disappear, because of the increasing in the multiple scattering, which produces a decreasing in intensity, due to the absorption in voids between the particles (Salisbury and Wald, 1991).

The spectral region associated with the transition from the surface to volume scattering is the *transparency region*, usually located between the first and the second restrahlen band. Here the features are due to stretching or bending modes, such as for the restrahlen bands. However in transparency bands are due to volume scattering, because the absorption coefficient is low and radiation can penetrate into grains. For transparency features the spectral contrast increases with decreasing particle size (Conel, 1969; Walter and Salisbury, 1989; Salisbury et al., 1992).

1.4 Directional Hemispherical Reflectance

In Section 1.2 I have briefly reviewed some space missions and their instrumentations, concentrating principally on the spectrometers. My work is a study of reflectance spectra of particulate mixtures, and it was thought for a possible application to Martian surface spectra.

Even if bidirectional reflectance has been widely used for this purpose, I prefer directional-hemispherical reflectance, which is the reflectance referred to a collimated beam which is scattered by a surface into the upper hemisphere. The main reason is that the directional-hemispherical reflectance is more easily related to emissivity by means of Kirchhoff's law (Hapke, 1993; Salisbury et al., 1994). In particular, in the infrared spectral range, the radiation absorbed by an opaque material, is then emitted at the same wavelength where such absorption has occurred. For this reason, the directional emissivity of a material can be determined measuring the hemispherical reflectance. Therefore, from the reflectance of a material illuminated by an incident collimated radiation at a defined angle and scattered into all directions (directional hemispherical reflectance), it is possible, using Kirchhoff's Law, to evaluate the emissivity toward the incident direction.

However, the Kirchhoff's law is applicable only on samples in thermodynamic equilibrium or, at least in thermal equilibrium when the material is isothermal and at the same temperature of the atmosphere toward which it radiates. Some works have been done in order to understand the validity limit of this law, because in general the atmosphere is cooler than the material. For example, Salisbury et al.

(1994) measured, in the thermal infrared spectral range, both directional hemispherical reflectance and emissivity of samples with a thermal gradient and compared the emissivity calculated using Kirchhoff's with that measured. As a conclusion they have shown that the Kirchhoff's law can be applied with a good precision to solid rocks and soils with a low thermal gradient. However the same gradient dominates the infrared radiation if the surface is composed of very fine particles with a decreasing density, such as frost or snow, and in such cases Kirchhoff's law could not be applied.

Fortunately, the Martian atmosphere, as well as the laboratory conditions, are sufficient to keep the thermal gradient low, because, from one side the Sun radiation enhances the thermal gradient, while, from the other side, the atmosphere, with its convective motion, reduces the thermal gradient within the regolith and the Kirchhoff's law can be considered fully valid.

The Kirchhoff's law is directly related to my work because one of its possible application is the deconvolution of Martian surface spectra in the NIR-MIR spectral range, $2.5 \div 25.0$ μm. Such spectral range includes the thermal infrared, which, for Mars, starts at about 4 μm, and is dominated by the radiation emitted by the planet. In such cases the Martian spectra could be obtained by measurements of both reflectance or emission, and in both cases it is possible, by means of Kirchhoff's law, to derive one from the other (Hapke, 1993; Salisbury et al., 1994). In conclusion Kirchhoff's law can be applied both for laboratory and Martian surface spectra.

Another important reason for using directional hemispherical reflectance is that, even if the orbiting spectrometers work in bidirectional reflectance, there are some problems related to such configuration. In fact, in the bidirectional reflectance a radiation is incident at a specific angle and collected at a fixed angle. In such condition some information dominate the spectra, such as the orientation of the grains, which is present in a laboratory measurements, but it is not present in remote sensing observations. In addition, the observed surface is not plane and, therefore, it is difficult to individuate a single incident direction and consequently a single emerging direction. In such conditions the radiation reaching the spectrometer is better simulated by a laboratory hemispherical reflectance configuration.

A last observation about the mathematical approach, because, as it is shown in Chapter 2 Equation 2.28, the hemispherical reflectance is the integral over the solid angle of the bidirectional reflectance (Hapke, 1993), so if the angle distribution is known, it is possible to calculate the hemispherical reflectance from the bidirectional.

As a conclusion I have thought that hemispherical reflectance is more appropriate for the object of my work: the study of mineral mixtures.

1.5 A work about the mixtures

In this chapter I have discussed about Mars because this study about reflectance spectra of particulate mixtures is aimed to a possible application to planetary surface spectra.

The reasons of such choice are different. I have just said that looking at a planetary surface, with remote sensing instruments, I do not expect that it is composed by only one mineral, but by a mixture of different minerals and rocks. Therefore a full understanding of the behaviour of materials in mixtures is necessary to understand better the surface spectra.

In addition, the mixtures spectral behaviour is not fully understood, especially in the NIR-MIR spectral range; in fact it has been demonstrated valid up to 2.5 μm by several authors (Clark, 1983; Mustard and Pieters, 1987, 1989; Johnson et al., 1983), but there are still some problems at longer wavelength.

However, to understand better the mixtures behaviour, it is necessary to do some preliminary observations. Different types of mixtures exist and for macroscopic minerals the principal two are *areal* and *intimate* mixtures.

In the areal mixtures, the surface is formed by several patches of a single and pure material, in the intimate mixtures, different types of particles are mixed homogeneously together in the whole volume (Hapke, 1993; Singer and McCord, 1979).

For each of this mixtures the evaluation of the resulting spectra is different, in fact for areal mixtures the resulting reflectance is a linear combination of the reflectance of each patch, weighted on the portion of surface occupied by each patch. On the contrary, for intimate mixtures, the resulting reflectance is a nonlinear function of

the reflectance of each component (Hapke, 1993; Singer and McCord, 1979) and it is given by the relations derived in the following chapter, using the Hapke Theory of Reflectance.

In addition, in this study I work only with binary mixtures, since, due to the many parameters involved, it is easier and, at the same time, not reductive to consider only two components.

Another observation can be made about the components of the mixtures. In fact I consider mixtures of the same mineral with components of different grain size, *granulometric mixtures*, and mixtures with different minerals with both different and similar grain size, *compositional mixtures*. In particular I use granulometric mixtures to check the hypotheses made, as I will show in Chapter 4, because mixtures of one mineral only have less parameters to keep under control. However, compositional mixtures are fundamental to understand the mixtures behaviour, without imposing any limitation.

In conclusion, in this work, I try to understand the spectral behaviour of mineral mixtures, as a function of both grain size of components, and wavelength. In addition I try, by means of Hapke theory (Hapke, 1993), to use the spectra of each component to calculate the spectra of the mixture, and compare it with the correspondent experimental spectrum of the mixture.

1.6 Summary

The necessity to have a fast deconvolution method, applicable to planetary spectra, capable of assessing the role of each component in a mixture of particulate materials, taking into account, at the same time, composition, abundance and grain size, is one of the major reason of this work.

In fact, in Chapter 2, I will shortly introduce the Radiative Transfer Equation to explain better the Hapke Reflectance Theory, which is the mathematical approach I use in this work. In particular, the Hapke theory describes the radiation matter interaction. Unfortunately, the reflectance described by Hapke depends on many variables, such as the abundance, the grain size, the distribution, the optical con-

stants, etc. Therefore, in order to simplify such theory and for using it both in laboratory and in remote sensing spectra, without losing any information, I have made some hypotheses.

The demonstration of such hypotheses is an important part of this work, and requires an adequate experimental apparatus, which will be fully explained in Chapter 3, where I will describe the procedure and the instruments used. In fact, the main issue of this work is the careful comparison between the theoretical predictions and the experimental spectra.

In Chapter 4, I will discuss and demonstrate the validity of the hypotheses made, which are basically three: (1) the particles are all identical and spherical; (2) the scattering is isotropic; (3) the extinction coefficient is equal to unit. I will show how such hypotheses are not restrictive and are easily to be applied to laboratory experience as well as to planetary spectra.

In Chapter 5 I will show the first result obtained: the extension of the validity of Hapke Theory of Reflectance (Hapke, 1993) to the whole NIR spectral range, up to the principal Christiansen frequency. In addition I will discuss some mixtures spectra, showing some discrepancies found between the theory and measurements and I will show some experimental results, which are the starting point of the main discussion of my work and are the basis for future work aimed to obtain a deconvolution method able to analyze the planetary surface spectra.

Finally, in Chapter 6, I will show that considering a mixture as areal, instead than intimate, is more correct in the MIR region. I will show some experiments which demonstrate such hypothesis and I will use the chi-square function as another proof of the validity of such work.

Chapter 2

Theoretical background

In this chapter I will describe the theoretical background used in this work. I will start with some definitions of the fundamental quantities (Section 2.1). In Section 2.2 I will introduce the general form of Radiative Transfer Equation (RTE), which controls the radiation field in a medium which absorbs, emits and scatters radiation. One of the solution of RTE is the Hapke Theory of Reflectance and it will be shortly illustrated in Section 2.3. In addition, I will introduce and discuss some hypotheses which are applied to Hapke Theory; such hypotheses from one side make the theory easier to be applied in most cases encountered in laboratory experience, while, from the other side, simplify the problem without reducing its applicability on remote sensing analysis of planetary surface spectra. However, such hypotheses will be demonstrated in this PhD thesis and they have been one of the principal subject of my work during these years. Finally, in Section 2.4, I will apply the Hapke Theory to particulate mineral mixtures, taking into account the hypotheses illustrated in the previous section.

2.1 Definitions

This work is a study of radiation-matter interaction, applied to a collimated beam which interacts with a particulate surface. Before considering the specific case, some general quantities must be defined (Hapke, 1993).

I consider, in this section, the radiation incident on the particles, characterized

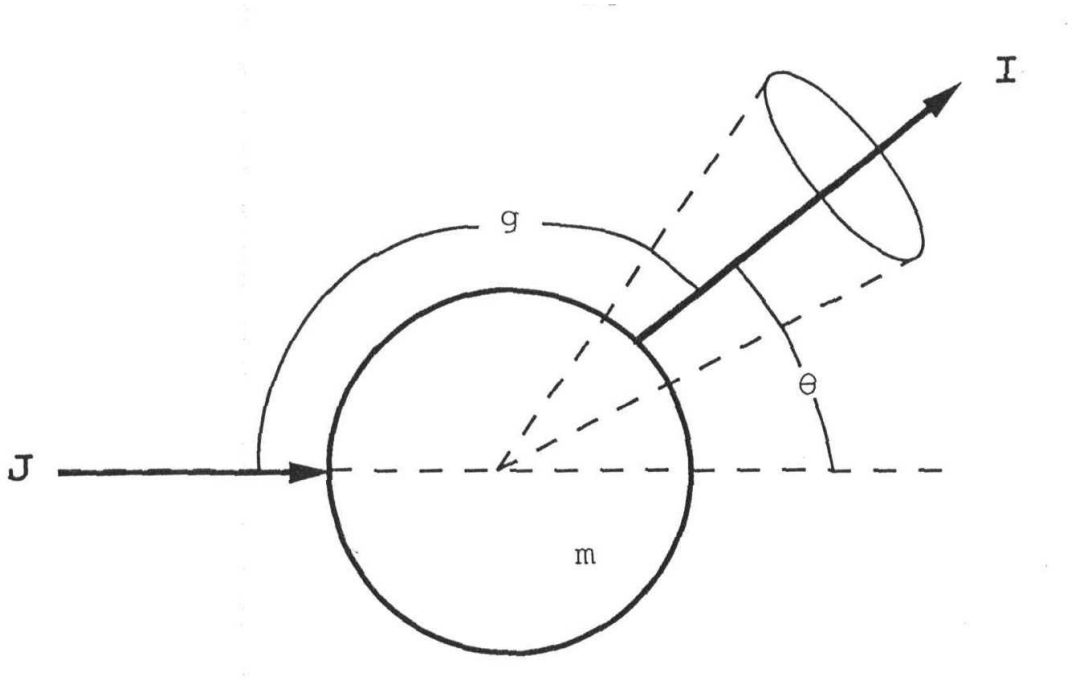

Figure 2.1: Scattering of a single particle.

by its *irradiance*, J, which is the power per unit area of a collimated beam. After the interaction with the matter, whose refractive index is $m = n + ik$, the radiation is characterized by its *radiance*, I, which is the amount of power, of an uncollimated beam, at position s, crossing unit area perpendicular to the direction of propagation Ω, traveling into the unit solid angle $d\Omega$.

If an incident beam, with irradiance J, interacts with a single spherical particle (see Figure 2.1), it could loose a part of the total energy, which can be absorbed or scattered (altogether extinguished). Even if, considering a particle as a perfect sphere is not the case of planetary regolith, this assumption is not too restrictive, because, if many particles are close together, then irregular shape can be neglected, as it will be demonstrated in this work.

The relation between the energy of the incident beam, J, and the extinguished, P_E, the scattered, P_S, and the absorbed ($P_A = P_E - P_S$) power, are:

$$\sigma_E = \frac{P_E}{J} \tag{2.1}$$

$$\sigma_S = \frac{P_S}{J} \tag{2.2}$$

$$\sigma_A = \frac{P_A}{J} \tag{2.3}$$

where σ_E, σ_S and σ_A are respectively the *extinction*, *scattering* and *absorption cross section* and $\sigma_E = \sigma_S + \sigma_A$

All these quantities (σ_E, σ_S and σ_A) have the dimension of an area, and their ratio with the geometrical cross sectional area ($\sigma = \pi\, a^2$, with a the radius of the particle) gives the *extinction*, *scattering* and *absorption efficiencies*, which are:

$$Q_E = \frac{\sigma_E}{\sigma} \tag{2.4}$$

$$Q_S = \frac{\sigma_S}{\sigma} \tag{2.5}$$

$$Q_A = \frac{\sigma_A}{\sigma} \tag{2.6}$$

with $Q_E = Q_S + Q_A$.

Another quantity, fundamental in this work, is the *particle single-scattering albedo*, w, which is the ratio of the scattered power to the extinguished power. Using the above relations:

$$w = \frac{P_S}{P_E} = \frac{\sigma_S}{\sigma_E} = \frac{Q_S}{Q_E} \tag{2.7}$$

The *particle phase function*, $p(g)$, describes the angular pattern into which the power P_S is scattered, so the scattered radiance, which is the power per unit area scattered into unit solid angle, is given by:

$$I(\Omega) = J(\Omega_0)\frac{\sigma Q_S p(g)}{\sigma Q_E 4\pi} = Jw\frac{p(g)}{4\pi} \tag{2.8}$$

where Ω_0 is the direction of the incident beam with irradiance J, Ω is the direction into which the radiance is scattered and g is the phase angle (Figure 2.1).

If a particle scatters isotropically, the particle phase function is:

$$p(g) = 1 \tag{2.9}$$

Finally ξ is the *cosine asymmetry factor*, i.e. the average value of the cosine of the scattering angle $\theta = \pi - g$, as it is shown in Figure 2.1:

$$\xi =< cos\theta > \tag{2.10}$$

All the quantities have been defined without making any hypothesis about the dimension of the particle compared with the wavelength, which is important for the description of the radiation-matter interaction. It is useful to define the *size parameter*, as the ratio of the particle size to the wavelength:

$$X = \frac{2\pi a}{\lambda} = \frac{\pi D}{\lambda} \tag{2.11}$$

where $D = 2a$ is the diameter of the particles and λ the wavelength of the incident radiation. The value of X defines the geometry of the interaction. If $X \ll 1$, the particles are known as *Rayleigh scatters* and the parameters, such Q_E, Q_S and Q_A could be derived by the Mie theory (Kerker, 1969; Bohren and Huffman, 1983). The case of $X \sim 1$ characterizes the resonance region. In such case, if the particles are not absorbed, the extinction and scattering efficiencies tend to oscillate. The case considered in this work is the geometrical optics region, for which $X \gg 1$. In such case, a portion of incident radiation could be scattered (Q_S) and a part of that could be diffracted (Q_d) by a large isolated sphere. However, if the particles of a medium are very close together, as in planetary regolith, the diffraction is effectively equal to zero. The size parameter and diffraction condition will be discussed in Section 4.1 and 4.3, because they are fundamental for developing the equations used in this work.

2.2 Radiative Transfer Equation

The Equation of Radiative Transfer describes how the intensity of a radiation field changes through a complex medium which absorbs, emits and scatters radiation. The principal assumption is that the inhomogeneities of the medium interact with the radiation independently of each other and incoherently.

Let $I(s, \Omega)$ be the intensity of radiation at the point s, propagating in the direction Ω, emitted or scattered by a particulate medium. Consider s, as in Figure 2.2,

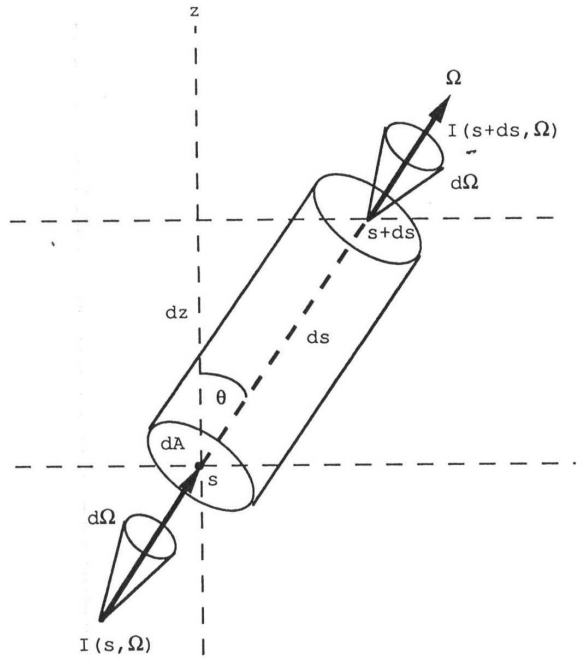

Figure 2.2: Geometry of RTE.

on a base of a cylinder of area dA, length ds and volume $dAds$. The radiation, passing through s in a solid angle $d\Omega$ in the direction of Ω is $I(s,\Omega)\ dA\ d\Omega$ and the power emerging from the top of the cylinder is:

$$I(s+ds)dAd\Omega = \left[I(s,\Omega) + \frac{\partial I(s,\Omega)}{\partial s}ds\right] dAd\Omega \tag{2.12}$$

The difference between the radiation entering at the bottom ($I(s,\Omega)$) and that emerging at the top is $(\partial I(s,\Omega)/\partial s)dsdAd\Omega$, and this reduction in energy is due to the absorption and scattering processes, or, equivalently, to the *extinction* process.

The reduction in power (ΔP_E) due to the extinction, which is the loss of energy related to the volume extinction coefficient ($E(s,\Omega)$) on a beam that propagates through the volume element $d\Omega$, is given by:

$$\Delta P_E = -E(s,\Omega)I(s,\Omega)dsdAd\Omega \tag{2.13}$$

If extinction acts only on the intensity, then:

$$\Delta P_E = \frac{\partial I}{\partial s}dsdAd\Omega = dIdAd\Omega \tag{2.14}$$

As already said, the extinction process is given by absorption and scattering (Section 2.1), so it can be separated into the *volume scattering coefficient*, $S(s, \Omega)$, and the *volume absorption coefficient*, $K(s, \Omega)$, as follows:

$$E(s, \Omega) = S(s, \Omega) + K(s, \Omega) \tag{2.15}$$

It is possible to calculate the increase in power (ΔP_S) due to the radiation scattered into the emerging beam, as follows:

$$\Delta P_S = \frac{1}{4\pi} G(s, \Omega', \Omega) I(s, \Omega') ds dA d\Omega' d\Omega \tag{2.16}$$

where $G(s, \Omega', \Omega)$ is the volume angular scattering coefficient of the medium, defined as the power, due to the radiation which comes from the direction Ω' ($I(s, \Omega')$), passing through the volume $dsdA$ and scattered into the direction Ω.

The volume scattering coefficient is given by the integral over all the directions of $G(s, \Omega', \Omega)$:

$$S^*(s, \Omega) = \frac{1}{4\pi} \int_{4\pi} G(s, \Omega', \Omega) d\Omega' \tag{2.17}$$

where the star is used in order to emphasize that the radiation is scattered into the emerging beam, and it is not that removed from the incoming beam ($S(s, \Omega)$).

Finally, the *volume emission coefficient*, $F(s, \Omega)$, is the power emitted per unit volume by an element at the point s into the solid angle about the direction Ω. So it is possible to define ΔP_F as the change of power due to the emission, as follow:

$$\Delta P_F = F(s, \Omega) ds dA d\Omega \tag{2.18}$$

Equating the sum of all the contributions ($\Delta P_S + \Delta P_E + \Delta P_F$) to $(\partial I / \partial s) ds dA d\Omega$ and dividing by $dsdAd\Omega$, it gives:

$$\frac{\partial I(s, \Omega)}{\partial s} = -E(s, \Omega) I(s, \Omega) + \frac{1}{4\pi} \int_{4\pi} I(s, \Omega) G(s, \Omega', \Omega) d\Omega' + F(s, \Omega) \tag{2.19}$$

This last equation is the general form of *Radiative Transfer Equation*.

2.2.1 Radiative Transfer Equation in a particulate medium

The Radiative Transfer Equation is a general equation which controls the interaction of radiation with matter, but such interaction, in a particulate medium, could change drastically with the dimension of the particles for a given wavelength of the incident radiation. This parameter will be taken into account during the following discussion.

The solution of the RTE requires the knowledge of the volume emission, scattering and absorbtion coefficients (F, S, K). The calculation of these coefficients depends on the characteristics of the particulate medium considered, such as the size of the particles (larger or smaller than wavelength), or their distribution (well separated or close together). However this work is focused on particles large compared with the wavelength ($X \gg 1$) and close together, as in a planetary regolith, and I will therefore describe only this case.

In such case individual rays interact only with a portion of the entire volume of a particle and many phenomena influence the radiative transfer coefficients, such as diffraction, non-uniform illumination of particles, coherent effects as well as particle density, porosity and shadowing; however, only diffraction is important in such case and the other phenomena can be neglected.

Diffraction. When the particles are close together, the diffracted rays could be neglected, and consequently Q_d, which is the portion of extinction due to the diffraction, can be ignored, so $Q_E = 1$. This condition on the extinction efficiency will be carefully discussed in Chapter 4, because it is a fundamental point of this work. In addition experimental work has been done in support of this hypothesis. However a condition must be added, because it is necessary to clarify for which separation of the particles it is possible to ignore the diffraction. Such estimation depends on the size parameter and the filling factor: $\phi \gg X^{-1}$ with $\phi = 4\pi a^3/3Z^3$ and $Z = N^{-1/3}$ is the mean distance between the particles.

This condition is valid if the particles are large, $X \gg 1$, and approximately in contact, such as in planetary regolith and in laboratory samples.

The radiative transfer coefficients. The main hypotheses of this work are that

the medium is composed of identical and spherical particles, large compared with the wavelength, close together and randomly oriented.

Considering N particles, with geometric cross-section area σ and extinction, Q_E, scattering, Q_S, and absorption, Q_A efficiencies, the *volume extinction*, *scattering* and *absorption coefficients* are:

$$E = N\sigma Q_E \tag{2.20}$$

$$S = N\sigma Q_S \tag{2.21}$$

$$K = N\sigma Q_A \tag{2.22}$$

In addition, the volume single-scattering albedo is:

$$w = \frac{Q_S}{Q_E} \tag{2.23}$$

In general, if the medium is composed of a mixture of different grains and the number of particles per unit volume will be given by $N = \sum_j N_j$, where N_j is the number of particles of type j with the geometric cross-section area σ_j and extinction, Q_{E_j}, scattering, Q_{S_j}, and absorption, Q_{A_j} efficiencies. In such case the volume extinction, scattering and absorption coefficients are:

$$E = \sum_j N_j \sigma_j Q_{E_j} \tag{2.24}$$

$$S = \sum_j N_j \sigma_j Q_{S_j} \tag{2.25}$$

$$K = \sum_j N_j \sigma_j Q_{A_j} \tag{2.26}$$

Similarly, the *volume single-scattering albedo* for the $j-th$ type of particle is:

$$w_j = \frac{Q_{S_j}}{Q_{E_j}} \tag{2.27}$$

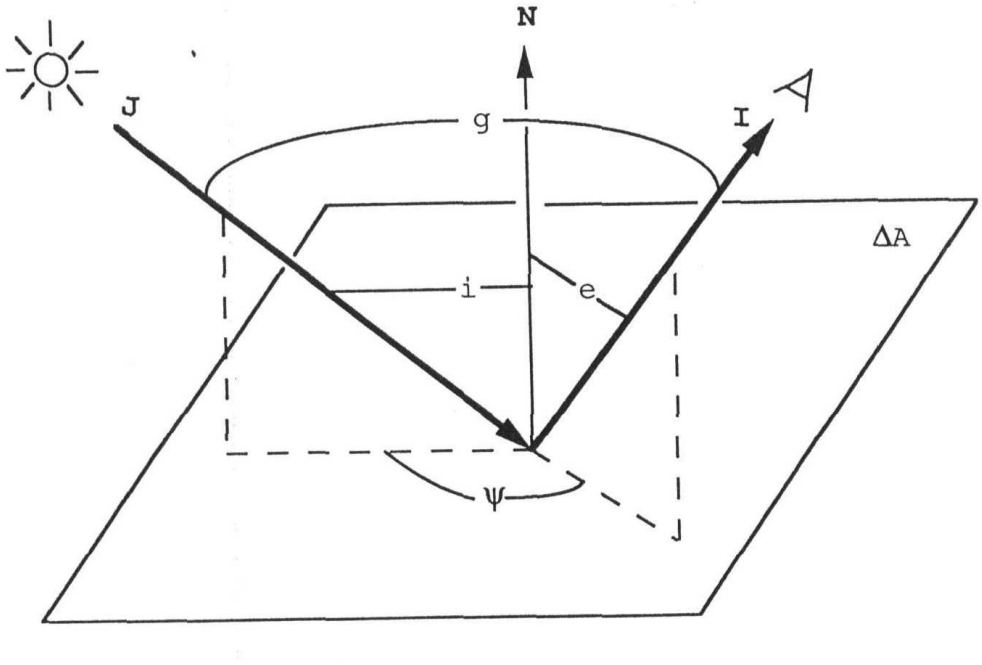

Figure 2.3: Geometry of Hapke theory of reflectance

2.3 The Hapke Theory

The Hapke theory of reflectance is a numerical approach for solving the RTE applied to a particulate medium (Hapke, 1993).

Reflectance is the fraction of incident light which is scattered or reflected by a material, such as in Figure 2.3. Because of the incident radiation which could be scattered in many directions and the radiation which could be collimated or not, the reflectance depends on the geometry. In particular two adjectives describe the geometry, the first is referred to the degree of collimation of the incident radiation and the second is referred to that of the detector, so the directional-hemispherical reflectance, or simply hemispherical reflectance, is the fraction of light scattered into the upward hemisphere by a surface illuminated by a collimated source. Bidirectional reflectance of a medium is defined as the ratio between the scattered radiance in the direction of the detector and the incident irradiance. In this work I use directional-hemispherical reflectance measurements because I think that such measurements are more appro-

priate, for the final purpose of this work, than the usual bi-directional reflectance measurements, as I have already explained in Section 1.4. In fact, while in laboratory the surface of the sample is flat enough for assuming the measured reflectance as bi-directional, different is the case of a remote sensing reflectance measurement, where the observed surface cannot be considered flat, but as composed by several planes oriented in different directions. Such situation is in between a laboratory measurement of bi-directional reflectance and one of directional-hemispherical reflectance. In addition, I have chosen to work in directional-hemispherical reflectance, because the largest part of the spectral range on which I focus my attention ($2.5 \div 25.0$ μm) is, as in the case of Mars, dominated by the radiation emitted by the planet and hemispherical reflectance is usually related to emission by means of the Kirchhoff's law ($R = 1 - \varepsilon$, with R the hemispherical reflectance and ε the emission) (Salisbury and Wald, 1991; Salisbury et al., 1994). However, the directional-hemispherical reflectance, r_h, is defined as:

$$r_h = \frac{1}{\mu_0} \int_{2\pi} r(i, e, g) \mu d\Omega_e \tag{2.28}$$

where $r(i, e, g)$ is the bi-directional reflectance, g the phase angle, $d\Omega_e$ is the element of the entire hemisphere into which the radiance is emitted, while μ and μ_0 are:

$$\mu = cose \tag{2.29}$$

$$\mu_0 = cosi \tag{2.30}$$

with e and i the emerging and the incidence angle respectively.

For the calculation of $r(i, e, g)$ consider Figure 2.4. Collimated irradiance J is incident on a particulate medium, composed of particles which absorb and scatter radiation. The radiation which arrives to the detector is I_D, the bi-directional reflectance is:

$$r(i, e, g) = \frac{I_D}{J} \tag{2.31}$$

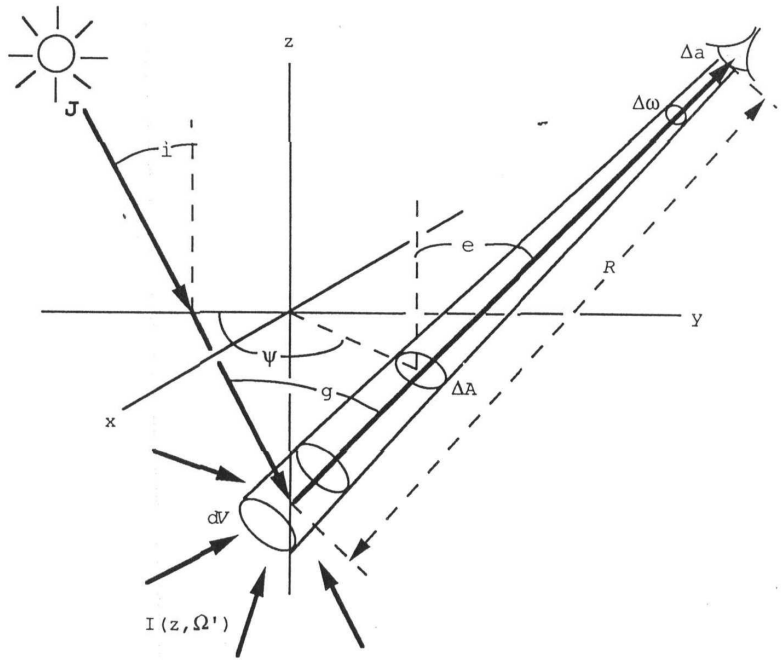

Figure 2.4: Geometry used for the calculation of bidirectional reflectance.

Solving RTE with two-stream method (Hapke, 1993), the resulting equation is:

$$I(\tau,\Omega) = I(\tau,\cos\vartheta) = \frac{Jw}{4\pi}\frac{1}{4\gamma^2\mu_0^2-1}\left[-\frac{(1-\gamma)2\mu_0(1+2\mu_0)}{1+2\gamma\cos\vartheta}e^{-2\gamma\tau}+\right.$$
$$\left.+\quad\frac{\mu_0}{\mu_0+\cos\vartheta}(4\mu_0^2-1)e^{-\tau/\mu_0}\right]. \tag{2.32}$$

where $\tau = 0$ is the level of the medium; considering that the radiance emitted by the surface at $\tau = 0$ is the same that arrives at the detector, the bidirectional reflectance becomes:

$$r(i,e,g) = \frac{w}{4\pi}\frac{\mu_0}{\mu_0+\mu}\frac{1+2\mu_0}{1+2\gamma\mu_0}\frac{1+2\mu}{1+2\gamma\mu} \tag{2.33}$$

where γ is the *albedo factor*, defined as:

$$\gamma = \sqrt{1-w} \tag{2.34}$$

Introducing the *Chandrasekhar function* $H(x)$, for which a good approximation

is:

$$H(x) \simeq \frac{1+2x}{1+2\gamma x} \tag{2.35}$$

The $r(i,e,g)$ can be rewritten as:

$$r(i,e,g) = \frac{w}{4\pi}\frac{\mu_0}{\mu_0+\mu}H(x_0)H(x) \tag{2.36}$$

This equation describes the bidirectional reflectance of a medium composed of particles that scatter light isotropically and independently from each other.

A general form takes into account also the opposition effect, $B(g)$, which is observed at small phase angle and it is due to the shadow caused by particles which are positioned between the source and the surface or between the surface and the detector. Introducing the opposition effect, the scattering is not isotropic and the equation becomes:

$$r(i,e,g) = \frac{w}{4\pi}\frac{\mu_0}{\mu_0+\mu}\{[1+B(g)]p(g) + H(x_0)H(x) - 1\} \tag{2.37}$$

As already said, in this work I use the directional-hemispherical reflectance, so, substituting the equation 2.37 into equation 2.28, developing $p(g)$ in Legendre polynomial at the second order and solving the integral, the hemispherical reflectance becomes:

$$r_h = \frac{1-\gamma}{1+2\mu_0\gamma} + \frac{w}{4}\frac{\mu_0}{1+2\mu_0}\xi\left[\frac{5}{4}\xi(3\mu_0^2-1) - 3\right] \tag{2.38}$$

The directional hemispherical reflectance, given by the relation 2.38, depends on several parameters. As a result the applicability of this equation is complicated and it is necessary to take into account a lot of parameters which could be neglected in many cases.

The first assumption that could be made is about the particle phase function. In fact it is possible to assume that particles scatter isotropically, so $p(g) = 1$ (Hapke, 1993, 2002; Mustard and Pieters, 1987). Assuming the isotropic scattering, since it is also $\xi = 0$, the relation becomes more simple:

$$r_h = \frac{1-\gamma}{1+2\mu_0\gamma} \tag{2.39}$$

In deriving Equation 2.39, in addition to the isotropic scattering hypothesis, I have also assumed that the opposition effect is always negligible (Hapke, 2002; Nelson and Hapke, 2000; Hapke et al., 1998). This is certainly true for my laboratory measurements, since, as it is described in Section 3.4, I use an integrating sphere. However, the opposition effect acts with two different mechanisms: the *Shadow hiding opposition effect* (SHOE), which is caused by radiation scattered once, and the *Coherent backscatter opposition effect* (CBOE), which is due to the multiply scattered component. However both of them are important for small phase angle, but this is not the case of almost remote sensing measurements, so I can neglected them.

As far as the isotropic scattering assumption is concerned, in this case it is equivalent to assume that the particles of laboratory samples do not have a preferred orientation or, equivalently, that they are randomly oriented. I have tested that such hypothesis is basically fulfilled, since I found no appreciable variation in the spectra taken with different orientations of the sample.

Using this relation it is possible to calculate the single scattering albedo, which will be useful for my aims.

2.4 The Hapke Theory for particulate mixtures

The aim of my work is studying particulate mineral mixtures, using directional hemispherical reflectance. In particular, starting with a spectrum of a mineral mixture, I aim to derive the components of the mixture, their grain size and their abundance. This is possible, for remote sensing reflectance spectra, using different techniques, and different measurements, but the process is slow. Obviously the use of a single technique, with a limited number of measurements, will be of great use.

For this reason, I am investigating a method which, starting from the spectrum of a mixture of particulate materials, is capable of assessing the role of each component of the mixture, taking into account, at the same time, composition, abundance and grain size. In particular such a procedure is already available in the visible and near infrared spectral range (VNIR, up to 2.5 μm) (Clark, 1983; Mustard and Pieters,

1987; Johnson et al., 1983), while in the near and medium infrared ($2.5 \div 25.0$ μm) the extension of such procedure has not produced so far satisfactory results (Montanaro et al, 2007). Such extension is important because the spectral range is covered by TES (Christensen et al., 2001) and by one of the channels of PFS (Formisano et al., 2005), and because in this range most of the fundamental vibrational bands characteristic of each mineral (Farmer, 1974; Estep-Barnes, 1977; Salisbury et al., 1992) are located.

In this work I have therefore used Equation 2.39, in order to trace the relation between the measured hemispherical reflectance and the corresponding single scattering albedo. For a particulate sample, composed by a large number of particles of different sizes, the effective single scattering albedo can be written as:

$$w = \frac{\sum_j \sigma_j Q_{S_j}}{\sum_j \sigma_j Q_{E_j}} = \frac{\sum_j \sigma_j Q_{E_j} w_j}{\sum_j \sigma_j Q_{E_j}} \tag{2.40}$$

where σ_j, Q_{S_j} and Q_{E_j} are the geometrical cross-sectional area, the scattering efficiency and the extinction efficiency of each particle, while $w_j = Q_{S_j}/Q_{E_j}$ is the single scattering albedo of the j-th particle. The sum is extended to all the particles of the sample (Hapke, 1993).

When considering a mixture, the above relation can be rewritten making firstly the sum on the particles of each component and then the sum on the various components of the mixture. If homogeneous components are correctly individuated, appropriate effective values can be used and the relation can be considerably simplified.

$$w_m = \frac{\sum_i N_i (\sum_j \sigma_j Q_{E_j} w_j)}{\sum_i N_i (\sum_j \sigma_j Q_{E_j})} = \frac{\sum_i N_i \overline{\sigma_i}\,\overline{Q_{E_i}}\,\overline{w_i}}{\sum_i N_i \overline{\sigma_i}\,\overline{Q_{E_i}}} \tag{2.41}$$

w_m is the single scattering albedo of the mixture, N_i the number of particles for unit volume of each component, while $\overline{\sigma_i}$, $\overline{Q_{E_i}}$ and $\overline{w_i}$ are respectively the effective values of the cross-sectional area, of the extinction efficiency and of the single scattering albedo of each component.

The above relation does not take into account the fact that when particles are close together, as for my samples, the effect of diffraction can be usually ignored

or, equivalently, it is possible to set $\overline{Q_{E_i}} = 1$ (Hapke, 1981, 1993; Hapke and Wells, 1981; McGuire and Hapke, 1995). Of course the size of particles is also important in order to introduce this simplification and this issue is discussed in the following chapter, where the effective dimension of particles is introduced. In addition, for easier applications, Equation 2.41 can be rewritten in function of the fraction of the mass of each component:

$$w_m = \frac{\sum_i \frac{M_i}{\rho_i \overline{D_i}} \overline{w_i}}{\sum_i \frac{M_i}{\rho_i \overline{D_i}}} \tag{2.42}$$

where $M_i = N_i \frac{4}{3} \pi \overline{a_i}^3 \rho_i$ is the mass for unit volume of the particles, ρ_i their solid density and $\overline{D_i} = 2\overline{a_i}$ the effective mean diameter of the particles of the i-th component.

In this work I compare the measured hemispherical reflectance of a mixture with the same quantity derived, by means of Equations 2.39 and 2.42, from the hemispherical reflectance measurements of each component. In fact, I evaluate w_i by means of Equation 2.39, while M_i is the measured mass of each component in the mixture, ρ_i its density and D_i is derived with a statistical approach from a size distribution measurement on the particles of each component, as it will be shown in the following chapter.

Chapter 3

Experimental procedure

In this chapter I will describe the experimental procedure used in this work. I will start with a description of the minerals used, in Section 3.1, and sample preparation, in Section 3.2. Then I will continue with a detailed description of the main instruments: in Section 3.3 the characteristics of *Malvern Mastersizer 2000* are discussed, while, in Section 3.4, the Spectrometer *Perkin Elmer 2000* is described with a particular attention of the study of instrumental accuracy and measurement repeatability. In addition, for each instrument, I will show the mineral size distributions and the mineral spectra of each sample. In the last section I will illustrate the preparation of mixtures.

3.1 Minerals

One of the interests of the Group of Astrophysics of Lecce is the study of Mars and, for this reason, all the materials are chosen with particular attention to their implications on Mars. In addition the choice is made considering different types of minerals, such as a sulphate, a carbonate and a silicate, in order to have different spectral features at different wavelengths, as well as a silicon oxide, which has its spectral features close to those of a silicate.

In particular, I have chosen a silicate: olivine (Forsterite, Mg_2SiO_4; Jackson Co. North Carolina), because it has been observed on Mars surface (Bandfield, 2002; Bibring et al., 2006); a quartz (SiO_2; Hot Springs, Arkansas), which, even if it is

not abundant on Mars surface, it is very well studied in the whole spectral range of interest (Bandfield, 2002; Spitzer and Kleinman, 1961; Wenrich and Christensen, 1996) and it is used in the theoretical mixtures as representative of unknown silicates.

In addition I have chosen dolomite as a carbonate ($CaMg(CO_3)_2$; Sinatengrun bei, Wunsiedel, Fichtelgebirge, Bayern; provided by Dr. F. Krantz, Bonn Germany) and gypsum as a sulphate ($CaSO_4 * 2H_2O$; Fremont Co., Colorado), for their importance for the Martian climatological history (Lellouch et al., 2000; Fonti et al., 2001; Bandfield et al., 2003; Arvidson et al., 2006), in particular because both of them are evaporite and their formation happens in presence of liquid water.

Together with the choice of the particulate minerals, the choice of the grain dimension is also important, because, from one side the grain size is correlated with the thermal inertia (Aumann and Kieffer, 1973; Edgett and Christensen, 1994; Dollfus et al., 1993), from the other side the spectral behaviour of each mineral changes with the grain size. In particular this last reason is important for my purpose because my work is focused on the understanding of the spectral behaviour of mineral mixtures, so I have chosen the grain size, taking into account the limits involved with the small and big grain sizes. Besides, for the choice of the grain size I have taken into account also the possibility of an application of this work to Martian surface. Therefore I have chosen ranges which are thought to be representative of the Martian regolith (63 $\div$ 125 μm, 100 $\div$ 200 μm and 200 $\div$ 300 μm) (Edgett and Christensen, 1994; Dollfus et al., 1993) together with ranges including smaller particles (1 $\div$ 20 μm, 20 $\div$ 50 μm and 37 $\div$ 63 μm), in order to check as their presence could affect the reflectance spectrum of a mixture. In fact it is well known that the smaller particles affect considerably the resulting spectra of a single mineral (Mustard and Hays, 1996).

In this way I can check the spectral behaviour of a mixture when the two components have similar or different spectra. In addition I can check the influence of different grain sizes of different minerals.

The main characteristics of the samples and minerals I used are listed in Table 3.1, together with a code which will be useful for the identification of minerals and mixtures in the rest of this work.

Table 3.1: Characteristics of the analyzed samples.

Material	Density g/cm^3	Size range μm	D[4,3][a] μm	D[3,2][a] μm	Code
Dolomite	2.84	106 ÷ 200	192	175	D1
		200 ÷ 300	307	290	D2
Olivine	3.32	1 ÷ 20	14	9	O1
		20 ÷ 50	48	39	O2
		106÷ 200	127	37	O3
Quartz	2.62	37 ÷ 63	60	52	Q1
		63 ÷ 125	114	98	Q2
Gypsum	2.3	20 ÷ 50	36	13	G1
		106 ÷ 200	169	53	G2

[a]D[4,3] and D[3,2] are the diameter of equivalent sphere in volume and in surface, respectively, see Section 3.3

3.2 Procedure

As discussed in Chapter 2, it is necessary to measure the reflectance of each component in order to calculate the reflectance of a mixture. Therefore, the experimental work consists of two parts: the first is related to single mineral characterization (grain size and reflectance) and the second is related to the comparison between theoretical reflectance of a mixture and the correspondent measured reflectance. The objective is to use well characterized minerals in order to obtain mixtures of known composition and compare them with the corresponding synthetic mixture.

For the production of all the particulate samples, I broke the bulk minerals with a grinder *Retsch Mortar Grinder RM 100*, an electric mortar which triturates the sample with the pressure of a silicon carbide pestle inside a rotating mortar of the same material. The mineral was ground with the pestle set in position 5 for 8 minutes.

The resulting powder was sieved with a *Retsch Sieve Shaker AS 200*, in order to obtain the following grain size classes:

- <20 μm;
- 20 ÷ 50 μm;

- $50 \div 106$ μm;
- $106 \div 200$ μm,
- $200 \div 300$ μm;
- $300 \div 425$ μm.

Unfortunately the sieving procedure is not well reproducible, since the result depends on the total sieving time. This is due to the fact that, since the particles are three-dimensional and, in general, not spherical, during the sieving process their orientation is crucial for a correct selection and a longer sieving time increases the probability that the particles orientate themselves on the smallest dimension and fall into the following sieve, with the consequence that the grain size of particles into each sieve will be, on average, bigger than the sieve dimension. Therefore in such case the sample obtained will be well separated and with a minor contamination of small particles, with respect to that obtained if the process lasts for a shorter time. In conclusion I have decided to sieve each mineral for about 20 hours reducing, in this way, the probability to have samples dimensionally contaminated.

Since having grains of well defined dimensional classes is of great importance, I checked the particle size with the *Malvern Mastersizer 2000* granulometer (see Section 3.3) and, when necessary, I washed the sample with 99.9 % pure alcohol, in order to better isolate the grain size of interest. In fact it is well known that small grains usually adhere to the surface of bigger grains and, even if their mass is a tiny fraction of the total mass, they affect considerably the resulting spectra (Mustard and Hays, 1996). During the washing procedure I put, in a test tube, a reasonable quantity of material with 99.9 % pure alcohol, and I shake the tube, in this way the motion of the dispersant breaks agglomerations and separates the small particles from the bigger ones. Then the dispersion is poured into the appropriate sieve, so that only the separated small grains pass through the sieve.

After the washing process I have checked again the grain sizes and, if necessary, I have continued the washing process until I obtained a sample of well defined grain size distribution, without contamination of smaller or bigger particles. The last

step is the spectral analysis of the selected samples, performed with *Perkin Helmer Spectrum 2000* (Section 3.4).

3.3 Malvern Mastersizer 2000

Many techniques can be used to obtain the size distribution of a particulate sample, but some of them might not be appropriate or repeatable, such as sieving (see Section 3.2) or microscopy, which, in particular, might not be representative, because only few particles are analyzed. A powerful technique is laser diffraction, based on the principle that every particle scatters incident light with an angle inversely proportional to its dimension. This technique is really important because it is based on a scientific principle, not on the capacity of the observer such as microscopy; the analysis is fast and repeatable.

For my measurements I use the *Malvern Mastersizer 2000*, based on the principle of laser diffraction. This granulometer allows to measure the grain size distribution of each sample. During the measurements, a focused laser beam (helium-neon laser, $\lambda = 0.63$ μm) passes through the examined sample. The particles, dispersed in an appropriate fluid, scatter the light, with an angle inversely proportional to their size. The scattered radiation is collected by fifty circular and concentric photosensitive detector placed on the focal plane, while others detectors are located at different angles for measuring wide angle scattering and backscattering by the smallest particles (Ran, 1998). A second laser beam, working at a shorter wavelength (solid-state light source, $\lambda = 0.45$ μm), is used for a better evaluation of the contribution by small particles; in this way the entire range of sizes between 0.02 and 2000.00 μm is conveniently covered. A scheme of the instrument is shown in Figure 3.1.

The actual size distribution is obtained using the Mie scattering theory (Van de Hulst, 1957; Kerker, 1969; Bohren and Huffman, 1983) and a statistical approach involving 5000 measurements. This theory uses the hypothesis of equivalent sphere to obtain many different geometrical and statistical parameters, in spite of the fact that the particles are not perfectly spherical. Under these conditions the output of the instrument is a volume distribution, equivalent to a weight distribution, if all

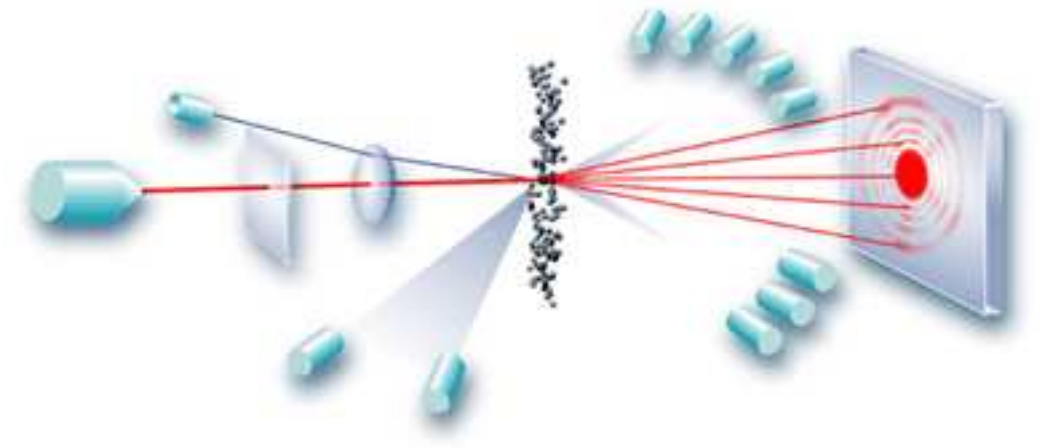

Figure 3.1: Optical scheme of granulometer: on the left side there are the two laser sources, the He-Ne laser on axis and the blue light at the top, the lasers are focused by two lens, then pass through the grains in the dispersant and the scattered light is detected by the cylindrical detectors placed at wide angles and by the circular and concentric photosensitive detectors placed on the focal plane.

the particles of the sample have the same density, which is the usual case. From this distribution it is possible to obtain a surface, length and number distribution, with the relative mean diameters even if these distributions are less accurate.

Among the many useful dimensional parameters that could be obtained starting from these distributions, I am particularly interested in the mean diameter of the equivalent sphere in volume (D[4,3]) (Alderliesten, 1991; Allen, 1999; Gabas et al., 1994), and in the mean diameter of the equivalent sphere in surface area (D[3,2]).

The *De Broucker diameter*, D[4,3], is defined as:

$$\frac{\sum d^4}{\sum d^3} = D[4,3] \tag{3.1}$$

The *Sauter diameter*, D[3,2], is defined as:

$$\frac{\sum d^3}{\sum d^2} = D[3,2] \tag{3.2}$$

3.3.1 Mineral grain size distribution

In Figure 3.2, 3.3, 3.4 and 3.5 the grain size distributions of all the minerals used for mixtures and listed in Table 3.1 are shown.

In particular both the dolomite distributions are narrow and this means that all the grains are quite similar in size (see Figure 3.2); instead both quartz samples (see Figure 3.4), although exhibit a good size distribution, without any tail of smaller or bigger particles, have broader distributions, meaning that the range of particle size is wider.

Olivine (see Figure 3.3) with grain size between $106 \div 200$ μm presents a tail of small particles. For this reason in Table 3.1 the dimensional value corresponding to that sample is lower than expected. Such small particles should be removed because, as I will show in Section 4.4, small particles dominates the reflectance spectrum of mixtures, as well as of single minerals, introducing contaminations which cannot be controlled. Olivine with grain size between 20 and 50 μm has a good grain size distribution, while the smaller olivine sample has a broad distribution which, however, is not a problem, since this sample has been used only for a particular mixture (as I will show in Section 4.2).

Finally both gypsum samples have a broad grain size distribution with a long tail of smaller particles (see Figure 3.5). These samples, as that of olivine $106 \div 200$ μm, are not fit for the study of mixtures and have been discarded, as I will show in Section 4.4. In fact gypsum is a mineral difficult to work with, since it reacts with atmosphere, in particular with water; in addition it is quite soft and easy to be damaged, during the sample preparation.

3.4 Perkin Helmer Spectrum 2000

Perkin Helmer Spectrum 2000 is a Fourier spectrometer and its optical scheme is divided into two levels. In the upper level, shown in Figure 3.6, there is the light source, an air-cooled wire coil operating at 1350 K, and the actual interferometer, a variation of the classical Michelson scheme, while lower level (shown in Figure 3.7) is entirely dedicated to the sample compartments and the detectors.

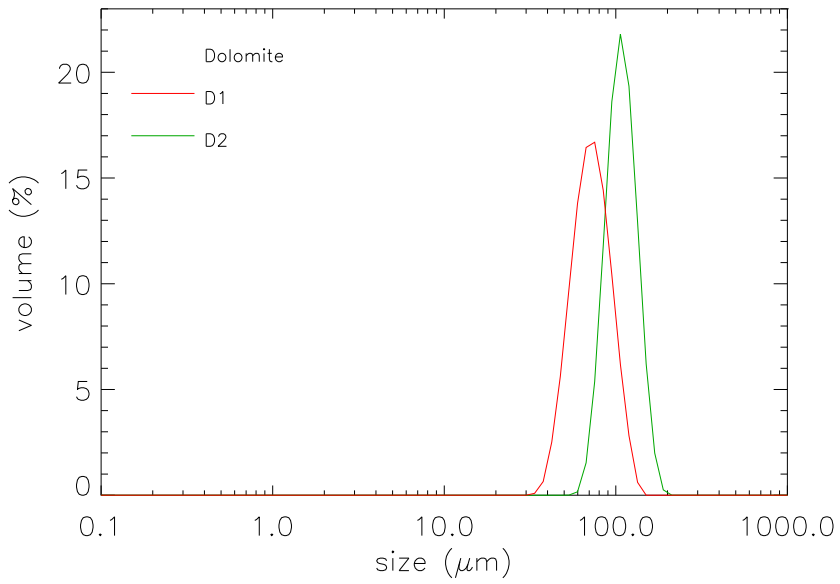

Figure 3.2: Measured grain size distribution of dolomite.

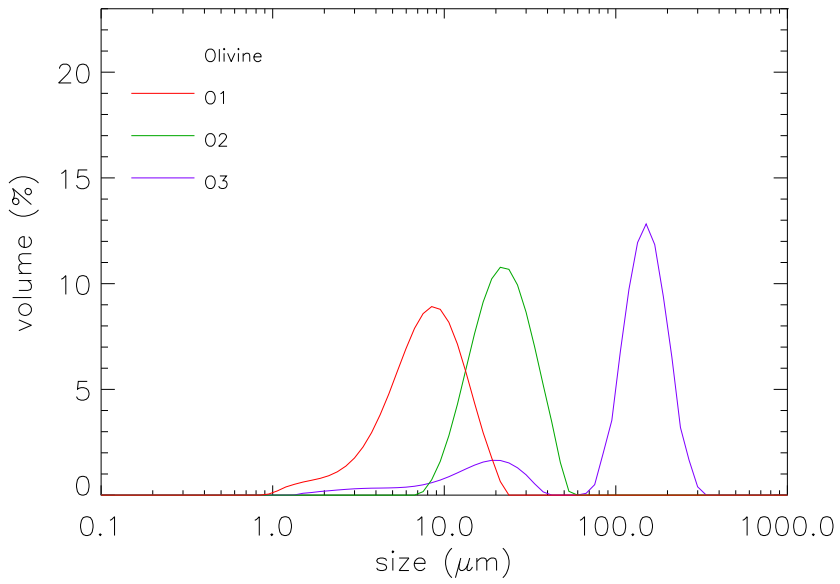

Figure 3.3: Measured grain size distribution of olivine.

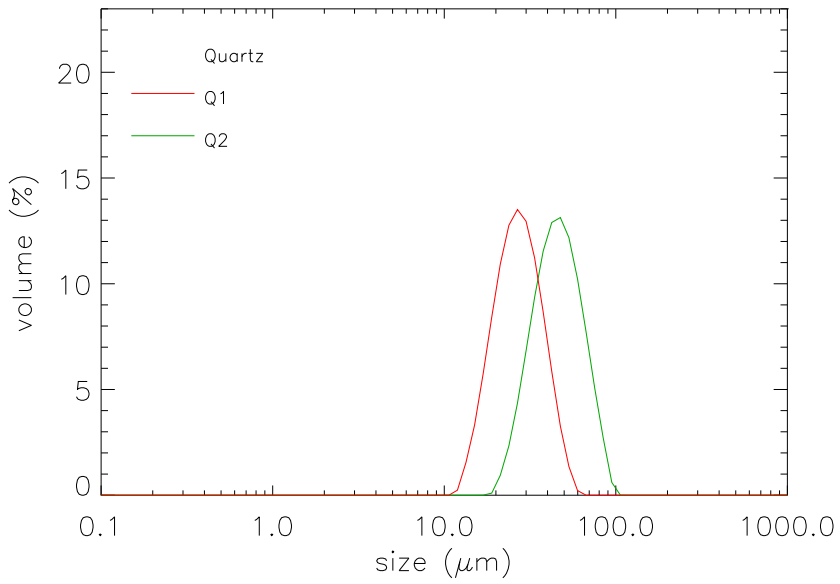

Figure 3.4: Measured grain size distribution of quartz.

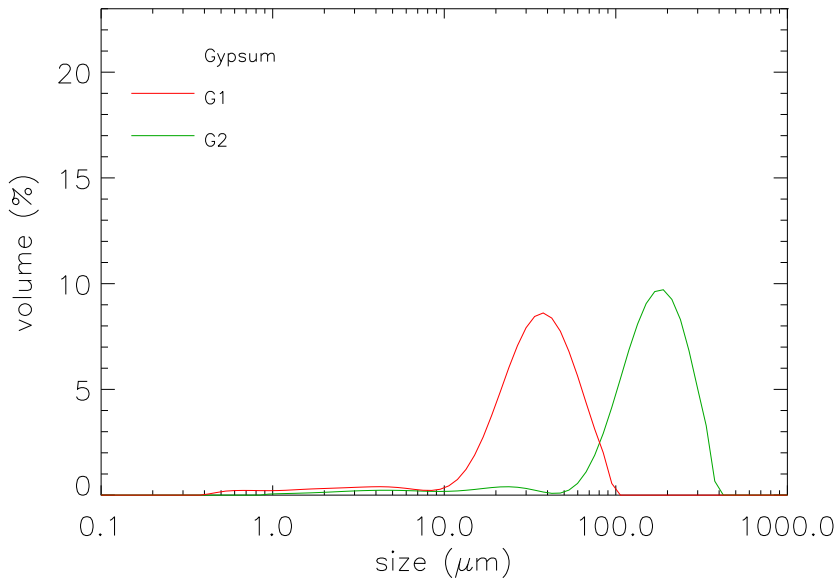

Figure 3.5: Measured grain size distribution of gypsum.

In the upper level, before entering in the interferometer, the light passes through a variable B-STOP aperture, important to calibrate the total energy and avoid saturation; then it passes through a J-STOP, which defines the field of view and the collimation of the beam. At the output of the interferometer the beam passes through a periscope, taking it to the lower level, where the instrument is built so that four different attachments can be mounted on its main body. A mirror system, operating via software, allows to choose the attachments in which the beam is directed. Each attachment can contain a sample compartment and a detector, but, if necessary, some of them can be substituted with special outfittings. The configuration of the instrument include two attachments working in transmission, one optimized for the NIR-MIR ($1.28 \div 27$ μm) spectral range, one optimized for the FIR ($17 \div 100$ μm) (obviously different beamsplitters should be used in the different spectral ranges). The third attachment is outfitted with an integrating sphere for directional hemispherical reflectance measurements and the last attachment has been removed and substituted with an accessory able to concentrate external sources into the instrument for emission spectroscopy.

For this study I have used only two channels: one in transmission and one in reflectance, both of them in the NIR-MIR spectral range.

Transmittance measurements are made using a KBr pellet (Fridmann, 1967), with a resolution of 4 cm^{-1}, a J-stop of 12.5 mm and a B-stop of 21.2 mm.

Directional-hemispherical reflectance of each mineral was measured in the reflectance channel equipped with an integrating sphere *Labsphere RSA-PE-200-ID* (internal coating in Infragold, diameter 70 mm and angle of incidence on the sample of 13°). The reflectance measurements are taken with a resolution of 4 cm^{-1}, the J-stop and the B-stop at their maximum aperture of 12.5 mm and 21.2 mm respectively. The sample is put into a black aluminium cylindrical dish with a diameter of 25.0 mm and a depth of 5.3 mm; the dish is filled with particulate material and the top surface is leveled with a spatula, in order to have a uniform but not packed sample. All the samples are prepared in the same way.

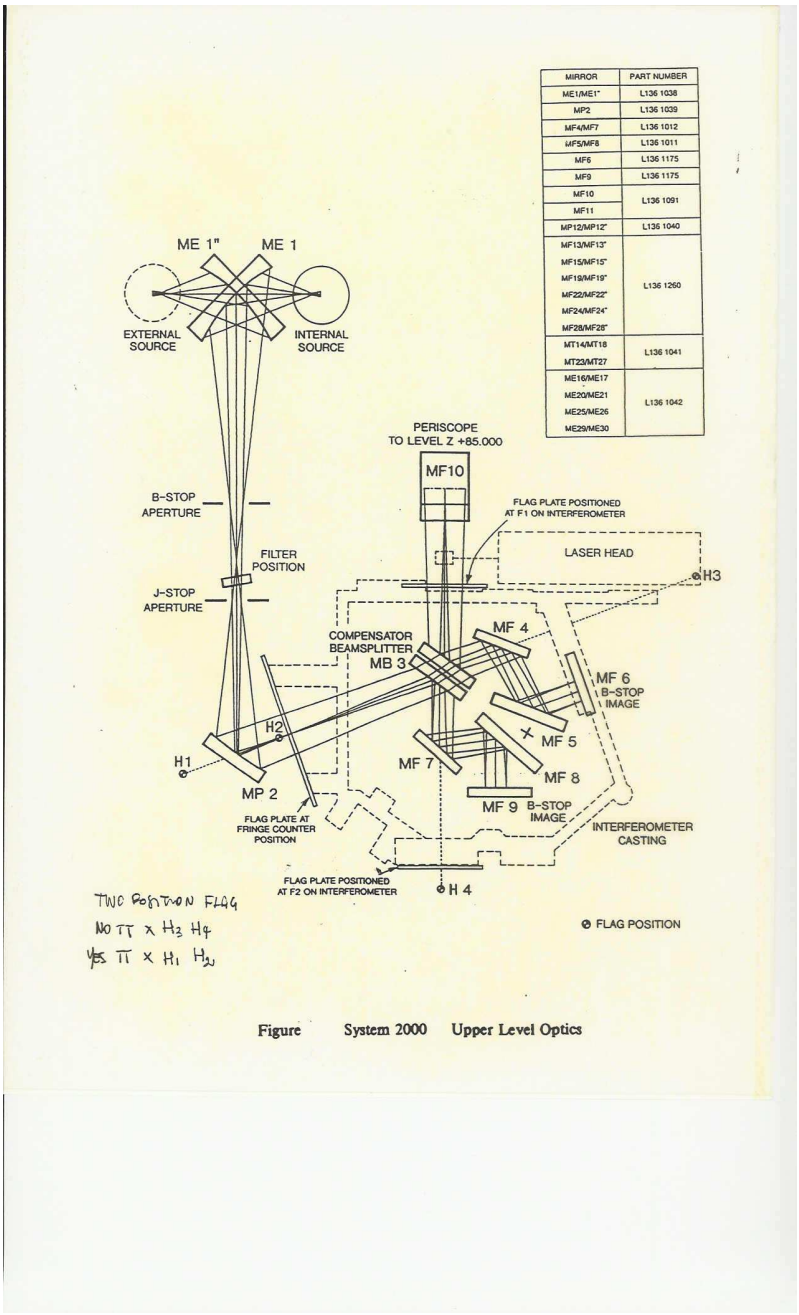

Figure System 2000 Upper Level Optics

Figure 3.6: Optical scheme of upper level of Perkin Helmer Spectrum 2000

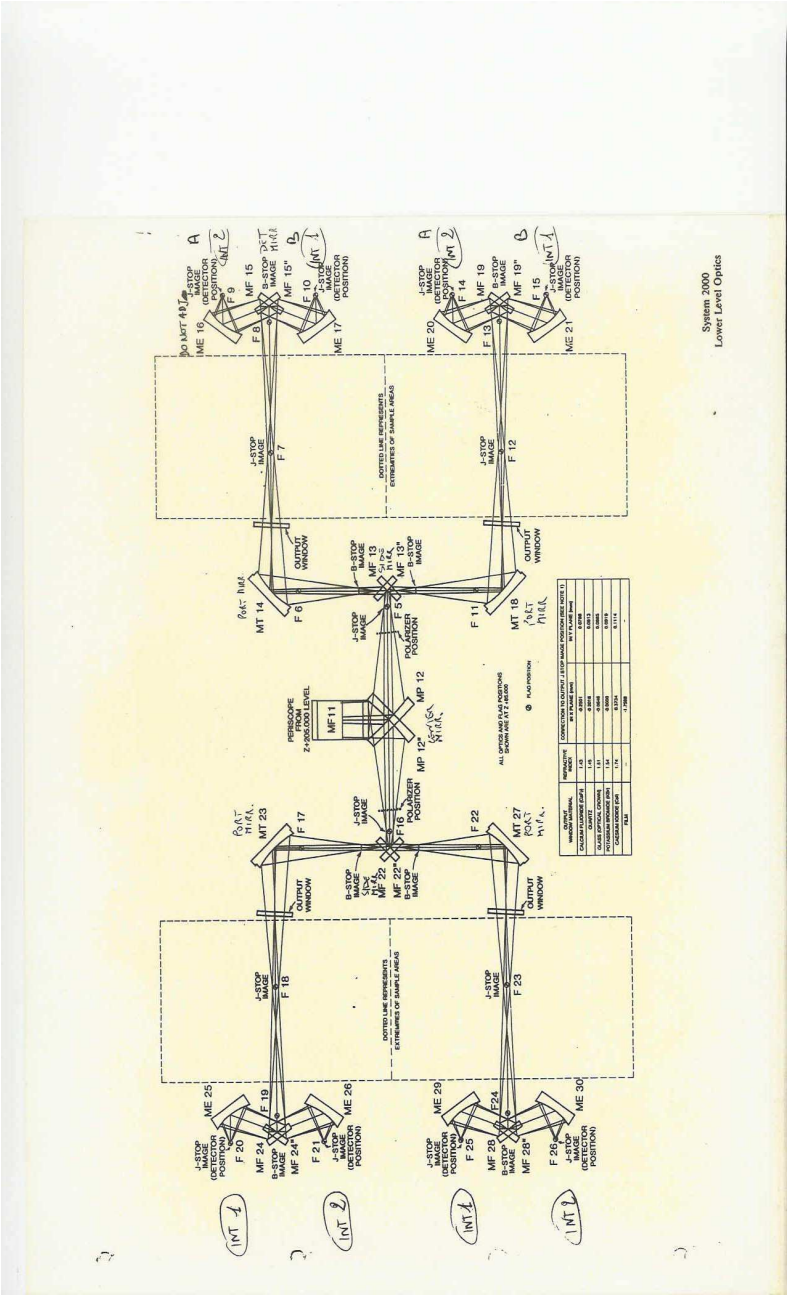

Figure 3.7: Optical scheme of lower level of Perkin Helmer Spectrum 2000

3.4.1 Precision

In this subsection I will describe all the tests made to find the best measuring procedure and to asses the instrumental precision.

The necessity for this kind of tests raised during the characterization of calcite both biotic and not (see Appendix A), because it was necessary to perform spectra with a very low noise. In this section I will report only the measurements more representative of these tests.

The measurements have been performed on the same sample of particulate calcite ($CaCO_3$), with a size range 20 $\div$ 50 μm, using three different spectral resolutions (4, 2 and 1 cm^{-1}).

For each resolution I performed different measurements, varying the number of scans, as follow:

- 20 scans of reference + 20 scans of sample, both of them 5 times, in order to obtain a total of 100 scans;
- 50 scans of reference + 50 scans of sample, both of them 2 times, in order to obtain a total of 100 scans;
- 100 scans of reference + 100 scans of sample;
- 200 scans of reference + 200 scans of sample, only for the measurement with 4 cm^{-1} of resolution.

The reference measurement is necessary because the spectrometer works in atmosphere and the sample measurement need to be normalized taking into account the effect of the atmosphere.

For every number of scans I have made different types of normalization, in particular I have made different means between the measurements made on the sample and on the reference, in order to see which is the best way for reducing instrumental errors, but all the spectra, obtained with different means on the same number of scans, are the same.

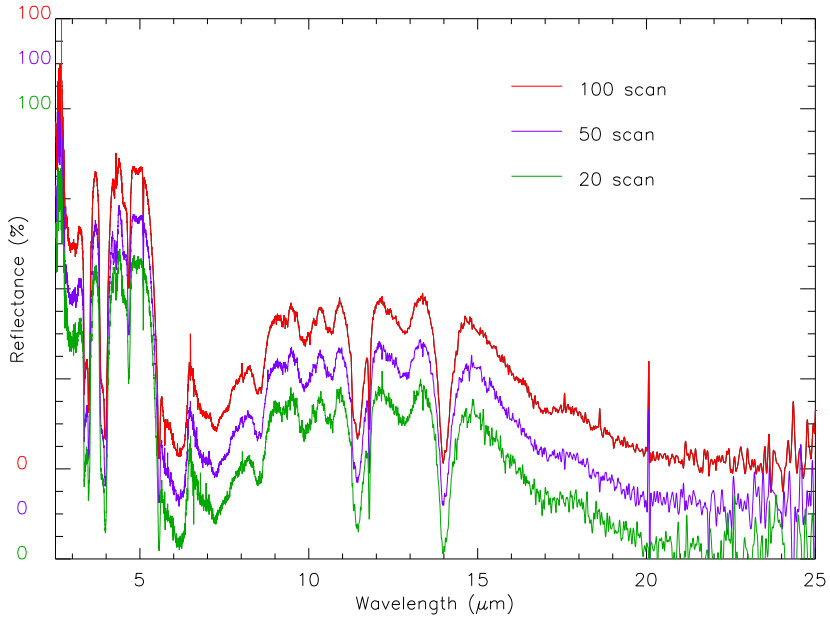

Figure 3.8: Comparison between the spectra obtained with a different numbers of scans for resolution of 1 cm^{-}1.

In Figure 3.8, 3.9 and 3.10 I show, for each resolution, the spectra measured with a different number of scans, shifted in steps of 10% each; in particular in Figure 3.8 I show the spectra measured at 1 cm^{-1} of resolution performed with 100, 50 and 20 scans; in Figure 3.9 I show the spectra measured at 2 cm^{-1} of resolution performed with 100, 50 and 20 scans and in Figure 3.10 I show the spectra measured at 4 cm^{-1} of resolution performed with 200, 100, 50 and 20 scans. As it can be seen for each resolution the spectrum with less scans is noisier. By comparing all the spectra it can be seen that the best spectrum is that performed with 4 cm^{-1} and 100 scans, since performing a spectrum with 200 scan does not improve appreciably the quality.

On the other hand, the use of higher resolution does not allow the detection of any other spectral features of the particulate sample. Finally it is worth noting that some instrumental disturbance is present in some spectra at about 20 μm.

I performed also other tests aimed to check the repeatability of the results and

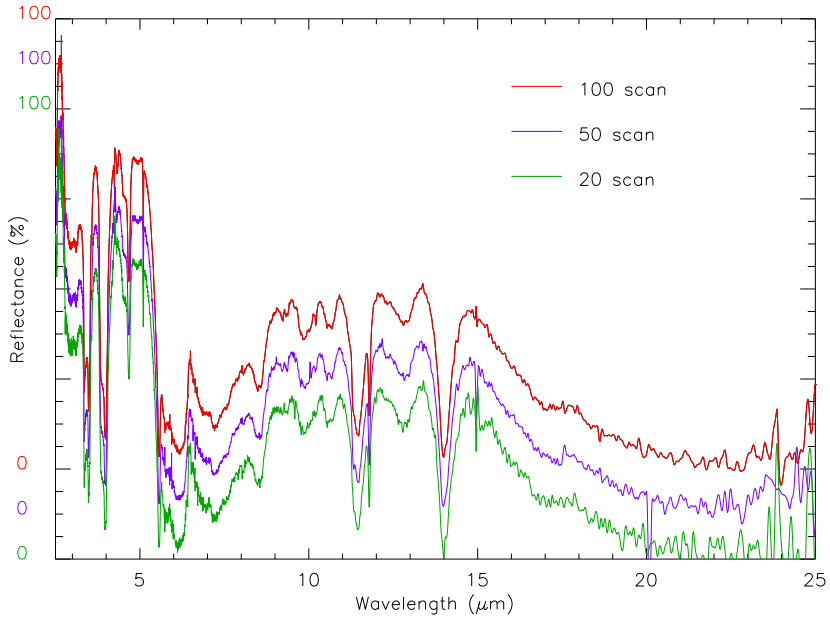

Figure 3.9: Comparison between the spectra obtained with a different numbers of scans for resolution of 2 cm^{-}1.

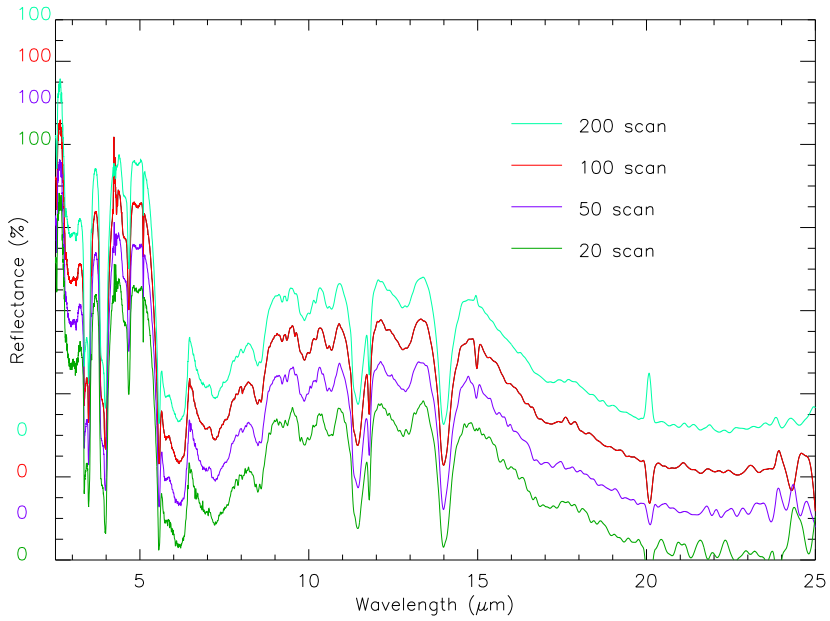

Figure 3.10: Comparison between the spectra obtained with a different numbers of scans for resolution of 4 cm^{-}1.

hence to evaluate the associated errors (the intrinsic precision of the instrument is about 1‰). In particular I performed a series of six different measurements of 100 scans each, according to the following scheme:

1. sample in the dish;
2. same sample in the dish rotated of 90 degrees;
3. same sample in the dish rotated of 180 degrees;
4. same sample in the dish rotated randomly;
5. same sample in the dish, randomly rearranged;
6. new sample of the same grain size, taken from the same bulk mineral.

All these measurements were performed on calcite samples with four different grain sizes, but I show only the spectra of calcite with grain size of 20 ÷ 50 μm, since all the samples show very similar results.

In Figure 3.11 I show the standard deviation calculated by means of the following relation:

$$\sigma = \sqrt{\frac{\Sigma_{i=1}^{N}(x_i - \overline{x})^2}{N-1}} \tag{3.3}$$

where $\overline{x}$ is the mean of x_i measurements, made following the scheme reported above (this equation is valid if $N < 20$, with N number of measurements).

As it can be seen the standard deviation is well below 1% in most of the spectral range (they are a little noisier above 21 μm) except for two spikes at about 4 and 15 μm, due to a not perfect compensation of the atmospheric CO_2, and a strong spike at 20 μm linked to the random instrumental effect mentioned above. In conclusion I can consider a spectrum performed with only one measurement of 100 scans with a standard deviation of about 1%.

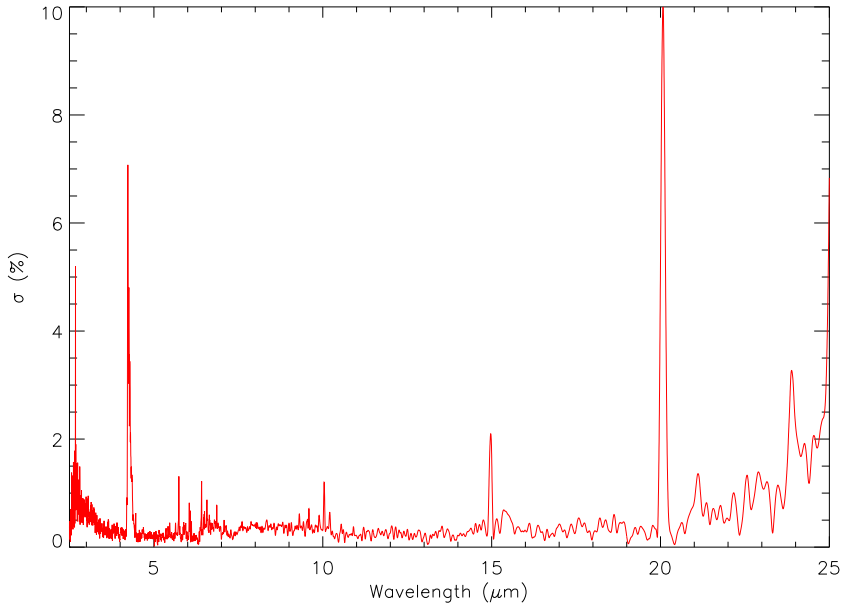

Figure 3.11: Standard deviation of calcite sample

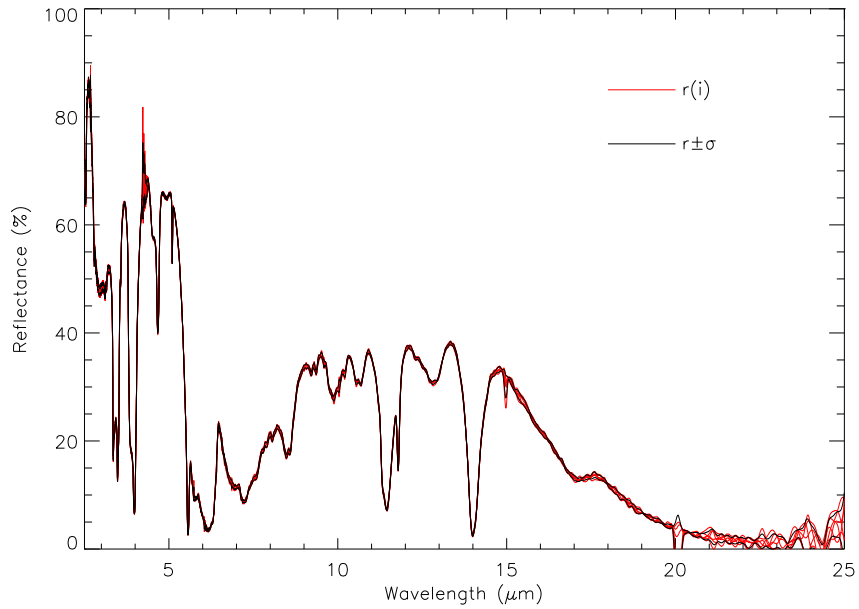

Figure 3.12: Reflectance spectra of the six calcite samples together with $r_m \pm \sigma$.

In Figure 3.12 I show the reflectance of the six measurements of the same calcite sample listed above, together with the spectra of $r_m \pm \sigma$. As it can be seen all the spectra are between the values of $r_m \pm \sigma$.

Once that the standard deviation of a standard measurement has been determined, it is possible to use it for assuming the validity of the results obtained in this PhD thesis. In particular I can evaluate the chi-square (χ^2) of all the comparisons between measured and calculated spectra, where the calculated reflectance is given by Equation 2.39 and 2.42, with the following relation (Taylor, 1982):

$$\chi^2 = \frac{\sum \frac{(r_m - r_c)^2}{\sigma^2}}{N} \tag{3.4}$$

where N is the number of points in each spectrum, r_m and r_c are respectively the measured and calculated values of hemispherical reflectance for each mixture and σ is the standard deviation calculated above.

This formula takes into account only the standard deviation made on a mineral sample, which could be lower than the standard deviation of a mineral mixture, as it will be explained in Subsection 6.3.1. In addition, further variability could be linked to the fact that the whole measurements are taken in a long lapse of time, so the environmental conditions are definitely not always the same. Finally, I consider only the standard deviation relative to the measured spectrum, ignoring, as usual, the experimental uncertainties associated with the theoretical spectrum, which, however, is derived by means of measurements on single minerals, as it can be seen in Equation 2.42 and 2.39. All these causes could affect the chi-square values and must be taken into account during the discussion of all the spectra.

3.4.2 Mineral spectra

Directional-hemispherical reflectance spectra are shown in Figure 3.13 for dolomite, in Figure 3.14 for olivine, in Figure 3.15 for quartz and in Figure 3.16 for gypsum. For each minerals the spectra corresponding to the grain sizes reported in Table 3.1 are shown.

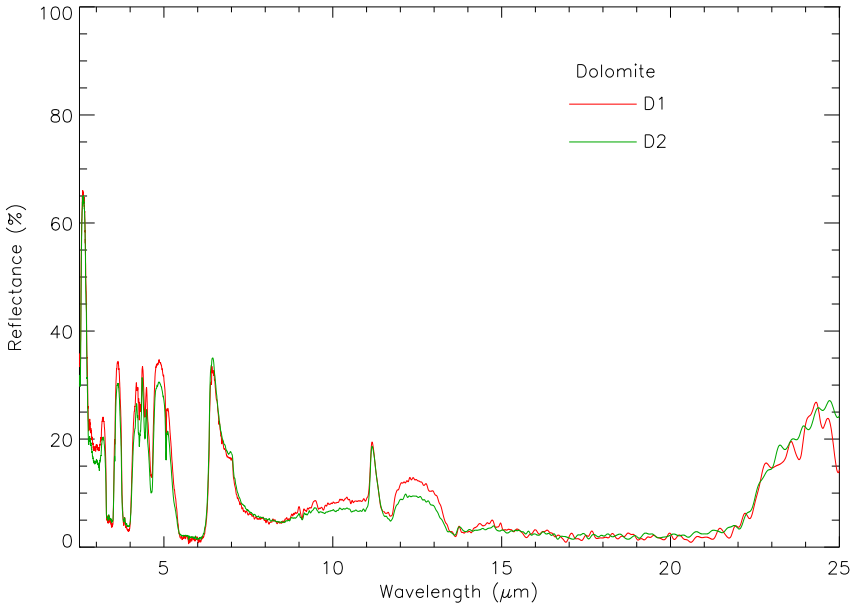

Figure 3.13: Measured reflectance spectra of dolomite.

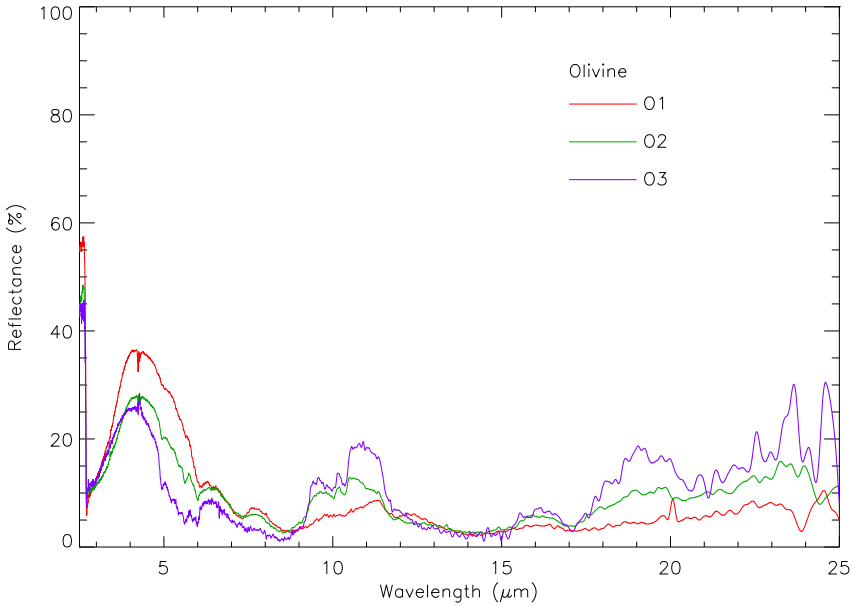

Figure 3.14: Measured reflectance spectra of olivine.

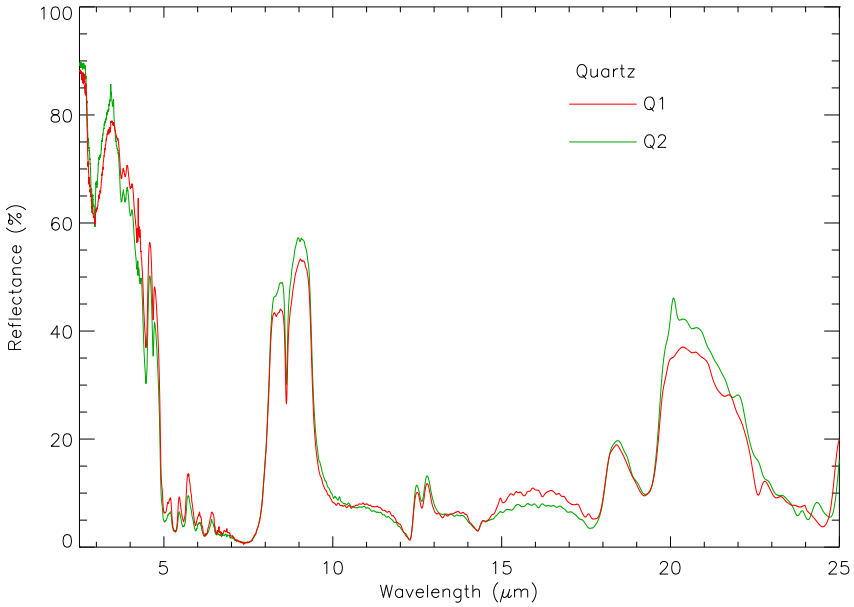

Figure 3.15: Measured reflectance spectra of quartz.

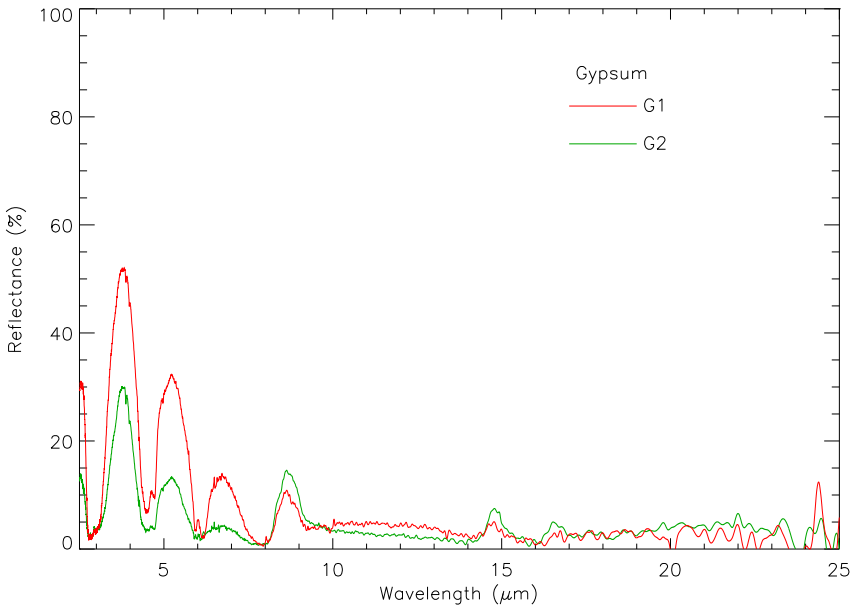

Figure 3.16: Measured reflectance spectra of gypsum.

The near and medium infrared spectral range ($2.5 \div 25$ μm) is really important for geochemical analysis because, as I have already explained in Section 1.3, it is the region where the most fundamental vibrational bands, characteristic of minerals and rocks, are present (Estep-Barnes, 1977). I have explained that the bands, which occur in reflectance spectra, depend on both by the real and the imaginary part of the refractive index, and change significantly with particle size (Salisbury, 1993; Salisbury and Wald, 1991), making the interpretation of reflectance spectra quite difficult.

The strongest fundamental vibrational bands, also called restrahlen bands, occur when the imaginary part of the refractive index, k, is greater than 0.1 (Salisbury, 1993; Mustard and Hays, 1996; Salisbury et al., 1992). These bands depend also on the grain size, because the band intensity decreases at the decreasing of particle size, as it can be seen in all the spectra shown in this section. This observed reduction in spectral contrast can be explained with the large number of small particles per unit volume, producing a lot of scattering between such particles and, therefore, causing a loss of energy and a reduction of the spectral contrast.

For dolomite the principal restrahlen band is between 6 and 8 μm and the second is at about 11 μm (see Figure 3.13): both are due to fundamental internal molecular vibration of CO_3 ions. In particular the first is due to C-O stretching vibration and the second to the bending mode (Farmer, 1974; Salisbury et al., 1992).

For olivine the principal restrahlen band is between 9 and 12 μm and it is due to the asymmetric stretching vibration Si-O-Si (Farmer, 1974; Salisbury et al., 1992), while the second begins at 17 μm and is principally due to the O-Si-O deformation or bending modes (Farmer, 1974; Salisbury et al., 1992) (see Figure 3.14).

For quartz the principal restrahlen band is between 8 and 10 μm and it is due to the stretching of Si-O-Si (Farmer, 1974; Salisbury et al., 1992), while the second is between 12 and 13 μm and the third starts at about 18 μm, both principally due to symmetric Si-O-Si stretching vibrations (Farmer, 1974; Salisbury et al., 1992)(see Figure 3.15).

For gypsum the principal restrahlen band is between 8 and 9 μm and the second is between 14 and 15 μm (see Figure 3.16), the first is due to asymmetric stretching

of S-O (Farmer, 1974; Salisbury et al., 1992) and the second is due to S-O bending modes (Farmer, 1974; Salisbury et al., 1992).

The Christiansen frequency occurs when the real part of refractive index is close to one (Salisbury, 1993) and the imaginary part is still small. Therefore there is very little backscattering and absorption, resulting in a minimum or reflectance spectra. These frequencies are associated to restrahlen bands because they occur just before such bands. In fact the principal Christiansen frequency is at 6 μm for dolomite, at about 9 μm for olivine, at about 7.5 μm for quartz and at about 8 μm for gypsum.

Absorption bands are principally due to volume scattering and generally increase for decreasing particle size. These bands are formed because in this spectral range the absorption coefficient is low, so radiation passes through grains before being scattered back to the detector, resulting in a minimum in reflectance spectra (Salisbury, 1993). The region of the absorption bands is between 2.5 and the principal Christiansen frequency, for all the minerals studied here.

Transparency features are associated with a change from surface to volume scattering. In this region the absorption coefficient is low and the grains are optically thin, so volume scattering occurs. In addition, transparency features are reduced if particle size increases. The dolomite has a transparency feature between 12 and 13 μm (see Figure 3.13), olivine between 15 and 17 μm (see Figure 3.14), quartz between 14 and 18 μm (see Figure 3.15), gypsum between 9 and 14 μm (see Figure 3.16).

3.5 Mixtures

The spectral behaviour of a lot of minerals is well known, and it has been discussed in the previous section for the minerals I have used. Now, the main problem is to understand how the physical processes, which cause different features, interact when different minerals are mixed together.

As already said in Section 1.5, to understand better the behaviour of minerals mixed together, I need to consider two different kinds of mixtures: the *areal mixtures*, where the surface is formed by several patches, each of a single and pure

material, and the resulting reflectance is a linear combination of the reflectance of each patch; the *intimate mixtures*, where different types of particles are mixed homogeneously together in the whole volume and the evaluation of the resulting reflectance is given by the relations derived in Chapter 2, in particular by the Equations 2.42 and 2.39 (Hapke, 1993; Singer and McCord, 1979; Mustard and Pieters, 1989).

For the preparation of the mixtures, I measure the mass of each component, using a precision analytical scale Sartorius Genius ME, with a typical accuracy better then 50 μg. The main characteristics of the mixtures used are listed in Table 3.2.

They can be divided in granulometric mixtures and compositional mixtures. The granulometric mixtures are used to verify all the hypotheses made in Chapter 2, in particular the hypothesis of isotropic scattering, of identical and spherical particles and the extinction efficiencies equal to unity. Such hypotheses will be demonstrated in Chapter 4. The compositional mixtures can be grouped into two different types according to their grain size distribution: the first group is formed by samples with a *good* grain size distribution (specifically O2D1, O2D2, Q2D1, Q2D2 and Q2O2) and the second group by samples with a *bad* grain size distribution (all mixtures with gypsum or O3)[a]. As it will be seen in Chapter 4, 5 and 6, the two groups of compositional mixtures are used at different times and for different scopes.

Even if the particle size actually involved in our laboratory work ranges between 20 and 300 μm, it is more correct to refer to the effective size D_i of each sample in order to check the validity of the large particles hypothesis (diffraction condition). As it can be seen in Table 3.1, the smallest of such values is 48 μm for olivine and 36 μm for gypsum and therefore the size parameter $X = \pi D_i/\lambda$ is respectively about 6 and 4.6 in the worst case ($\lambda = 25$ μm). So, we can conclude that the diffraction condition is basically satisfied for all the samples we used, in the whole spectral range (McGuire and Hapke, 1995). However such subject will be discussed in more detail in the following chapter, because it is a central point of this work.

[a]The meaning of *good* and *bad* is related to the results obtained for each component in the size distribution analysis, shown in Figures 3.2-3.5 and discussed in Section 3.3.1.

Table 3.2: Granulometric and compositional mixtures analyzed in this work.

Granulometric mixtures		
Sample	**Components**	**Volume percentage**[a]
O1O2	O1	33% (1.56 g)
	O2	67% (3.16 g)
D1D2	D1	50% (1.99 g)
	D2	50% (1.99 g)
Q1Q2	Q1	50% (0.70 g)
	Q2	50% (0.70 g)
Compositional mixtures		
Sample	**Components**	**Volume percentage**[a]
O2D1	O2	50% (1.99 g)
	D1	50% (1.70 g)
O2D2	O2	75% (2.99 g)
	D2	25% (0.85 g)
Q2D1	Q2	50% (1.84 g)
	D1	50% (1.99 g)
Q2D2	Q2	75% (2.75 g)
	D2	25% (1.00 g)
Q2O2	Q2	50% (1.84 g)
	O2	50% (2.32 g)
G1O3	G1	59% (2.00 g)
	O3	41% (2.00 g)
G1O3	G1	27% (1.00 g)
	O3	73% (4.01 g)
G2O3	G2	59% (2.93 g)
	O3	41% (2.95 g)
G2O3	G2	22% (0.98 g)
	O3	78% (4.89 g)
D1O3	D1	54% (2.80 g)
	O3	46% (2.80 g)
D1G2	D1	45% (2.80 g)
	G2	55% (2.81 g)

[a]The relative amount of each component, in weight, is reported in brackets.

Chapter 4

Verification of the main hypotheses

In this chapter I will explain and verify all the hypotheses made during the theoretical discussion. They are: (*i*) extinction efficiency equal to unity; (*ii*) isotropic scattering; (*iii*) identical spherical particles. However, before starting, it is important to make some preliminary discussion about the size parameter, Section 4.1, which influences deeply the radiation matter interaction, and I will show that the theoretical approach, made considering the geometrical optical region, is valid for my aims. In Section 4.2 I will discuss and verify the three hypotheses using granulometric mixtures. In addition, in Section 4.3, I will show that the extinction efficiency is equal to unity also for compositional mixtures, with the consequence that the diffraction condition is valid for all my samples. In Section 4.4 I will show the importance of a good size distribution and its implications on the compositional mixtures. Finally, in Section 4.5, I will summarize all the results shown in this chapter.

4.1 Size parameter

Before starting with the discussion of the hypotheses made in this work, it is important to make a preliminary consideration about the size parameter, defined in

Section 2.1:

$$X = \frac{2\pi a}{\lambda} = \frac{\pi D}{\lambda} \tag{4.1}$$

where $D = 2a$ is the diameter of a particle and λ the wavelength of the incident radiation.

I have just said that this parameter is very important for the radiation matter interaction; in fact, the Hapke Theory of Reflectance is valid only for particles bigger than wavelength, or, equivalently, $X \gg 1$. On the other hand, the samples used in this work have a grain size both large and small, in order to study their behaviour and the influence of small particles in mixtures, as already said in Section 3.5. In conclusion, it seems clear how a thorough discussion about such parameter is fundamental at the beginning of this work.

In Table 4.1, I report the value of X for each mineral used, calculated using the D[4,3] defined in the previous chapter.

Table 4.1: Size parameter of each mineral used, calculated using the D[4,3] reported in Table 3.1 .

	D1	D2	O1	O2	O3	Q1	Q2	G1	G2
$\lambda = 2.5$ μm	241	386	18	60	160	75	143	45	212
$\lambda = 25$ μm	24.1	38.6	1.8	6.0	16.0	7.5	14.3	4.5	21.2

As it can be seen looking this table, the values of X tend to oscillate from a small value, in the worst case of the smallest olivine, to a large value, for the biggest dolomite.

Looking at such values, it seems that my study involves both the resonance region, which occurs when $X \cong 1$, and the geometrical optics region, which occurs when $X \gg 1$. However, it is not so, because I will show that all my samples can be considered bigger than the wavelength. In fact, the hypothesis of $X \gg 1$ implies that a portion of incident radiation could be scattered (Q_S) and, within such portion, a smaller portion could be diffracted (Q_d), but, if the particles of a medium are very close together, as in laboratory samples, the diffraction is effectively equal to zero.

However, in laboratory samples, the portion of light diffracted can be considered as well as that not diffracted, because it is impossible to distinguish the origin of

the radiation incident on a particle. So, the spectrometer measures, by means of an integrating sphere, the radiation scattered towards the detector, and the role of diffraction is included into the measured reflectance. If its contribution is relevant, a comparison with theoretical spectrum will reveal a disagreement due to the absence of such contribution in the calculated spectrum. As I will show in this chapter, the experiments verify also such hypothesis.

The smallest value of X occurs only for the smallest olivine, which will be used only for granulometric mixtures. However, this kind of mixtures is used only for demonstrating the hypotheses made during the theoretical discussion. As it will be shown in the following section, the fact that all the hypotheses will be demonstrated independently to the particle size, is a proof that the diffraction condition is valid for all the laboratory samples, independently of their size.

Such conclusion will be discussed also at the end of this work, with an accurate set of experiments, which demonstrate the occurrence of such condition.

4.2 The validity tests using granulometric mixtures

The hypotheses, made during the theoretical approach and which will be fully discussed and verified in this chapter, are:

1. extinction efficiency equal to unity;
2. isotropic scattering;
3. identical spherical particles

In order to verify such hypotheses, the use of granulometric mixtures is very useful. In fact, these mixtures are made up of only one kind of mineral with two different grain sizes. Looking at the mixtures behaviour, described principally by Equation 2.41, it seems clear how using only one mineral is important to avoid many parameters. In fact, the Hapke theory states that, if particles are not identical, the resulting reflectance is given by Equations 2.40 and 2.39, where the sum, in the

albedo equation, is extended to all the particles of a sample. At the same time, if particles are of different minerals, the equation is extended to all the particles independently to their type. However, considering mixtures of the same material, is easier for the verification of the hypotheses made, because important parameters, such as the optical properties, are basically the same.

The first hypothesis is about the *extinction efficiency*. Such value is equal to unity because the diffraction condition is valid for particles close together, as for laboratory mixtures. However, I want to check directly such hypothesis with a preliminary work, shown in Section 4.3, made both on granulometric and compositional mixtures. In fact this hypothesis is easy to check for granulometric mixtures because the extinction efficiency is related to the optical constants of a material, and as it is well known, their behaviour does not change with the particle size, as it can be seen in Figure 4.1 where I show the extinction efficiency measured for both the dolomite samples. Such values have been calculated, starting from a transmittance measurement, using the following relation:

$$\frac{Q_E}{a} = \frac{4}{3}\frac{\rho S}{M}\ln\frac{1}{T(\lambda)} \tag{4.2}$$

valid for grains of radius a embedded in a pellet of section $S \cong \pi r^2$, where r is the pellet radius, M the mass of grains and ρ the density of the mineral, while $T(\lambda)$ is the measured transmittance (Fridmann, 1967).

Both these samples show that the optical behaviour is the same and it is independent to the grain size, but the intensity changes with the size, in particular the Q_E of the biggest dolomite is about twice that of the smallest one. In Figure 4.2, I show an example of theoretical spectrum calculated both with the measured Q_E and with the hypothesis of $Q_E = 1$.

Even if the use of two different techniques at the same time is debatable, this figure is useful to understand that the use of the hypothesis $Q_E = 1$ could be not restrictive. However, in the following section, I will make other considerations about the extinction efficiency, in case of compositional mixtures.

The assumptions of *Isotropic scattering and identical spherical particles* can be considered together, because the hypothesis of identical spherical particles is related

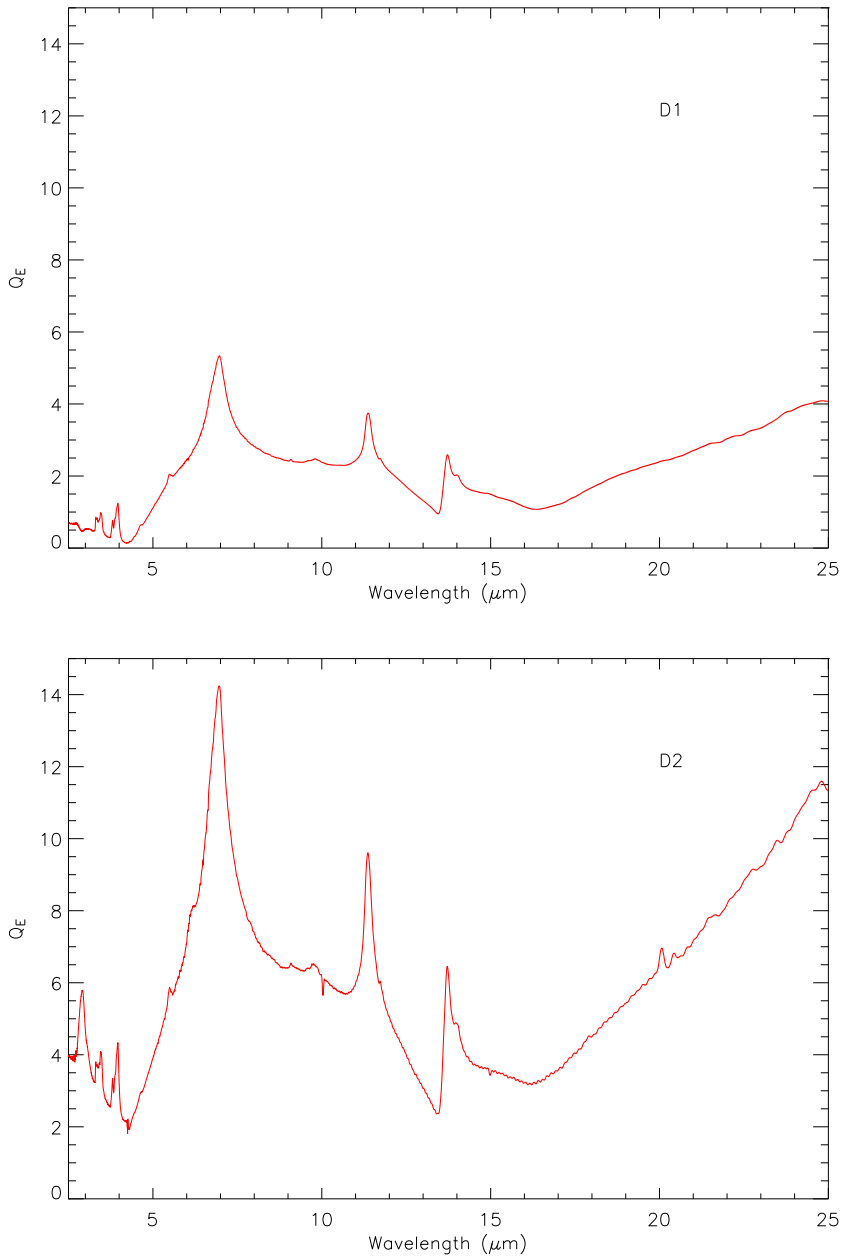

Figure 4.1: Q_E measured in transmittance configuration and calculated by means of Equation 4.2, for D1 and D2 samples.

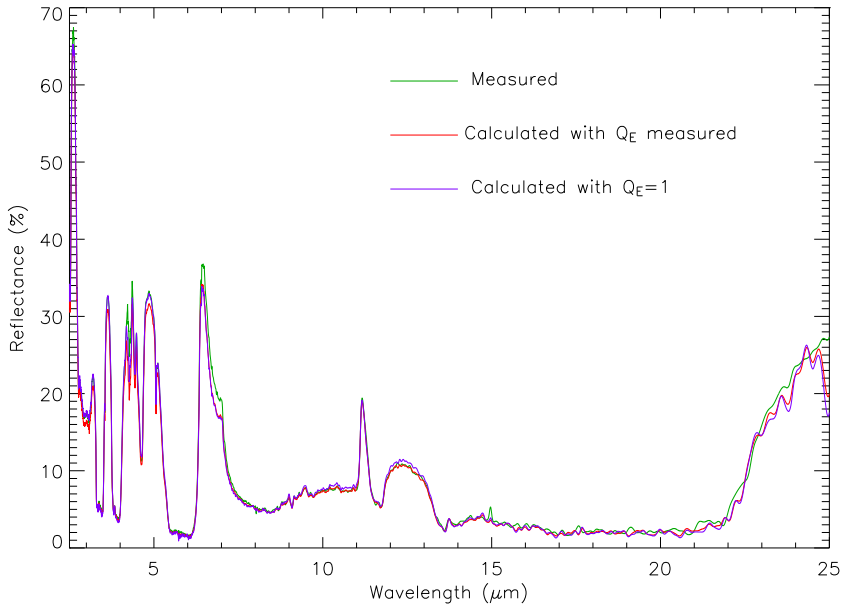

Figure 4.2: Comparison between measured and theoretical spectra for D1D2. The theoretical spectra are calculated with the Q_E measured using equation 4.2 and with the hypothesis of $Q_E = 1$.

to the isotropic scattering. In Figure 4.3 I show the other two granulometric mixtures used, the O1O2 and the Q1Q2. The theoretical spectra have been calculated applying the diffraction condition, since I have shown its validity.

As it can be seen, the agreement is quite good for both the spectra, independently from their component size.

The good agreement is due to the fact that the two hypotheses made are valid for this kind of mixtures.

The isotropic scattering means that the radiation incident on the sample is scattered in all the directions with the same intensity. Considering that the components of each mixture are of the same mineral, in this case the only thing which influences the mixture is the geometry of the interaction between the radiation and the sample, because the optical properties are similar for each component and, as I have already shown, they do not influence the spectrum. In fact, the spectra, shown in Figure 4.2, demonstrate that when I consider or do not consider the optical properties, I ob-

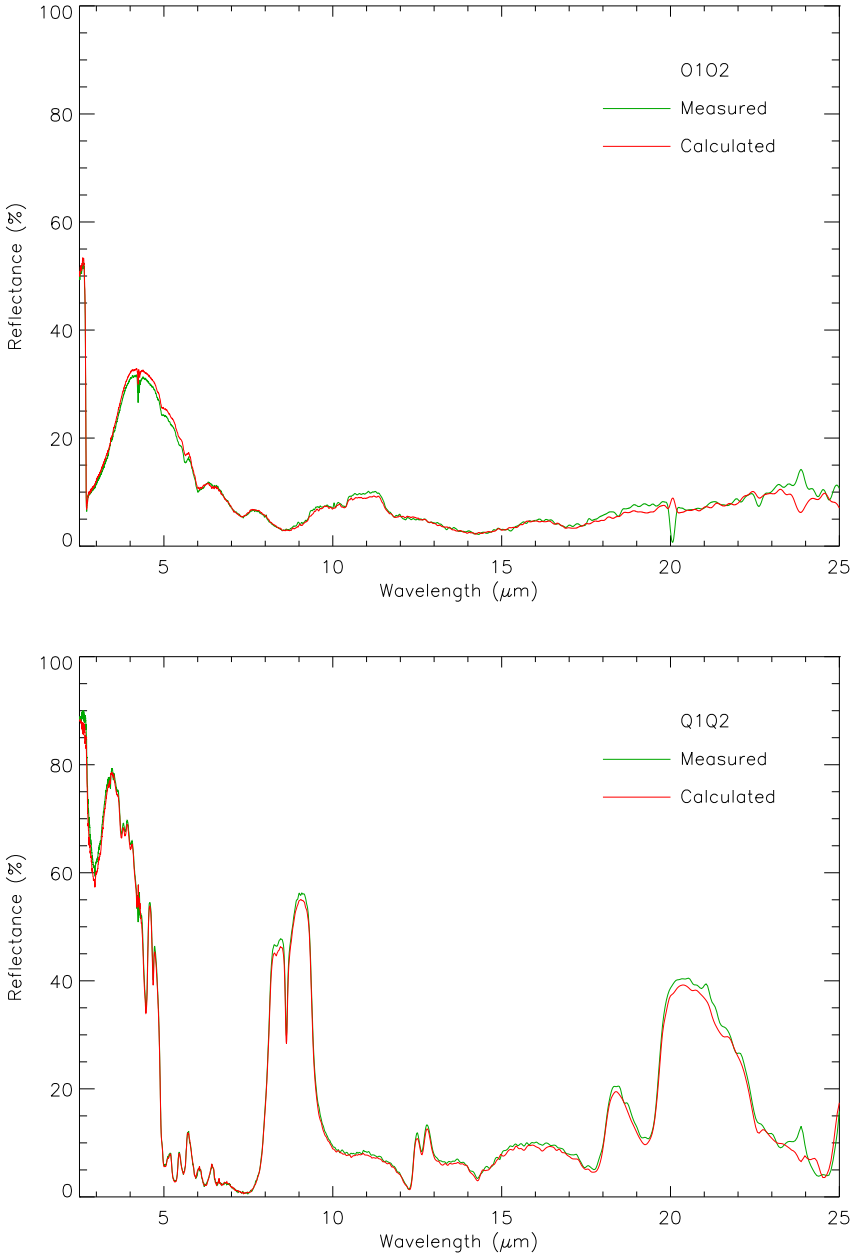

Figure 4.3: Comparison between measured and theoretical spectra for O1O2 (top panel) and for Q1Q2 (bottom panel). Both the theoretical spectra have been calculated applying the hypothesis of $Q_E = 1$.

tain the same results. In addition, it is important to stress that the validity of the isotropy hypothesis can be evaluated only with this kind of mixtures and there is no reason for not extending such result to compositional mixtures.

All these spectra show not only that the scattering is isotropic, but also that the spherical hypothesis is not restrictive. In fact, the irregularity in the shape of the particles does not influence the measured spectra. It is plausible that the shape irregularity is conveniently averaged due to the high volumetric density of the grains.

About the hypothesis of identical particles, a discussion is necessary. In particular, even if such hypothesis is fully demonstrated for granulometric mixtures, because the agreement is quite good, it could not be so for compositional mixtures.

In fact, the impact on the mixture spectrum of the different size of the two components is less important for the granulometric mixture due to the fact that the optical properties are basically the same. On the other hand, in compositional mixtures, the grain size, influencing the band depth, can produce major effects on the mixture spectrum, when affecting features in different spectral position.

As a conclusion, I have verified all my hypotheses for granulometric mixtures and it is reasonable to consider them valid also for compositional mixtures. However, in the following section, I will discuss such hypotheses also for compositional mixtures, showing that they can be considered valid in the whole spectral range.

4.3 About the extinction efficiency

As already discussed in Section 4.1, the diffraction condition implies also some restrictions about the extinction efficiency, which must be equal to unity. In this section I will show an additional test made on compositional mixtures about this subject.

As in the previous section, I base my considerations on the mathematical approach shown in Chapter 2. In Figure 4.4 I show the comparison between the theoretical and the measured reflectance spectrum for two mixtures involving gypsum and olivine (top panel) and quartz and olivine (bottom panel). For both of them the theoretical spectrum has been calculated using Equation 2.42, with $Q_{E_i} = 1$. As

it can be seen, in both spectra the agreement is not good.

At first, I thought that the reason of such discrepancies could be the assumption $Q_E = 1$. In the restrahlen bands, where the discrepancies are bigger, the absorption coefficient is larger than the scattering coefficient ($Q_A \gg Q_S$), and the assumption of $Q_E = Q_A + Q_S = 1$ could not be valid anymore. Therefore, I thought that it could be necessary considering separately Q_S and Q_E, instead of their ratio w.

Unfortunately, the only method to evaluate the extinction efficiencies is to use transmittance measurements, and as I have just said in Section 4.2, this is a rather controversial issue.

To avoid the use of two different techniques at the same time (transmittance and reflectance), I thought to use reflectance measurements of albedo to calculate the scattering and extinction efficiencies. However, in this case, the number of variables is always larger than the number of equations (Montanaro et al, 2007), and this is true even using three binary mixtures, for which a system of six equations with six variables, like the following system (where the index 1, 2 and 3 are referred to each mineral component), has ∞^3 solutions and therefore cannot be of any help:

$$\begin{cases} w_1 = \frac{Q_{S_1}}{Q_{E_1}} \\ w_2 = \frac{Q_{S_2}}{Q_{E_2}} \\ w_3 = \frac{Q_{S_3}}{Q_{E_3}} \\ w_{1+2} = \frac{\frac{M_1}{\rho_1 D_1} Q_{E_1} w_1 + \frac{M_2}{\rho_2 D_2} Q_{E_2} w_2}{\frac{M_1}{\rho_1 D_1} Q_{E_1} + \frac{M_2}{\rho_2 D_2} Q_{E_2}} \\ w_{1+3} = \frac{\frac{M_1}{\rho_1 D_1} Q_{E_1} w_1 + \frac{M_3}{\rho_3 D_3} Q_{E_3} w_3}{\frac{M_1}{\rho_1 D_1} Q_{E_1} + \frac{M_3}{\rho_3 D_3} Q_{E_3}} \\ w_{2+3} = \frac{\frac{M_2}{\rho_2 D_2} Q_{E_2} w_2 + \frac{M_3}{\rho_3 D_3} Q_{E_3} w_3}{\frac{M_2}{\rho_2 D_2} Q_{E_2} + \frac{M_3}{\rho_3 D_3} Q_{E_3}} \end{cases} \tag{4.3}$$

It is worthwhile to stress that the importance of Q_E is due also to the fact that the radiation is all extinguished by the sample, but I cannot say how much radiation

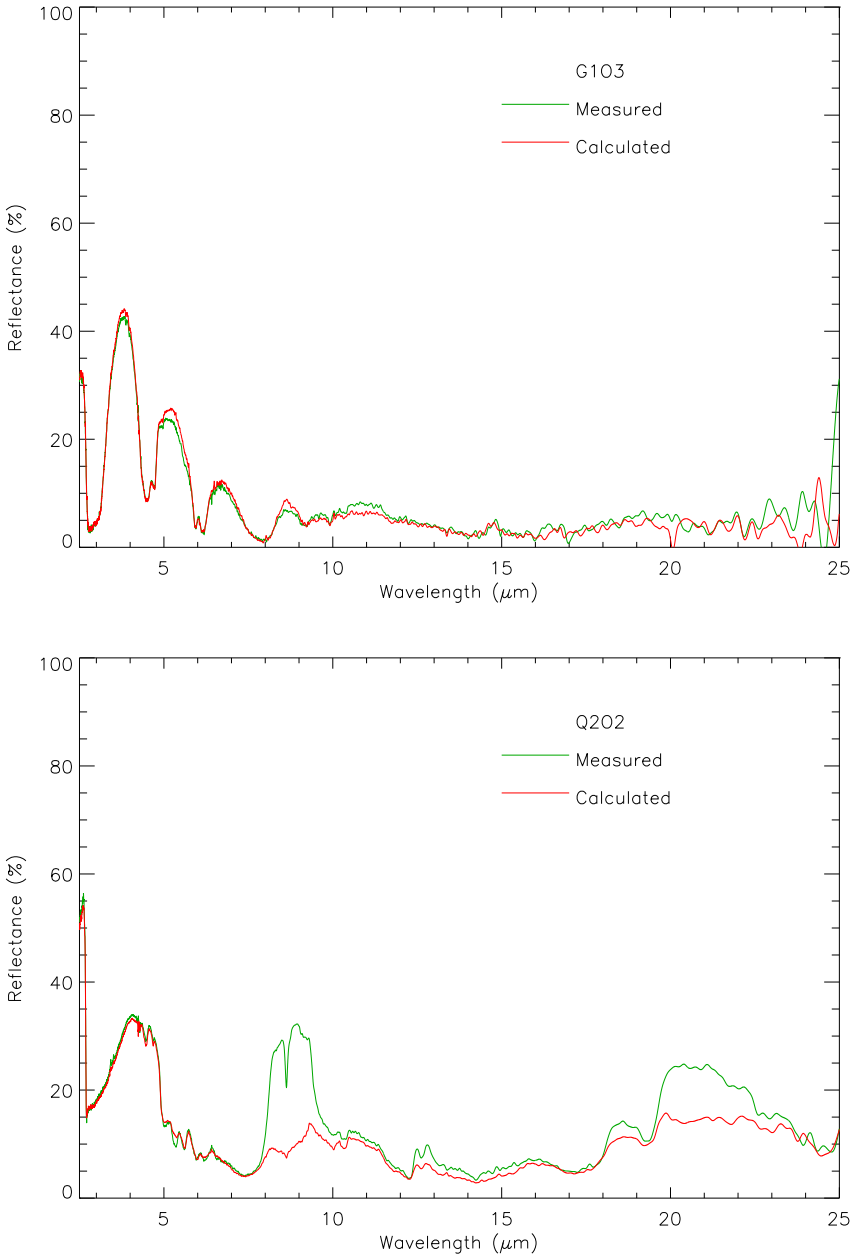

Figure 4.4: Comparison between measured and calculated spectra of G1O3 (top panel) and Q2O2 (bottom panel).

is extinguished by the first component and how much by the second component. In particular, the diffraction condition is valid for particles bigger than wavelength and close together: if both such conditions are verified, there is no diffraction and the radiation is all extinguished by the sample.

In fact, dealing with compositional mixtures, the assumption that no radiation is transmitted must be referred to the whole mixture, and I cannot set $Q_E = 1$ for each component. Therefore, I do not know how each mineral extinguishes the radiation, since it is necessary to take into account not only the relative amount but also the effect of the optical behaviour of each component of the mixture.

In order to take into account the spectral behaviour of each component, I need to derive the extinction efficiency, Q_E, of each sample. Unfortunately, the only method is by means of transmittance measurements and using Equation 4.2.

Even if the use of the above procedure is not always applicable, in my case the bands considered are active both in reflectance and in transmittance. Moreover, I use the values of Q_E, derived by transmission measurements (in Figure 4.5 I show the Q_E calculated for other two samples, olivine and quartz, used for the calculation of the following spectra), only as weight factors, able to account for the actual extinction ascribable to each component of the mixture.

Unfortunately, comparing the reflectance spectra obtained with the measured extinction efficiencies with those obtained with the assumption of $Q_E = 1$, I do not obtain good results in all cases. In fact, in Figure 4.6 I report an example of a mixture for which the use of the measured Q_E improves the agreement in the whole spectral range, but in Figure 4.7 the the agreement improves for the restrahlen bands of quartz and worses for those of dolomite.

The fact that the use of the measured extinction efficiency does not improve all the theoretical spectra is not surprising. In fact, the diffraction condition implies also that Q_E is equal to unity. The problem is that such condition is valid for particles close together, and bigger than the wavelength. The first hypothesis is respected. For the second it could not be so, as I have explained in Section 4.1. However the grains are close together and no radiation passes trough the sample; moreover it is impossible to distinguish the radiation which directly arrives on a particle from that

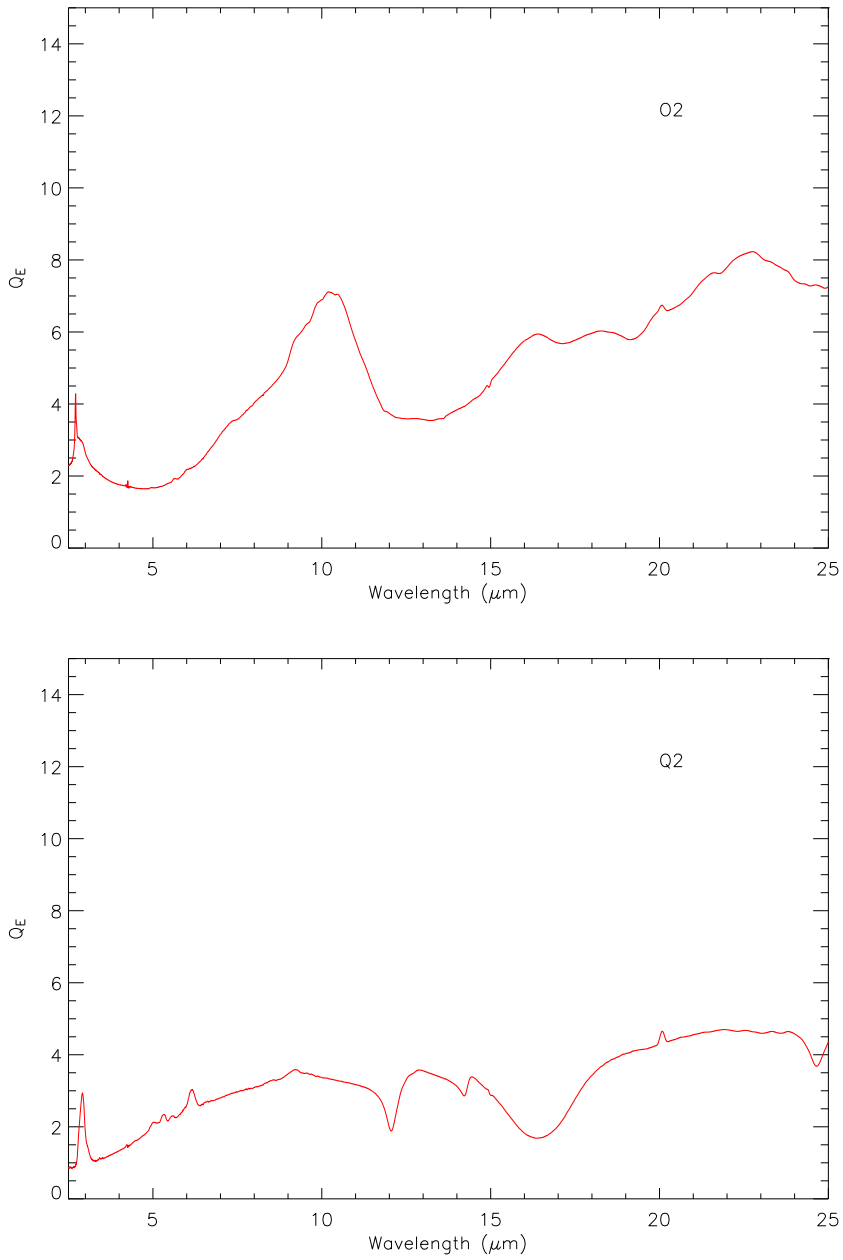

Figure 4.5: Q_E measured in transmittance configuration and calculated by means of Equation 4.2, for O2 and Q2 samples.

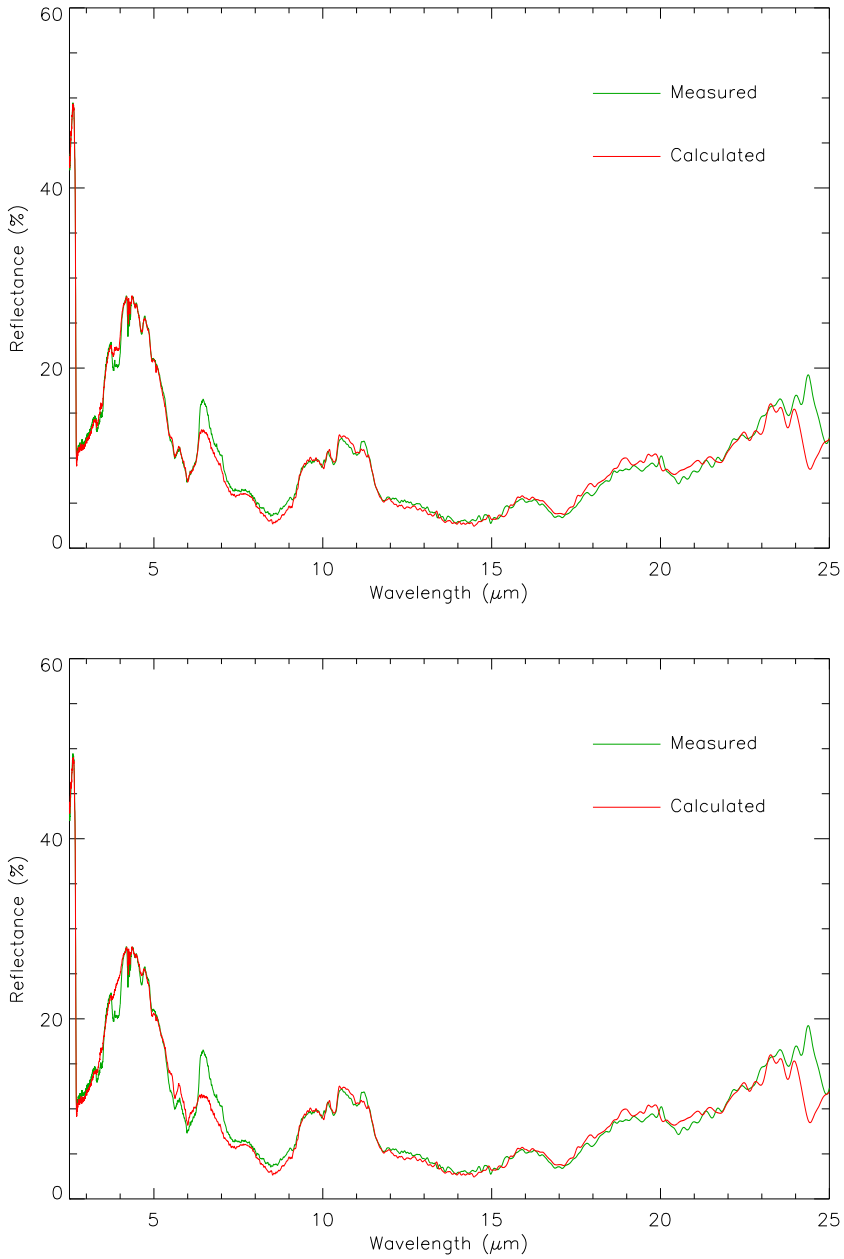

Figure 4.6: Measured and theoretical spectra of mixture O2D2. In the top panel the theoretical spectrum is calculated using the Q_E measured in transmittance configuration, in the bottom panel with the normalization of $Q_E = 1$.

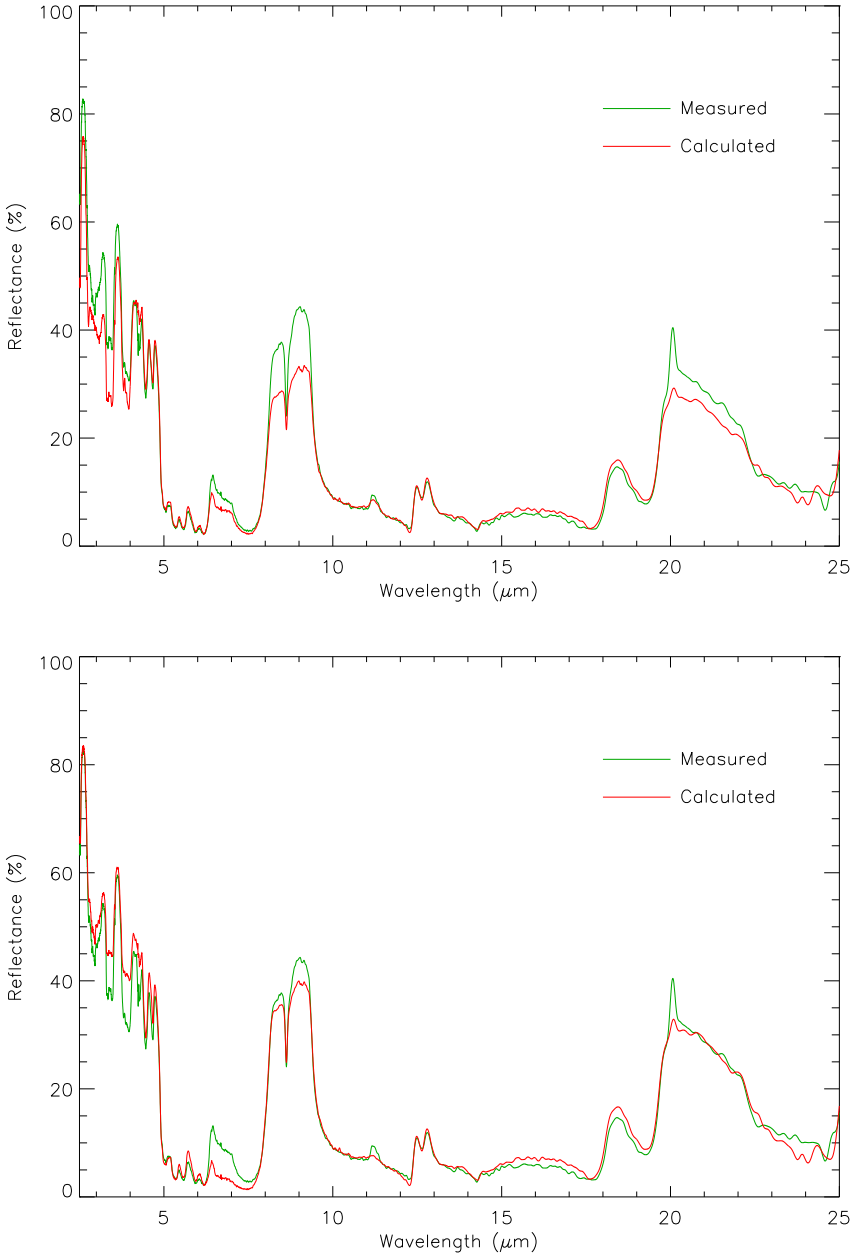

Figure 4.7: Measured and theoretical spectra of mixture Q2D2. In the top panel the theoretical spectrum is calculated using the Q_E measured in transmittance configuration, in the bottom panel with the normalization of $Q_E = 1$.

which is diffracted before arriving to the same particle. In such case, it is possible to say that the diffraction condition is valid also in my case.

4.4 The grain size

When I have discussed the theoretical approach, in Chapter 2, I have made an important hypothesis about the particles, which are considered spherical and identical. Unfortunately, it is impossible to check directly the spherical hypothesis, but it is only possible to deduce its validity, as I have shown in Section 4.2. In addition I can make some considerations about the identical spherical particles.

Such hypothesis could not be valid for all the samples. In fact, as it can be seen in Figures from 3.2 to 3.5, not all the samples have a good size distribution: for example the biggest sample of olivine, O3, presents a tale of small particles, while both the gypsum samples have a wide size distribution. In such cases it is possible that the hypothesis of identical particles could not be valid and this could be the explanation of the disagreement between the measured and calculated spectra, shown, for example, in the top panel of Figure 4.4.

In Section 3.3, I have explained how, using the Mie scattering theory (Van de Hulst, 1957; Kerker, 1969; Bohren and Huffman, 1983), the output of the granulometer is a volume distribution, and I have mentioned that it is possible to calculate other distributions (in surface, in length and in number of particles) and, accordingly, many different effective diameters could be evaluated considering different properties.

In Figure 4.8 I show the grain size distribution of dolomite, gypsum and olivine, as a function of volume, surface, length and number, and in Table 4.2 I list some effective diameters of the same material, obtained using different distributions. As it can be seen the dolomite sample is very uniform, in fact all its size distributions are very close to each other and this implies that all the particles are very similar in size and shape. On the contrary, both gypsum and olivine results are very different for different distributions, with the consequence that size and shape of olivine and gypsum particles should vary in a much larger range. This is due to the fact that a

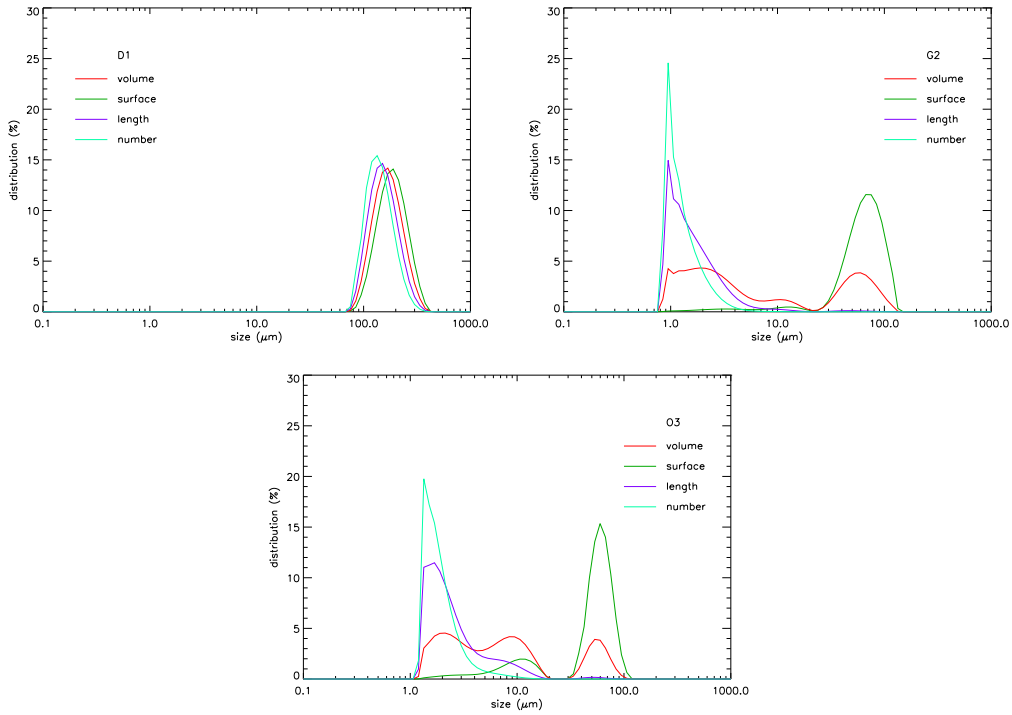

Figure 4.8: Grain size distribution of D1, G2 and O3 samples. In each panel the volume, surface, length and number distribution is reported.

distribution in number or in volume produces different results because the physical properties taken into account to calculate each distribution are very different. For example a big particle has a big volume, so it weighs more than many small particles in a volume distribution, on the contrary those small particles weigh more than a big particle in a number distribution.

In Table 4.2 I list only some effective diameters which can be evaluated. The purpose is to show how the different distribution produces very different values. The D[4,3] and D[3,2] are independent from the distribution. The d(0,x) is defined as the diameter for which the $10x$ percentage of particles has a diameter smaller than d(0,x), so the d(0,9) is the diameter for which the 90% of particles has a diameter smaller than such value, as well as for the 50% of particles have a diameter smaller than d(0,5).

As a conclusion, it is possible that the D[4,3] effective diameter is not adequate

Table 4.2: Mean diameter (in μm) calculated by means of different size distributions.

material	D[4,3] μm	D[3,2] μm	distribution	d (0,9) μm	d(0,5) μm
Dolomite D1	192	175	Volume	274	184
			Surface	250	166
			Length	227	150
			Number	205	137
Gypsum G2	169	53	Volume	277	164
			Surface	176	5
			Length	4	2
			Number	3	1
Olivine O3	127	37	Volume	205	136
			Surface	139	10
			Length	11	3
			Number	4	2

for all the samples. To understand if this is the case, I have made some tests: I have calculated the theoretical spectra, of all the mixtures composed of samples with a *bad* grain size distribution, using different effective diameter values. In Figure 4.9 I show only some examples of these theoretical spectra, for the mixture G2O3, using some of the different diameters which can be evaluated; in particular I show the theoretical spectra calculated using all the diameters listed in Table 4.2.

As it can be seen, considering different values is not the answer of such problems. At the same time, every diameter is related to some characteristics of the size distribution, and therefore the reason of the observed spectral discrepancies does not depend on any characteristics linked to the size or shape of the particles.

As a consequence of this discussion, such disagreement could be related only to the quality of the size distribution. In fact, looking with more attention to the various panels of Figure 4.9, it is possible to notice that the influence of small particles plays a relevant role in the measured spectrum. For example, the restrahlen bands of olivine, at about 11 μm, could be higher, and the small band which starts at about 17 μm is difficult to be recognized. This depends on the influence of small particles, because they produce an increase in multiple scattering with a consequent increase of energy lost during such scattering.

In conclusion, I must neglect all the mixtures composed of particles with a *bad* size distribution. However, such distributions could be studied in future, when the mixtures behaviour will be better understood.

4.5 Summary

In this chapter I have verified that all the hypotheses made are basically fulfilled.

In particular I have shown that the particles size can be effectively considered larger than the wavelength, and, therefore, the mathematical approach is valid for all my samples.

The first hypothesis is about the extinction efficiency. This parameter is an expression of the optical properties of every mineral, so it could be fundamental. However, if particles are larger than the wavelength and close together, such value can be considered as equal to unity. This means that the diffraction can be neglected, and this is certainly true for all my samples. Such conclusion is supported by experimental measurements made both on granulometric and compositional mixtures. In particular, the granulometric mixtures prove that the diffraction condition is valid, also for small particles, and there is no reason not to extend this result to compositional mixtures, for which the use of a measured extinction efficiency does not produce any improvement.

I go on with the discussion on isotropic scattering. The fact that the spectra of granulometric mixtures, calculated using the equation derived with the application of such hypothesis, are in agreement with those measured, is sufficient to demonstrate that the scattering is isotropic. In fact, if it were not so, the agreement would not be so good, because the isotropic scattering depends only on the geometry of the radiation matter interaction.

Finally some considerations on the hypothesis concerning the shape of the particles. If the particles could not be considered identical and spherical, a discrepancy would be noticed in both granulometric and compositional mixtures. The fact that the agreement is good for granulometric mixtures means that the shape irregularities are conveniently averaged, due to the high volumetric density of the grains. However,

the effects on the mixture spectrum of the different particle sizes are less important for the granulometric mixture, for which such effects are compensated by the similar behaviour of the particles optical properties; on the other hand, in compositional mixtures, the grain size, influencing the band depth, can produce major effects on the mixture spectrum, when features in different spectral position are induced. In addition, some of the components of the mixtures have not a *good* size distribution. It is therefore reasonable to assume that both the variations of the optical properties in function of the particle size and the *bad* particles size distribution could play an important role, in the observed disagreement between theoretical and measured spectra of some compositional mixtures. From one side a wrong interpretation of the size could produce wrong results in calculated spectra, from the other side the presence of small particles in the mixtures could affect the measured spectrum. The importance of small particles in mixtures, as well as in the spectrum of a single pure material (Mustard and Hays, 1996), has been discussed in this chapter.

As a conclusion, this chapter is fundamental for the application of mixture laws derived in Chapter 2. In the following chapter I will show that such laws are valid only in the NIR range. After this range other considerations must be made, because the disagreement is due to reasons which are not considered neither in Chapter 2 nor in this chapter.

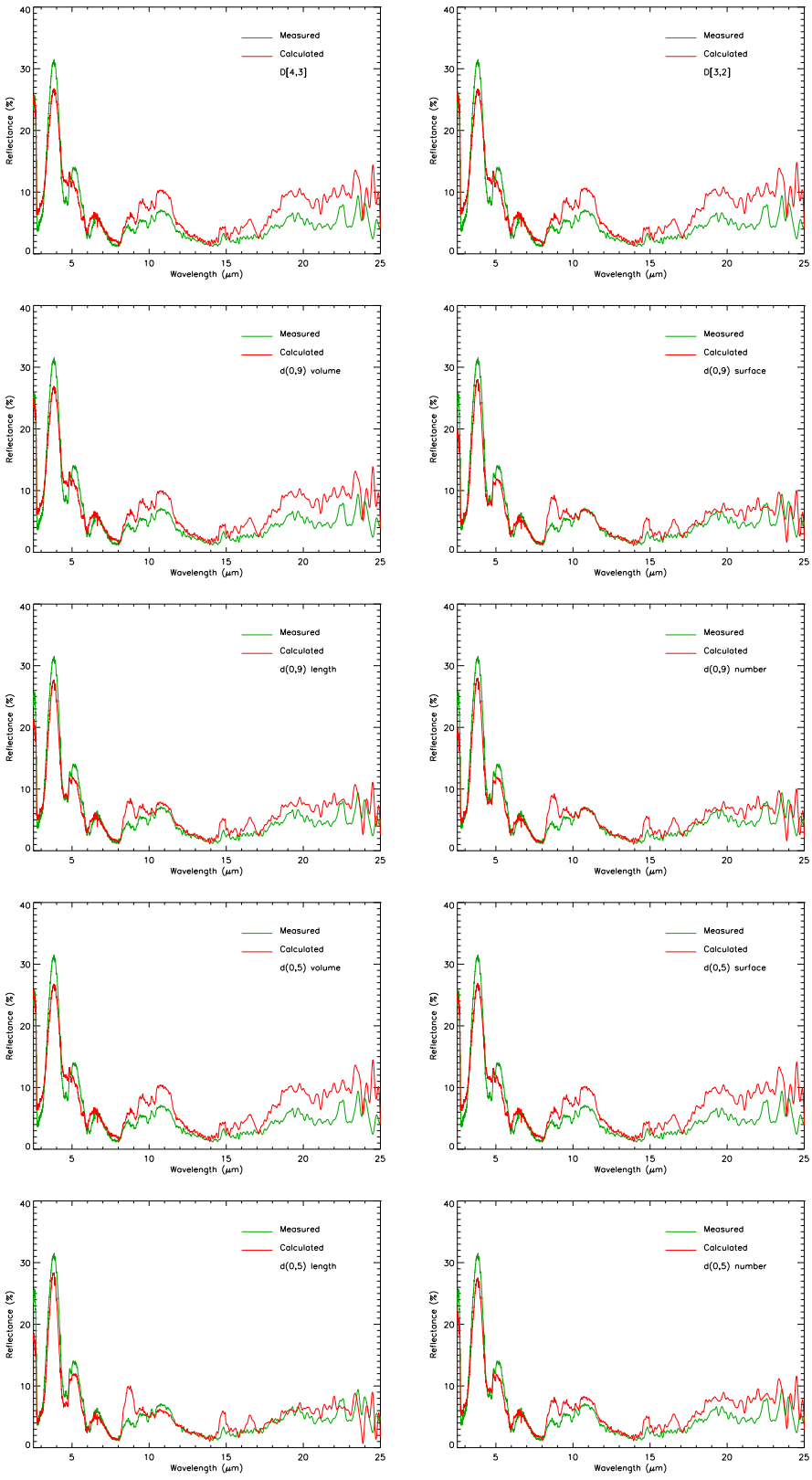

Figure 4.9: Comparison between measured and calculated spectrum of G2O3 mixture. In each panel the spectra calculated using different values of diameter are shown.

Chapter 5

Preliminary results

In this short chapter I will show the first results of my work, in particular the comparison between measured and calculated spectra of each mixture, demonstrating the validity of Hapke Theory of Reflectance for particulate mixtures up to the principal Christiansen frequency. All the synthetic spectra have been calculated taking into account the validity of the hypotheses and the discussion made in the previous chapter. In Section 5.1 I will show the spectra of the selected mixtures, in the whole spectral range. In Section 5.2 I will focus my attention on the first part of the spectrum, where absorption bands occur, and I demonstrate the validity of the Hapke approach for the calculation of a synthetic spectrum of an intimate mixture, within the hypotheses made. In Section 5.3, I will discuss a possible explanation of the disagreement for a mixture spectrum. Finally, in Section 5.4, I will summarize the work shown in this chapter and demonstrate the validity of Hapke Theory of Reflectance up to the first Christiansen features.

5.1 A first comparison

In Chapter 4, I have explained that the granulometric mixtures have been used for the demonstration of the hypotheses made on the theoretical approach and I have concluded the chapter saying that, in this work, I have neglected all the mixtures where the components have a *bad* size distribution (as defined in Section 3.5). In particular, from this moment, I will exclude all the mixtures involving both the

gypsum samples and the biggest olivine. As a conclusion, the mixtures which will be discussed in this chapter, are those with a *good* grain size distribution: O2D1, O2D2, Q2D1, Q2D2, Q2O2. In fact, for all these mixtures, the grain size distribution of each component does not show any tale and is rather narrow (see Figures 3.2-3.5).

In Figure 5.1 I report the comparison between the measured and calculated spectra for all the mixtures listed above. As it can be seen, the agreement is quite good for the two mixtures involving olivine and dolomite, and it is bad for the three mixtures involving quartz.

In particular, looking with more attention, for the mixture O2D1 the agreement is good up to the first restrahlen band of dolomite, approximately 6 μm, for which the agreement is not very good. After this band the agreement becomes good again. The only exception is at 24.5 μm, for an instrumental effect.

For the mixture O2D2, the agreement is like that of mixture O2D1, with the only exception that the disagreement in the restrahlen band of dolomite is worse.

The agreement of these two mixtures deserves a comment about the size of the components. In fact, the olivine sample is rather small and, if the diffraction condition were not respected, the agreement would not be so good, especially at longer wavelength, where the size parameter becomes smaller. Therefore, as I have discussed in Chapter 4, the hypothesis about the size parameter (particles bigger than wavelength) and about the diffraction condition (particles close together) and their implication on the extinction efficiency (which is equal to unity), are all valid.

More complicated is the discussion of the other spectra. In fact for all these spectra the disagreement is very strong and it is necessary a deep analysis for every band.

In the mixture Q2D1, the agreement is quite good in the absorption range, up to the first restrahlen band of dolomite (6 μm). Both the first and the second restrahlen bands of dolomite have a larger band depth in the measured spectrum than the calculated one. The same happens for the first and the third restrahlen bands of quartz. On the contrary, in the region where the second restrahlen band and the transparency features of quartz occur (between 12 and 20 μm), the agreement is very good.

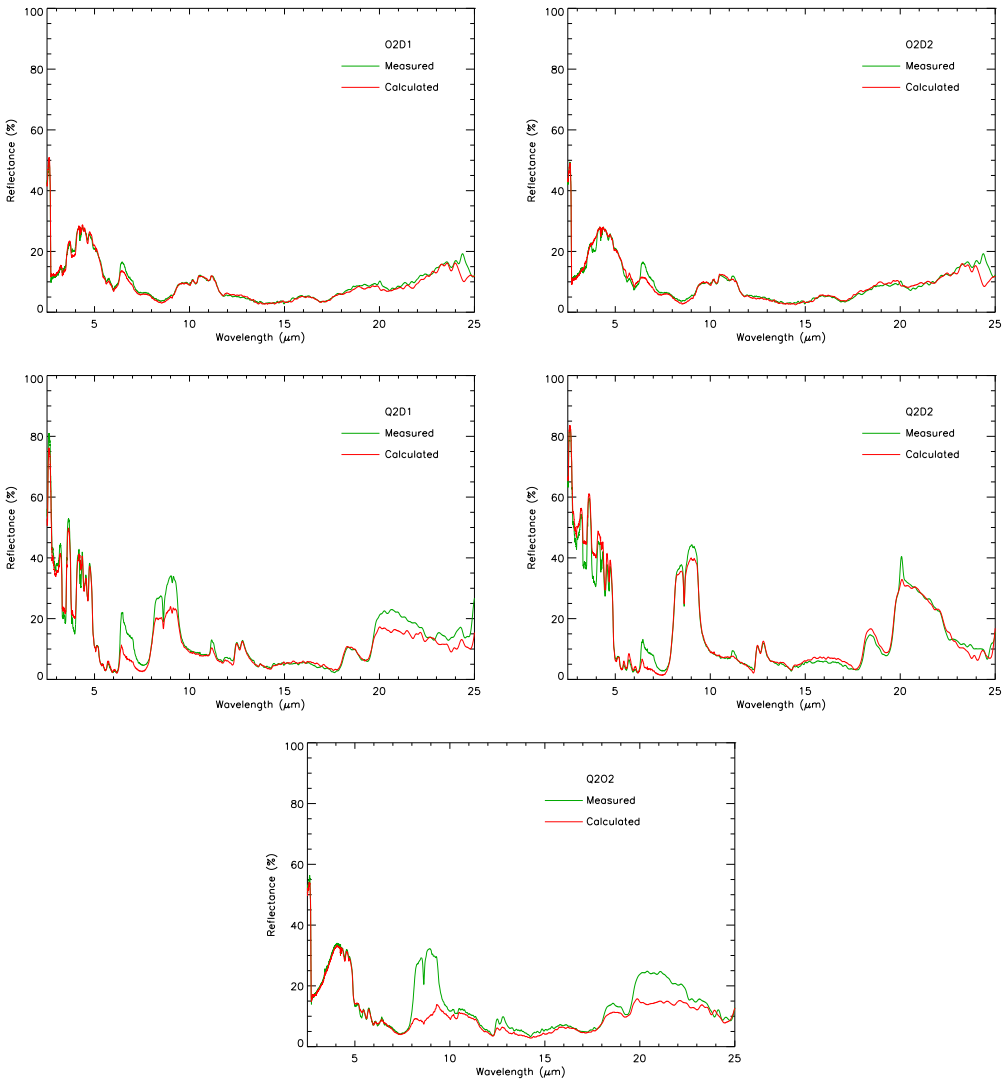

Figure 5.1: Comparison between measured and calculated spectra for mixtures: O2D1 (top left panel), O2D2 (top right panel), Q2D1 (middle left panel), Q2D2 (middle right panel) and Q2O2 (bottom panel).

The spectrum of the mixture Q2D2 is quite different. The agreement is bad in the absorption region, with the exception between 5 and 6 μm where the agreement is good. Both the first and the second restrahlen bands of dolomite are basically absent in the calculated spectrum. The agreement in all the restrahlen bands of quartz is not very good, and in the transparency region the agreement is worse than that of the Q2D1 mixture.

In these last two spectra, it seems that dolomite sometimes dominates the measured spectrum and sometimes does not. However it is only an appearance, because, as I have just shown in Section 4.3, in particular in Figure 4.7, if it were so, the use, in the theoretical calculation, of the extinction efficiency, which is a parameter taking into account the optical properties of each mineral, would improve the synthetic spectra.

The case of Q2O2 is more complicated. In fact, the comparison between the measured and calculated spectra is good up to the principal Christiansen features of quartz, at about 7.5 μm, but then the agreement is bad. In particular the agreement is good where the contribution of olivine is accounted for the measured spectrum, but, above 7.5 μm, the spectrometer seems to see only quartz, with a consequent disagreement between the two spectra.

However, the above discussion suggests that most of the differences between the calculated and the experimental spectrum occur principally in the restrahlen bands of each component. Since such bands are characterized by large values of the complex part of the refractive index ($k > 0.1$), only a small amount of energy passes through the sample and the scattering and absorption properties are basically controlled by first surface reflection (Salisbury, 1993; Mustard and Hays, 1996; Salisbury et al., 1992).

In conclusion, Hapke reflectance theory for intimate mixtures seems not to be valid in the whole spectral range, but only up to the first Christiansen feature. However, to demonstrate that, it is necessary to divide the spectrum into two parts: the first, the NIR region, up to the principal Christiansen feature and the second, the MIR region, above such frequency. In this chapter, I principally focus my attention on the NIR region.

5.2 The NIR region

The range between 2.5 μm and the first Christiansen frequency (NIR spectral range) is where the absorption features occur. As I have already said in Section 1.3, such bands are dominated by volume scattering, because the absorption coefficient is low, therefore the photons survive inside the particles and, before arriving to the detector, interact with many particles (Salisbury et al., 1992).

The equation of reflectance I have used for the calculation of synthetic spectra, is basically due to the assumption that the particles are mixed homogenously together, such as in the intimate mixtures, defined in Section 1.5 and used also for the Equation 2.42. Naturally such hypothesis have a meaning if the radiation penetrates into the sample, as it happens in this region.

As it can be seen in Figure 5.1, in this range the agreement between the measured and calculated spectra is, in most cases, good, even if the two mixtures involving quartz and dolomite do not show a very good agreement. In particular the detector measures more dolomite with respect to that present in the calculated spectra. This could be due to the fact that quartz is smaller than the dolomite sample, and, probably, the smaller grains could penetrate between the dolomite grains. In this way the lower level of the mixture could be richer of quartz than the upper one, with the consequence of a non-homogeneous distribution of each component.

5.3 About the homogeneity

I have concluded the previous section with an hypothesis about the inhomogeneous distribution of each component of a mixture in the NIR range.

In addition, in Section 5.1, I have shown that in the mixture Q2O2, in the MIR spectral range, the instrument measures only the contribution due to the quartz, ignoring olivine. This fact could be explained with the same hypothesis of a non homogeneous distribution.

In fact, the olivine, which is smaller than the quartz, could percolate more deeply in the sample and therefore be more abundant in the lower part, while the upper

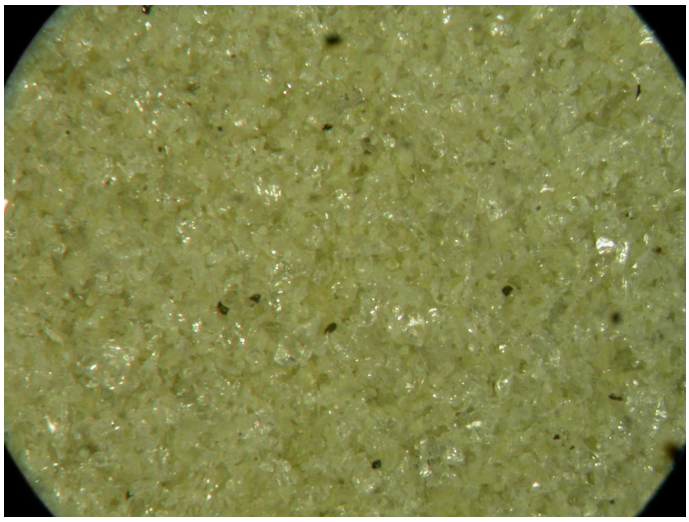

Figure 5.2: A photo, taken by means of a microscope, of the sample Q2O2, before making the spectroscopic measurement.

level is richer in quartz. Therefore, the instrument measures the contribution due to olivine only in the NIR range, where the low absorption coefficient allows the radiation to penetrate into the sample,while, in the MIR range the radiation does not penetrate, the contribution due to quartz dominates the resulting spectrum.

However, such hypothesis is quite difficult to demonstrate. In Figure 5.2, I show a photo of the mixture Q2O2, taken before making the measurement. Such photo has been taken with a camera, *Nikon Coolpix 4500*, assembled on a microscope *Nikon SMZ 1500*, at 10x of magnification. Looking at such picture, it is quite difficult to recognize each component; in particular it is possible to see particles bigger than others, but it is impossible to count them and it is impossible to determine the real contribution of each component.

Therefore, finding a solution to this problem seems to be not very easy; in particular it is not easy to find an accurate method for the determination of the real distribution of each component.

However, it is possible to perform an experiment, which could demonstrate the importance and the implication of a good distribution of each component in a mixture. Such experiment will be shown in the following section and it will be the

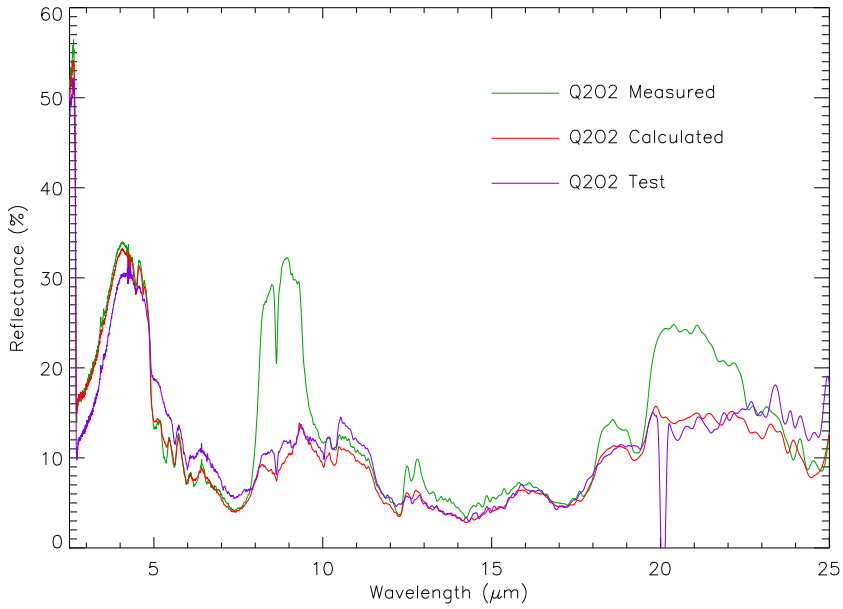

Figure 5.3: Comparison between the measured spectrum and the calculated spectrum of mixture Q2O2 and another spectrum measured after covering the surface with a 0.04 g of olivine.

principal object of the Chapter 6.

5.3.1 A first experiment about the homogeneity

In this section I will describe a qualitative experiment designed for showing the influence of a non-uniform distribution of each component on a mixture spectrum.

The experiment consists in performing directional-hemispherical measurements of a mixture, before and after covering the exposed surface with small variable quantities of each of the two components.

The first significative result is shown in Figure 5.3, where I show, for the mixture Q2O2, the measured spectrum, the calculated spectrum and another spectrum measured after covering the surface with a 0.04 g of olivine (less than the 1% of the mixture volume).

As it can be seen, this spectrum is very similar to that of the calculated mixture Q2O2. The major disagreement is at 20 μm for an instrumental spike. So, a very

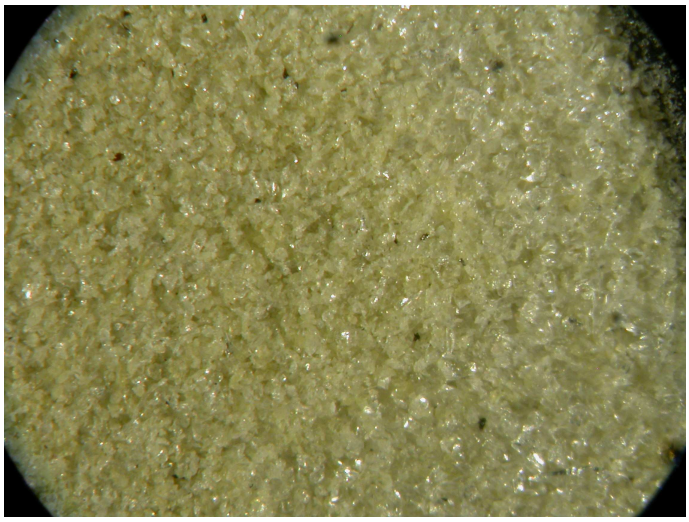

Figure 5.4: A photo, of the sample Q2O2, taken by means of a microscope after covering the surface with 0.04 g of olivine.

small quantity of one component causes a big variation in the resulting spectrum. This fact implies two possibilities: the first is about the non-homogeneous distribution of each component in an intimate mixture; the second is about the role of the mixture surface, which becomes fundamental in the spectral range of the restrahlen bands.

Another evidence is shown in Figure 5.4, taken in the same way of the other shown in Figure 5.2, of the same sample after covering the surface with 0.04 g of olivine and, it is possible to see that the mineral distribution seems more homogeneous. In fact, in this figure, it is possible to notice that the bigger grains are less than those present in Figure 5.2 (in both figures the small grains are those with a darker color, while the bigger grains are those with a brighter appearance).

In conclusion, the mixture after covering the surface with a small quantity of olivine shows a more homogeneous distribution than before, and produces a spectrum more similar to that calculated for the original mixture, with respect to the spectrum of the original Q2O2 mixture.

5.4 Conclusion

In this short chapter I have discussed the first result of this PhD. thesis: the extension of the spectral range where it is possible to apply the Hapke Theory of Reflectance.

In fact, the Hapke Theory states that, if particles are bigger than the wavelength, close together and mixed homogeneously, the resulting spectrum is given by the Equations 2.39 and 2.42. In particular, such equations, which supply the albedo of a particulate mixture, is obtained considering an intimate mixture, i.e. a mixture with the particles mixed homogeneously together. Only under such condition the resulting reflectance is given by Equations 2.39 and 2.42.

In this chapter I have shown that the hypothesis of particles bigger than wavelength and close together, continue to be valid also for the mixtures involving the smaller olivine grains. In spite of that, the spectra of some mixtures reveal a disagreement between the measured and the calculated spectra. Such discrepancy can be due to a *bad mixing* of the components, but, unfortunately, such bad mixing does not depend on the sample preparation method, which is the same for all the mixtures. It could, instead, depend on the particles themselves: for example small particles could percolate among big particles, producing a non homogeneous distribution of each component. Such inhomogeneity produces discrepancies between the measured and calculated spectra of intimate mixtures, even if it does not invalidate the mathematical approach.

In Figure 5.5, I show the comparison between measured and calculated spectra for the mixture Q2D2 in the NIR range. In the left panel I show the calculated spectrum with the true mass of each component, and, in the right panel, I show the calculated spectrum obtained varying the relative abundance of each component: in particular, the mass of dolomite has been modified from 25% to 39% of the total mixture mass. As it can be seen, the agreement improves in the right panel and this suggests the inhomogeneity in the distribution of the components could be the cause of the observed spectral disagreement.

As already said, it is impossible to control effectively the distribution of the

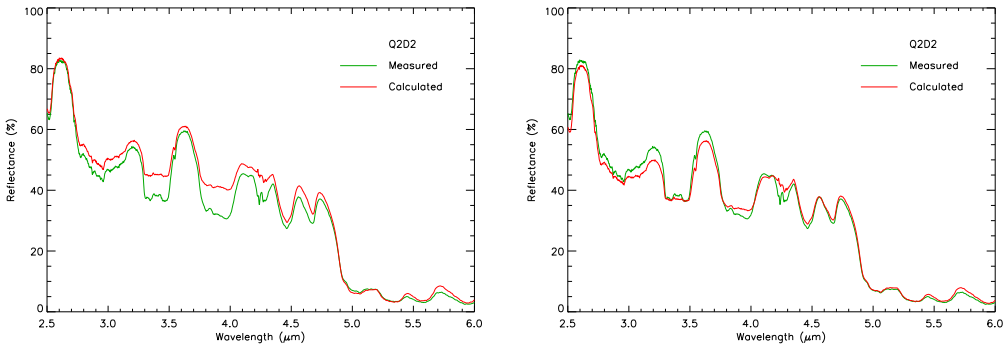

Figure 5.5: Comparison between measured and calculated spectra for the mixture Q2D2 in the NIR range. In the left panel the calculated spectrum with the true mass of each component is shown, while, in the right panel, there is the calculated spectrum varying the abundance of each component: in particular, the mass of dolomite has been modify from 25% to 39% of the total mixture mass.

particles. However, the fact that the distribution of each component is not homogeneous, in the NIR region, does not influence the validity of the Hapke theory of reflectance for intimate mixtures. In fact, if the mathematical approach is valid, the characteristics of each components will be referred to the mixture effectively measured.

In the following chapter I will show that, considering a mixture as areal instead than intimate, is more correct. However such approach produces another problem: in fact, if the distribution of each component is not homogeneous, then determining the real surface abundance of each component should become difficult. Such problem can be overcome minimizing the chi-square function.

Chapter 6

Results and discussion

In this PhD thesis I have shown that, using Hapke Theory of Reflectance for particulate mixtures, if particles are close together and mixed homogeneously, it is possible to reproduce, with a good agreement up to the first Christiansen frequency, the spectrum of a measured mixture starting from the reflectance of the components. Above this wavelength, the agreement between the measured and calculated spectra becomes worse.

In the previous chapter I have discussed the possibility that the observed disagreement, in the NIR range, could be due to inhomogeneities in the component distribution. In Section 6.1 I will show other measurements, which demonstrate that such inhomogeneities are fundamental and, in the MIR range, become the major reason of disagreement. In particular, in Subsection 6.1.1, I will experimentally demonstrate that, in the MIR range, the radiation does not penetrate into the sample, and the mixture reflectance is due only to the surface. In Section 6.2 I will use the same type of experiments to confirm the intimate approach in the NIR spectral range. If, in the MIR region, only the surface of a mixture interacts with radiation, it would be more correct considering a mixture as areal, instead than intimate, and this will be proved in Section 6.3 and confirmed in Subsection 6.3.1, where I will discuss both approaches, intimate and areal, with the help of the chi-square function. In Section 6.4 I will draw some conclusions, I will illustrate some pending problems and I suggest some possible actions necessary to improve this work.

6.1 Other experiments

In Section 5.3.1, I have shortly shown an experiment made on mixture Q2O2. Such experiment consists in performing directional-hemispherical measurements of a mixtures, before and after partially covering the exposed surface with small quantities of one of the two components of the mixture. In that section I have also discussed only one of the consequences that such experiment reveals: the inhomogeneity of the component distribution. However, the result of such experiment has also other implications and in this section I will discuss them.

The experiment, performed on Q2O2 and Q2D1 mixtures, consists of some reflectance measurements of a mixture, varying both the component and the quantity of the material added.

In particular, the experiment consists in making the following measurements for the mixture Q2D1:

1. original mixture at 50% in volume;
2. adding 0.02 g of dolomite on the surface;
3. adding 0.05 g of dolomite on the surface;
4. adding 0.02 g of quartz on the surface;
5. adding 0.05 g of quartz on the surface.

For the mixture Q2O2 the measurements are:

1. original mixture at 50% in volume;
2. adding 0.02 g of olivine on the surface;
3. adding 0.04 g of olivine on the surface;
4. adding 0.01 g of quartz on the surface;
5. adding 0.03 g of quartz on the surface.

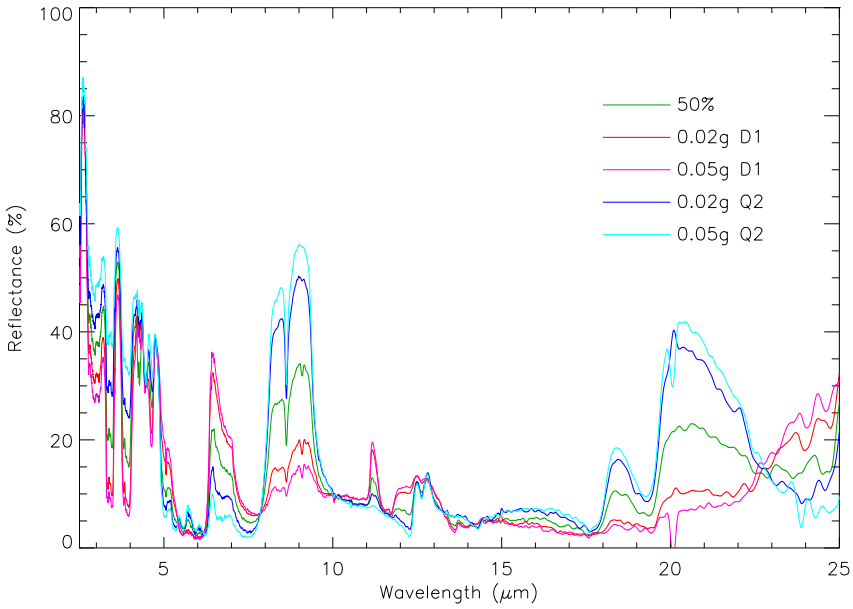

Figure 6.1: Directional hemispherical reflectance measurements for all the variations of the mixture Q2D1.

After each measurement I have mixed again the sample.

In Figure 6.1 and 6.2, I show the reflectance measured for all the steps listed above. In addition, I examine each sample with the microscope, even if, unfortunately, it is very difficult to understand if the added mineral covers the surface homogeneously.

Looking at Figure 6.1, it is better to take separately into account those measurements for which the dolomite is the added component, and those for which it is the quartz, taking always as reference the starting mixture in which the components are mixed at 50% in volume. When dolomite is added, the corresponding bands reach quickly their maximum intensity and this happens both in the NIR range and in the restrahlen region. On the other side, the first restrahlen band of quartz becomes gradually smaller, while the second and the third restrahlen almost disappear together with the transparency features. The only band of dolomite that does not reach rapidly full intensity is the first absorbing band just before 3 μm.

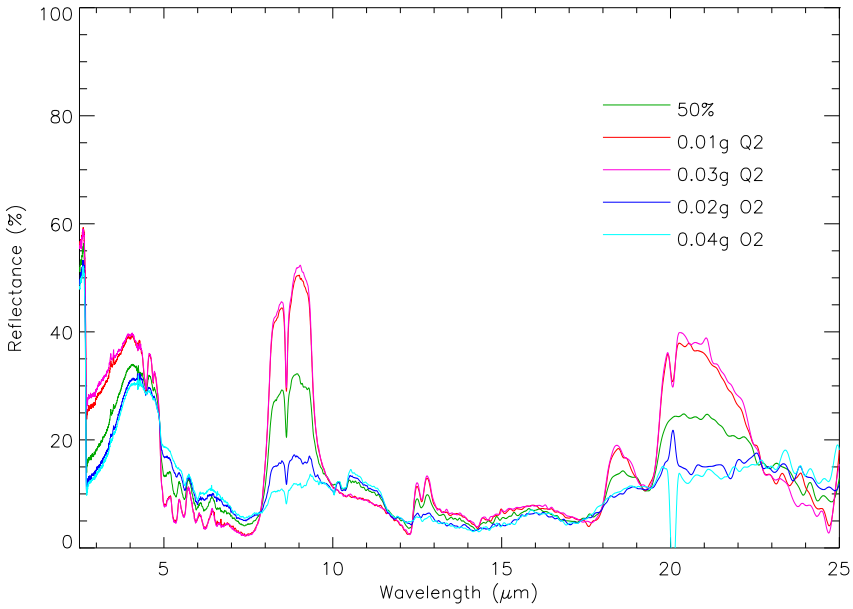

Figure 6.2: Directional hemispherical reflectance measurements for all the variations of the mixture Q2O2.

When quartz is added, the dolomite bands progressively disappear, and the bands of quartz, reaching quickly their maximum intensity, are the second restrahlen as well as the transparency feature. The first and the third restrahlen bands become larger more gradually.

In the Q2O2 mixture, both the measurements, when quartz is the added component, reveal that the bands of quartz are all at their maximum intensity, while the bands of olivine quickly disappear. When olivine is the added component, the discussion is more complicated. In fact, the first restrahlen band of quartz progressively becomes smaller, while the other bands disappear at once.

However, both olivine and quartz have their bands at very similar wavelength: for example the second restrahlen band of olivine starts at 17 μm and goes on up to 25 μm, while the third restrahlen band of quartz is composed of a smaller feature at about 18 μm and another larger band starting at 19 μm and going up to 23 μm; the transparency feature is between 15 and 17 μm for olivine and between 14 and 18 μm

for quartz (see Section 3.4.2). Therefore, it is not easy to distinguish the bands in a very accurate way, especially when the added component is olivine, whose features are very small due to the small grain size.

From such discussion, it is clear that a small quantity of a mineral could cause the corresponding bands to reach an intensity close to that of the single component, while canceling the bands of the other component. At this point it is important to understand more precisely how much mineral is necessary to cause such effects, since such amount is definitely related to the penetration depth of the incident radiation.

6.1.1 An estimation of the radiation penetration depth

To estimate quantitatively the penetration depth of radiation in a mineral mixture, I reported the above results in a plot, with the quantity of added mineral, in percentage of the total volume, in abscissa and the normalized intensity of a band in ordinate. Each band is normalized respect to the same band in the spectrum of the single mineral.

Such plot has been made for all the restrahlen bands of each component of the two mixtures Q2D1 and Q2O2. In Figure 6.3 I show the plots obtained for the Q2D1 mixture: the restrahlen bands of quartz, at 9 μm, in the top left panel and at 20 μm in the top right panel; the two restrahlen bands of dolomite on the bottom panels at 6 μm on the left and at 11 μm on the right. In Figure 6.4 I show the plots obtained for the Q2O2 mixture: the two restrahlen bands of quartz at 9 μm and at 20 μm on the top left and right panel respectively, and in the bottom panel the restrahlen band of olivine at 11 μm. In all these plots the trend, although probably not linear, has been considered as linear, in first approximation, for sake of simplicity.

Looking at these plots, it is possible to calculate the quantity of one of the components that must be added to cancel the bands of the other. In particular, looking at the plot in the top left panel of Figure 6.3, it is necessary to add approximately 1.3% of the total volume of dolomite on the surface in order to cancel the first restrahlen band of quartz. In other words, since adding a small quantity of one component on the surface results in canceling the bands of the other component, this means that

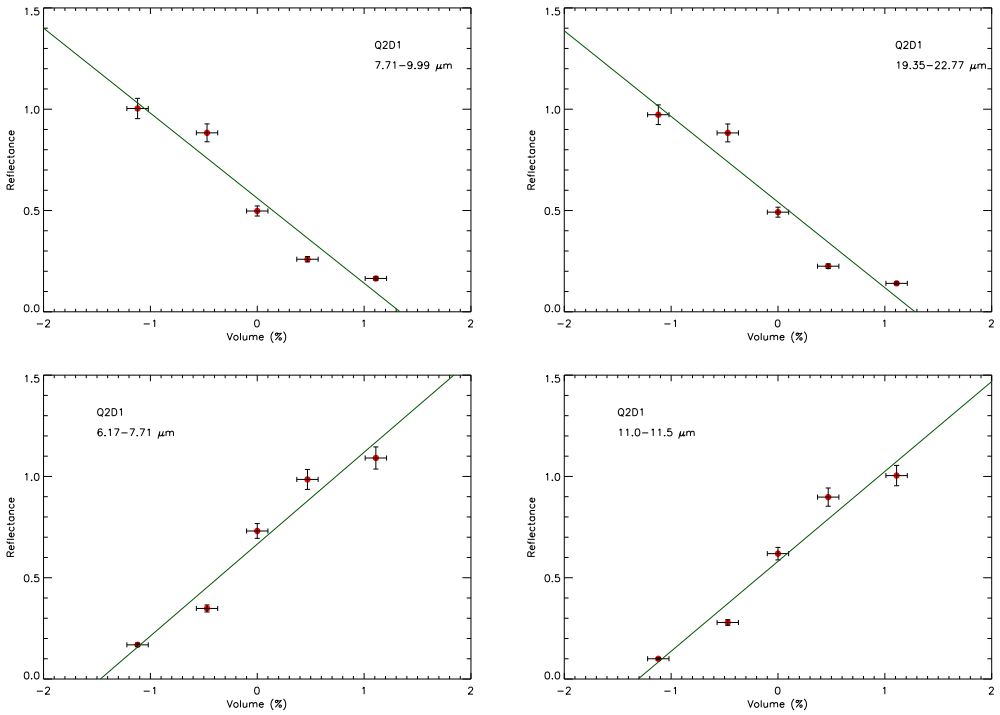

Figure 6.3: Plot of the normalized intensity (in the mixture Q2D1) of the two restrahlen bands of quartz on the top panels (9 μm at left and 20 μm at right), and of the two restrahlen bands of dolomite on the bottom panels (6 μm at left and 11 μm at right) as a function of the quantity of mineral added on the surface, in percentage of the total volume.

the radiation interacts only with the mineral added and it is not able to reach the underlying mixture. Obviously such quantity is a function of wavelength as well as the penetration depth of radiation.

To estimate the penetration depth of the radiation, we can start assuming that the total volume of the particles, contained in the dish, corresponds to a given fraction of the volume of the dish. The fraction is given by a factor, φ, which is the ratio between the volume of the mixture (V), calculated considering the weighted the mass of the sample, and the volume of the dish (V_d), so the volume of the sample is:

$$V = V_d \varphi \tag{6.1}$$

For both the mixtures, $\varphi = 0.50 \pm 0.03$.

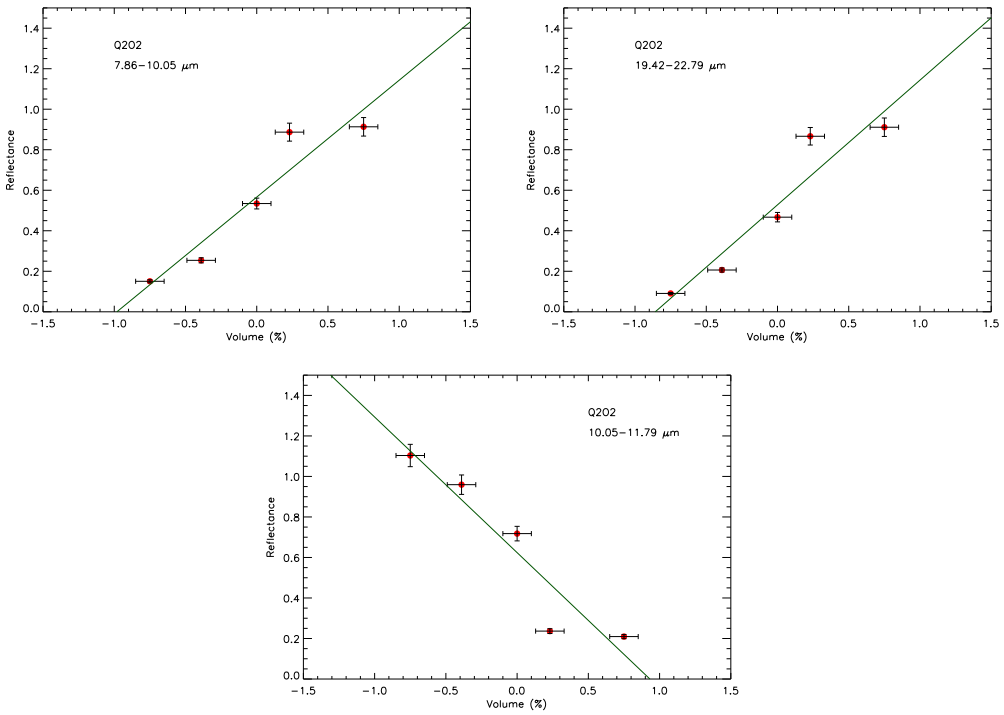

Figure 6.4: Plot of the normalized intensity (in the mixture Q2O2) of the two restrahlen bands of quartz on the top panels (9 μm at left and 20 μm at right), and of the restrahlen band of olivine at 11 μm in the bottom panel, as a function of the quantity of mineral added on the surface, in percentage of the total volume.

The dish is cylindric, and its volume is:

$$V_d = \pi r_d^2 h_d \tag{6.2}$$

where r_d is the radius of the dish (12.5 mm) and h_d its depth (5.3 mm).

Consider, now, the mineral added on the surface: the volume occupied in the dish is given by the relation:

$$V_m = \pi r_d^2 h_m \varphi \tag{6.3}$$

where V_m is the volume of the added mineral and h_m its thickness. V_m is calculated using the plots, and it is the quantity of mineral that must be added to cancel the band; in other words it is the abscissa corresponding to ordinate zero. Therefore h_m, which is the thickness of the mineral added to cancel the spectroscopic influence

of the other component, must be also the maximum thickness which the radiation can penetrate at that wavelength, i.e. the penetration depth.

In conclusion, the relation which describes the penetration depth, is:

$$h = \frac{V_m}{\pi r_d^2 \varphi} \tag{6.4}$$

Extrapolating, from the linear trend shown in the Figure 6.3 and 6.4 , it is possible to find the quantity of one component necessary to cancel completely the band of the other component from the spectrum of the mixture, and the corresponding penetration depth of radiation.

I have applied such discussion to the plots of the restrahlen bands of the mixture Q2D1, shown in Figure 6.3. For the first restrahlen band of quartz (corresponding to the plot on the top left panel) I must add 0.022 cm^3 (0.063 g) of dolomite to cancel completely the effects of quartz. The corresponding penetration depth, according to Equation 6.4, is approximately 86 μm. For the third restrahlen band of quartz, at about 20 μm, shown in the top right panel of the same figure, the quantity of dolomite to add is about 0.021 cm^3 (0.060 g), which corresponds to a thickness of about 83 μm. On the other hand, to cancel the first restrahlen band of dolomite at 6 μm, shown in the bottom left panel of the same figure, it is necessary to add about 0.025 cm^3 (0.065 g) of quartz, which corresponds roughly to a thickness of 96 μm of quartz; the quantity of quartz to add for canceling completely the second restrahlen band of dolomite, at about 11 μm on the bottom right panel, is 0.022 cm^3 (0.058 g), which corresponds to a thickness of about 84 μm.

In the same way, in the mixture Q2O2, to cancel the first restrahlen band of quartz, between 8 and 10 μm, it is necessary to add about 0.053 g of olivine, which corresponds to about 60 μm and to cancel the second restrahlen band of quartz, above 20 μm, it is necessary to add about 0.046 g of olivine, which corresponds approximately to 55 μm. On the other hand, to cancel the first restrahlen band of olivine, between 10 and 11.8 μm, it is necessary to add 0.040 g of quartz, corresponding to about 60 μm.

In Table 6.1 I summarize the values found for all the restrahlen bands of both samples, Q2D1 and Q2O2. As it can be seen, the values of the penetration depth

Table 6.1: Penetration depth for mixture Q2D1 and Q2O2.

Q2D1

sample	Quartz bands		Dolomite bands	
	$8 \div 10$ μm	$18 \div 23$ μm	$6 \div 7$ μm	$11 \div 11.5$ μm
dolomite	86 μm	83 μm		
quartz			96 μm	84 μm

Q2O2

Sample	Quartz bands		Olivine bands
	$8 \div 10$ μm	$18 \div 23$ μm	$10 \div 11.8$ μm
olivine	60 μm	55 μm	
quartz			60 μm

for different bands of the same mineral are comparable and this is a confirmation that the penetration depth of the radiation is basically linked to each mineral, even if the values found seem to be a function of wavelength: in fact they decrease with increasing wavelength. In this respect, I recall that, during the discussion of the experiment made on mixture Q2D1, in Section 6.1, in particular during the discussion of Figure 6.1, I have noticed that the only band of dolomite that does not reach immediately its maximum intensity is the absorbing band at $2.6 \div 3.2$ μm. Since the same behaviour is not followed by the other two dolomites bands, at $3.3 \div 3.5$ μm and $3.7 \div 4.0$ μm, such occurrence seems to be a confirmation of a larger penetration depth with decreasing wavelength. Unfortunately, at this stage, I do not have enough data to discuss quantitatively such dependence.

However, the most important point is the comparison between the values found for the penetration depth of the radiation and the average size of the particles of each mineral. It is important that only 86 μm of dolomite are sufficient to cancel the first restrahlen band of quartz, since such value is smaller than the mean size of dolomite, which is 192 μm. The conclusion is that a photon, in the MIR spectral range, is not able to reach the underlying quartz, with the consequence that the quartz restrahlen band disappears from the reflectance spectrum of the mixture.

The same discussion can be applied to all the considered cases, with the only exception of olivine, in Q2O2 mixture, whose mean size (48 μm) is slightly smaller than the evaluated penetration depth (60 and 55 μm).

At this point I can draw some conclusions.

Such experiments have shown that the surface distribution of the grains is fundamental, since, the radiation, in the MIR range, does not penetrate deeply into the sample. The most important conclusion is that considering a mixture as intimate, in this spectral range, is not correct, because the radiation "sees" only the first layer of the mixture. From such conclusion two consequences can be derived. The first is about the kind of mixture: in fact, if radiation does not penetrate, it is probably more correct to consider the mixture as areal, instead than intimate, and the disagreement between the measured and calculated reflectance spectra could be due to a wrong interpretation of the mixture. The second is about the NIR spectral range: in fact such experiments can be made also in this range, and if considering the mixture as intimate is correct, then I will find a much greater penetration depth implying that several layers of the two components, mixed homogeneously, together, must be considered. In the following two sections I will discuss both hypotheses, starting from the latter about the confirmation of the intimate mixture in the NIR spectral range.

6.2 Intimate mixture in the NIR range

In this section I will show other experiments made on the same mixtures. Such experiments are another proof of the validity of Hapke approach for the reflectance of intimate mixtures, up to the principal Christiansen feature.

For this reason I have added a larger quantity of material on the surface of the mixtures Q2D1 and Q2O2, in order to check the penetration depth of the radiation in the NIR spectral range. Unfortunately, in this range the choice of the bands is limited to the presence, in the spectrum of each component, of features with a sufficient intensity and easily recognizable.

In particular, for the mixture Q2D1, the bands large enough are those of dolomite, while those of quartz are smaller or near some bands of dolomite; so I have added quartz to the mixture and controlled its thickness in correspondence of the cancelation of the dolomite bands, with the following samples:

1. original mixture at 50% in volume;
2. adding 0.07 g of quartz on the surface;
3. adding 0.08 g of quartz on the surface of the previous sample;
4. adding 0.06 g of quartz on the surface of the previous sample;
5. adding 0.10 g of quartz on the surface of the previous sample;
6. adding 0.19 g of quartz on the surface of the previous sample.

For the mixture Q2O2 the measurements are made considering an olivine band, located at about 2.2 μm. I consider this band, because for canceling the two bands of quartz I need a very large quantity of olivine in volume, and performing such measurements with an appreciable accuracy should be quite difficult. So the samples I have prepared are:

1. original mixture at 55% of quartz in volume;
2. adding 0.13 g of quartz on the surface;
3. adding 0.13 g of quartz on the surface of the previous sample;
4. adding 0.09 g of quartz on the surface of the previous sample.

In Figure 6.5 I show the reflectance spectra of the samples for Q2D1 and in Figure 6.6 of the samples of Q2O2.

In Figure 6.5 (now the component added is always quartz), the absorbing bands of dolomite are in the range 2.6 $\div$ 3.2 μm, 3.3 $\div$ 3.5 μm and 3.7 $\div$ 4.0 μm, but the first is in the same range of a quartz band. The quartz bands are at about 2.6 $\div$ 3.4 μm, 4.35 $\div$ 4.6 μm and 4.65 $\div$ 4.7 μm. As it can be seen, the dolomite bands become smaller and progressively disappear. The second band of quartz (4.35 $\div$ 4.6 μm) is the same for all the samples, while the third does not change anymore when the the quantity of quartz added is about 0.21 g.

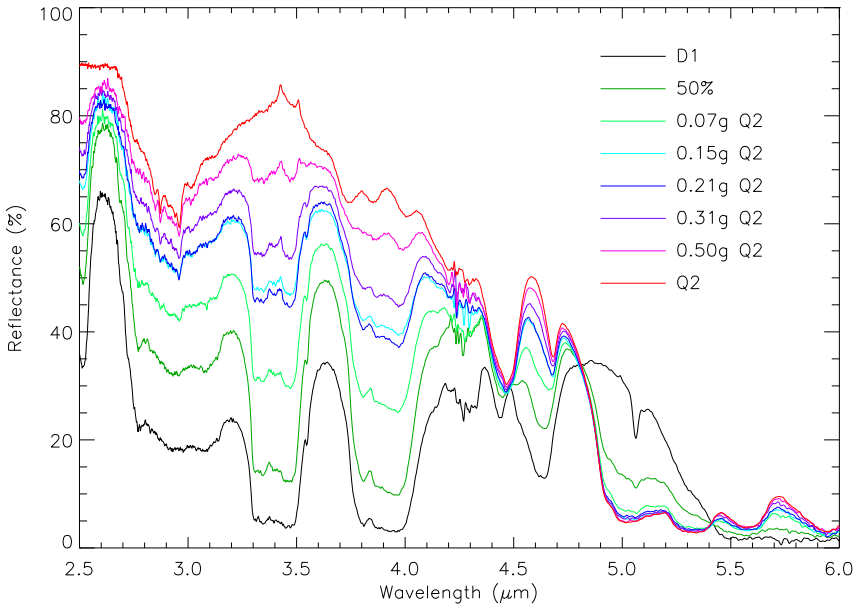

Figure 6.5: Directional hemispherical reflectance measurements for all the new samples of mixtures Q2D1 in the NIR spectral range.

In Figure 6.6, the reflectance spectra of both the components are quite similar: both of them have a maximum at 2.5 μm and then fall down steeply in a deep band between 2.6 and 3.4 μm for quartz and with a deep minimum at 2.6 μm for olivine. After such band, quartz has a reflectance larger than that of olivine, which has a low reflectance without any band in the whole range. The two small bands of quartz at 4.35 $\div$ 4.6 μm and at 4.65 $\div$ 4.7 μm, reach very rapidly an almost stable configuration. The first band of quartz, at about 3 μm, becomes progressively deeper, without reaching a stable configuration. However, in this case I have extended the range to shorter wavelengths, in fact, in Figure 6.6 I show the reflectance spectra starting from 2 μm instead than from 2.5 μm. This is due to the fact that at about 2.2 μm there is a small olivine band, which I consider for the calculation of the penetration depth.

I can make plots, similar to those of the previous section, for some of the bands discussed, and, following the discussion I have already made in the MIR range, I can

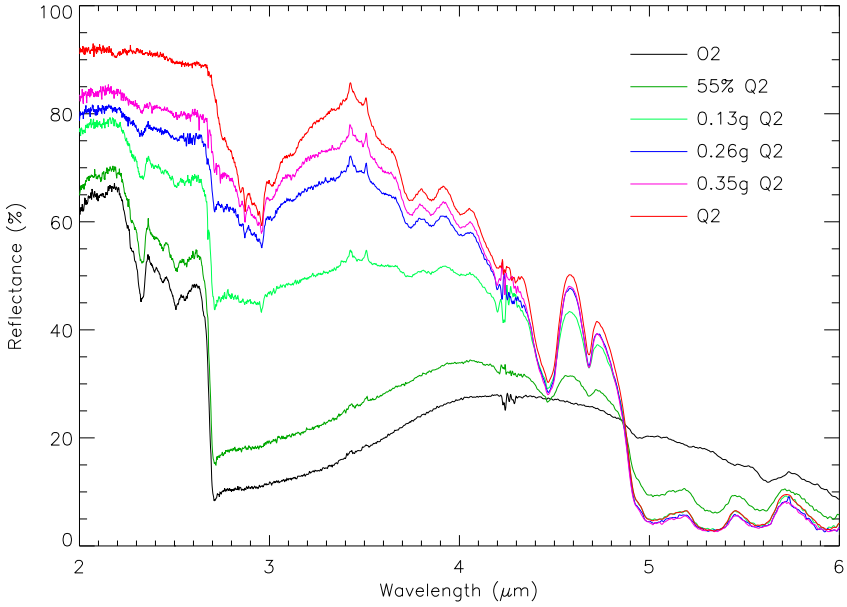

Figure 6.6: Directional hemispherical reflectance measurements for all the new samples of mixtures Q2O2 in the NIR spectral range.

evaluate the quantity of a given component necessary to mask completely the band of the other component from the spectrum of the mixture, and the corresponding penetration depth of radiation. The plots are shown in Figure 6.7 and 6.8

In this case, I have found some difficulties in performing the measurements due to the large volume of material to be added and this is the reason for a not perfect alignment of the experimental points reported in Figure 6.7 and 6.8.

In the mixture Q2D1 I have considered first the band at $3.22 \div 3.64$ μm. Here I must add 0.265 cm^3 (0.694 g) of quartz to cancel completely the absorbing band of dolomite, which corresponds to a penetration depth of 1020 μm. For the second band of dolomite (at $3.64 \div 4.09$ μm) the needed quantity of quartz is 0.229 cm^3 (0.600 g), corresponding to a penetration depth of 880 μm. Such values are much larger than the quartz mean size and the incident radiation interacts with about 10 layers of quartz before being reflected.

In the mixture Q2O2 I have considered the band at $2.21 \div 2.35$ μm and I

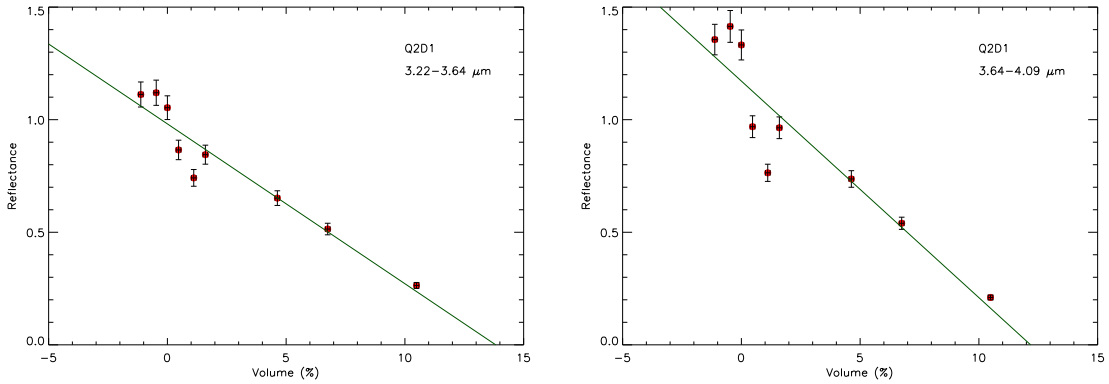

Figure 6.7: Plot of the normalized intensity of the two absorbing bands of dolomite, in mixture Q2D1 (left panel at 3.22 ÷ 3.64 μm and right panel at 3.64 ÷ 4.09 μm) in function of the quantity of mineral added on the surface, in percentage of the total volume.

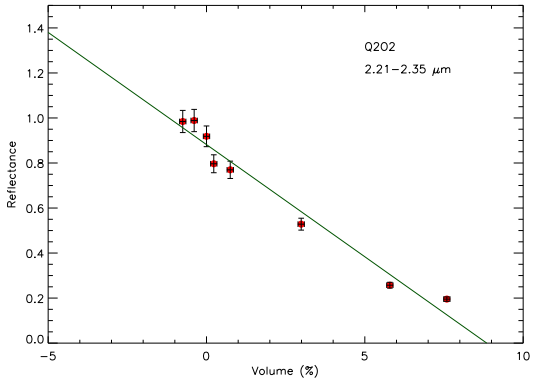

Figure 6.8: Plot the normalized intensity of the absorbing band of olivine in mixture Q2O2 at 2.21 ÷ 2.35 μm, in function of the quantity of mineral added on the surface, in percentage of the total volume.

must add 0.163 cm^3 (0.427 g) of quartz to cancel completely the absorbing band of olivine, which corresponds to a penetration depth of 627 μm. In this case the radiation interacts with at least 6 layers of quartz, before being reflected.

In conclusion, in the NIR range, considering a mixture as intimate is correct. In fact, in more than 6 layers of mineral, it is plausible to assume that both the components of the mixture are present in their defined proportion. The most important result is that in the NIR range much more material must be added than

that necessary in the MIR range, and that the thickness of the latter is comparable with the size of the particles involved.

Such experiments are another proof of validity of Hapke approach for reflectance of intimate mixture in the NIR range. So the validity range of such theory can be extended from 2.5 μm, which is the value tested by several authors (Clark, 1983; Johnson et al., 1983), to the principal Christiansen frequency of the mixture.

6.3 The mixing areal model in the MIR spectral range

The experiments, illustrated in Section 6.1 and discussed in Subsection 6.1.1, have shown that the radiation does not penetrate into the sample because it is extinguished by the first layer of mineral, with the obvious consequence that the surface becomes fundamental for the interpretation of a mixture spectrum. In addition, I have concluded the Section 6.1 making an hypothesis about the most correct way for the interpretation of the mixture spectra, in the MIR spectral range, as areal, instead than intimate, such as in the NIR range.

In this section I show that such hypothesis is correct, because using the areal mixing model, the agreement between calculated and measured spectra improves considerably.

In Section 1.5 I have only defined the areal mixtures saying that their surface is formed by several patches of a single and pure material and the resulting reflectance is a linear combination of the reflectance of each patch, weighted on the relative portion of surface.

Considering a mixture composed of minerals mixed together as areal is problematic, because there is no way for the determination of the real portion of surface occupied by each component. In fact, the experiment made, in particular that shown in Section 5.3.1, demonstrates that in a mixture the components are not mixed homogeneously, so I cannot use the abundance of each mineral to calculate the theoretical reflectance.

In Figure 6.9 I show the comparison between the measured and the theoretical

spectra, calculated using the areal mixing model, assuming that the percentage in volume of each component were the same of the portion of surface occupied.

As it can be seen comparing the Figure 5.1, where I report the spectra calculated with intimate approach, with the Figure 6.9, where I consider the mixture as areal, the agreement in the MIR range, improves for every mixtures with the only exception of O2D1.

However, for a better understanding of the real surface abundance of each component I can use the chi-square function, described in Subsection 3.4.1. In fact, the minimum value of chi-square corresponds to a best fit between measured and calculated spectra. The chi-square values will be discussed in the following subsection. In Figure 6.10 I show the resulting spectra, where the theoretical reflectance has been calculated considering the mixtures as areal and the corresponding portion of surface occupied by each component has been calculated using the lowest value of chi-square found for the mixture in the MIR range and listed in Table 6.2.

As it can be seen, the agreement improves for every mixtures, where I consider the lowest value of chi-square, for the determination of the portion of surface occupied.

It is interesting to notice that the values of surface occupied, for which the chi-square is the lowest, can be divided into two groups: the first is composed of mixture O2D1 and O2D2, for which the percentage of surface is very different from the volumetric fraction (in O2D1 the olivine varies from 50% to 84% and in O2D2 from 75% to 82%), and the second group, with the remaining mixtures, for which the values are very similar, when not the same, to the volumetric ones (in Q2D1 the percentage of quartz varies from 50% to 53%, while in Q2D2 and in Q2O2 the percentage remains the same). In addition the group for which the percentage is different is composed of mixtures for which the intimate approach produces a good agreement, while for the group whose percentage does not vary appreciably is composed of mixtures whose intimate approach produces a very bad agreement. Understanding the reasons of such behaviour could be the subject of a future work.

Comparing the two different approaches (intimate, shown in Figure 5.1, and areal, shown in Figure 6.10), it is possible to notice that the agreement improves in all the spectra.

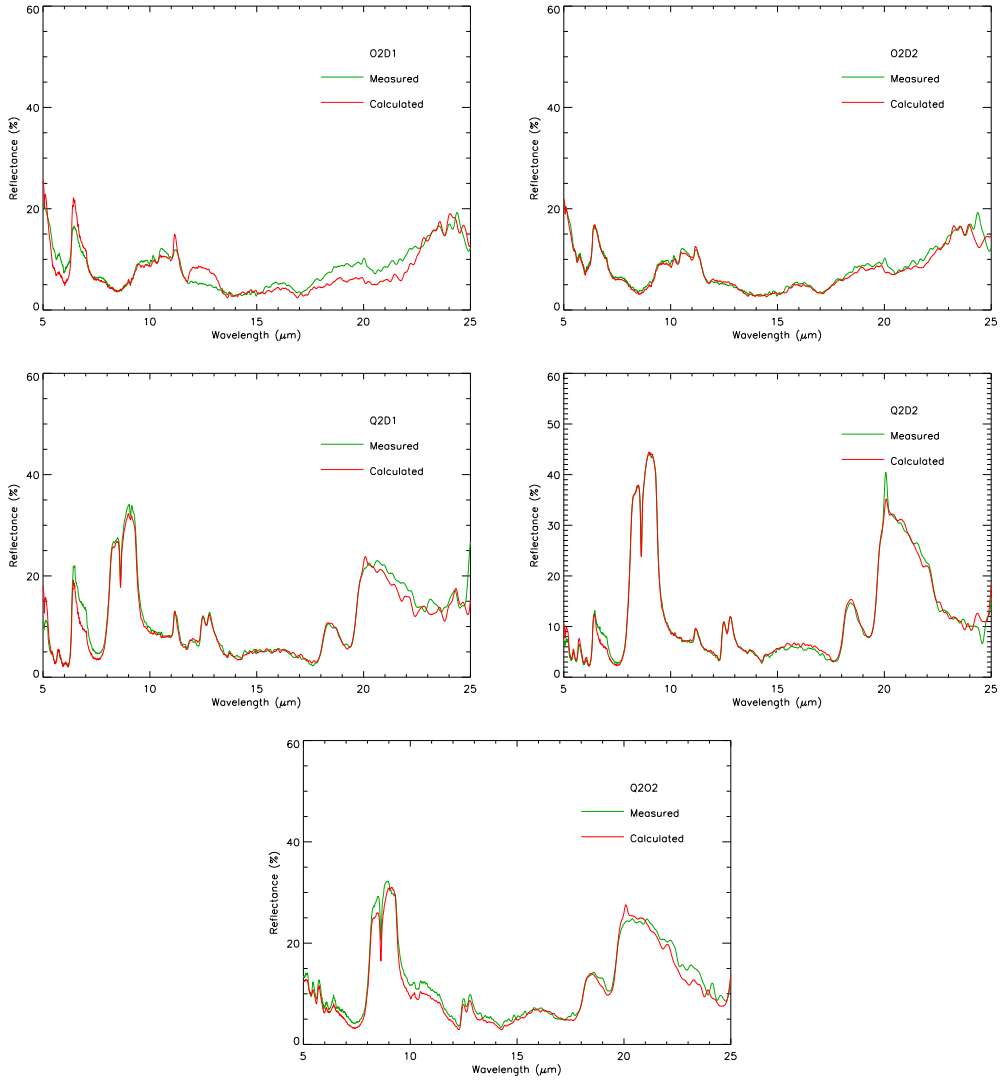

Figure 6.9: Comparison between measured and theoretical spectra for mixtures: O2D1 in the top left panel, O2D2 in the top right panel, Q2D1 in the middle left panel, Q2D2 in the middle right panel and Q2O2 in the bottom panel. The theoretical spectra have been calculated using the areal mixing model, with the named proportion.

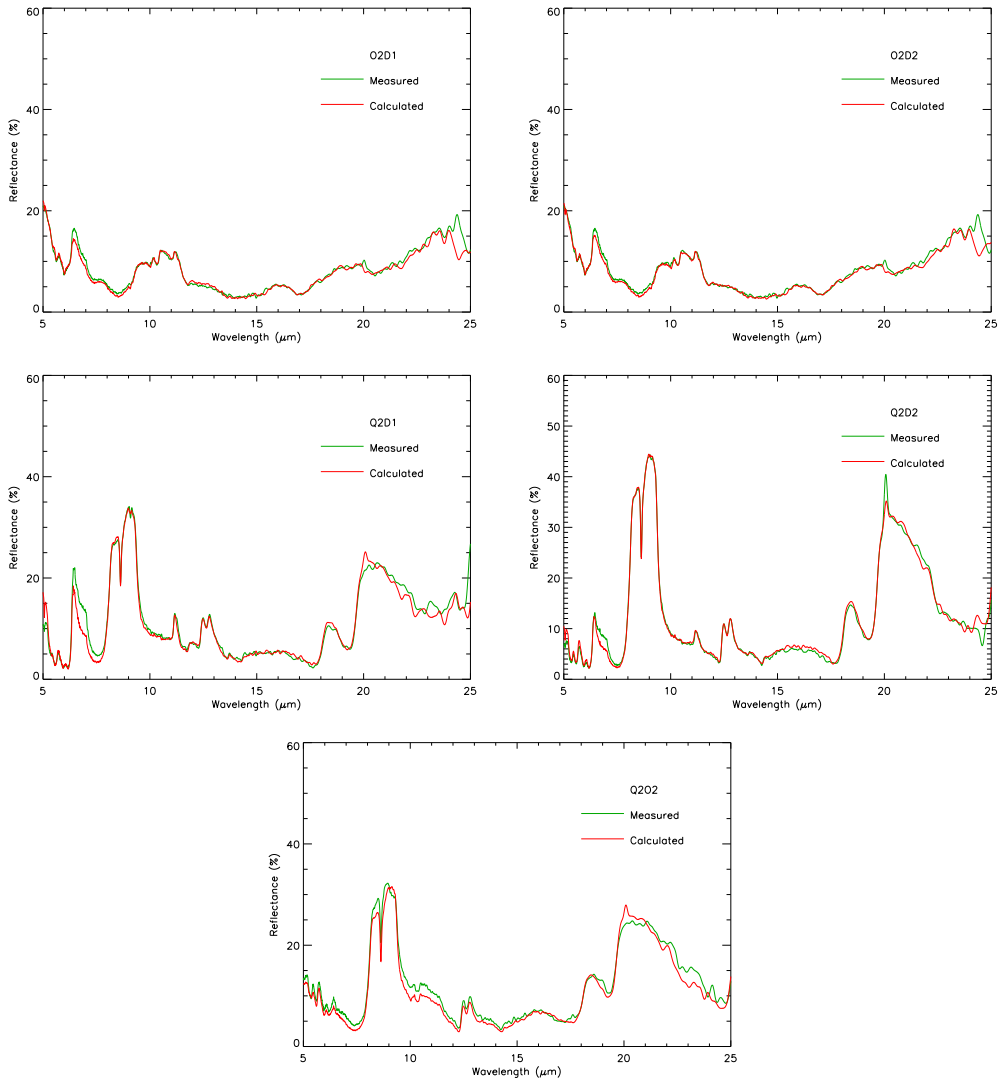

Figure 6.10: Comparison between measured and theoretical spectra for mixtures: O2D1 in the top left panel, O2D2 in the top right panel, Q2D1 in the middle left panel, Q2D2 in the middle right panel and Q2O2 in the bottom panel. The theoretical spectra have been calculated using the areal mixing model, where the corresponding portion of surface occupied by each component has been calculated using the lowest value of chi-square found for the MIR range and shown in Table 6.2.

Looking the mixture O2D1 in Figure 6.10, the only residual disagreement is in the first restrahlen band of dolomite, for which, however, the agreement improves when it is considered as areal.

The mixture O2D2 shows a behaviour similar to that of O2D1, but the disagreement is worse, if it is considered as intimate, and becomes very good if it is considered as areal.

The three mixtures involving quartz show a considerably disagreement when they are considered as intimate (Figure 5.1): in particular, the mixture Q2D1 shows disagreement in the two restrahlen bands of dolomite and in the first and third restrahlen band of quartz, while, if it is considered as areal, the agreement becomes good everywhere with the only exception of the first restrahlen band of dolomite.

The mixture Q2D2 shows a behaviour like that of mixture Q2D1: in particular there is disagreement in the two restrahlen bands of dolomite and in the first and in the third restrahlen band of quartz, when it is considered as intimate, while, if the mixture is considered as areal, the agreement becomes good everywhere with the only exception of the first restrahlen band of dolomite.

Finally, for the mixture Q2O2, when it is considered as intimate, the agreement is very bad, because the spectrum is dominated by quartz, while, in the areal approach, the agreement becomes much better.

In conclusion, considering a mixture as areal in the MIR spectral range, seems to be the most correct form to simulate a mixture spectrum. Such discussion is confirmed also in the following subsection, where I will show the chi-square values found when such mixtures are considered as intimate or areal.

6.3.1 Chi-square

In Table 6.2 I report the chi-square values for compositional mixtures with a *good* grain size distribution. In particular I report the values found using, in the Equation 3.4, the calculated reflectance (r_c) in three different ways: the intimate approach, the areal approach with the volumetric percentage, the areal approach with the percentage corresponding to the lowest chi-square value. The chi-square

Table 6.2: Chi-square values for mixtures with a *good* grain size distribution, calculated for three different spectral intervals.

Sample	**Approach**[a]	χ^2		
		2.5-25 μm	**2.5-5 μm**	**5-25 μm**
O2D1	Intimate (50%)	7.5	13.5	6.8
	Areal (50%)	87.6	206.6	72.8
	Areal	4.8 (84%)	11.7 (83%)	3.9 (84%)
O2D2	Intimate (75%)	12.5	25.6	10.9
	Areal (75%)	6.3	17.1	4.9
	Areal	3.3 (82%)	9.2 (82%)	2.6 (82%)
Q2D1	Intimate (50%)	112.2	59.0	118.8
	Areal (50%)	160.3	1096.3	43.3
	Areal	147.3 (46%)	407.0 (32%)	38.5 (53%)
Q2D2	Intimate (75%)	54.8	262.0	28.9
	Areal (75%)	152.7	1279.9	11.7
	Areal	109.4 (67%)	268.6 (54%)	11.7 (75%)
Q2O2	Intimate (50%)	350.0	7.4	392.9
	Areal (50%)	235.5	1926.8	23.9
	Areal	155 (37%)	40.8 (15%)	23.9 (50%)

[a]The percentage is in volume for the intimate mixture and in area for the areal mixtures, and is relative to the first component.

has been calculated in the whole spectral range and two separate spectral regions, NIR and MIR; for a homogeneous evaluation of the values obtained, I have chosen as separating wavelength between the two regions the value of 5 μm, good for all the mixtures, since the principal Christiansen frequency has different values for each mixture.

Looking at this table, the first observation is relating to the calculated values of chi-square, since they appear too high to suggest a reasonable agreement. This is due to several causes, all linked to the comparison of whole spectra, but, in first approximation, I can consider as *good values* all those lower or just above ten, for which a very good visual agreement is obtained between the considered spectra.

As I have explained in Section 3.4.1, the reasons of a possible high value of chi-square could be: (*i*) the standard deviation, calculated on a single mineral, instead of than for a mixture; (*ii*) considering only the standard deviation relating to the

Table 6.3: Chi-square values for granulometric mixtures, calculated for three different spectral intervals.

Sample	**Approach**[a]	χ^2		
		2.5-25 μm	**2.5-5 μm**	**5-25 μm**
D1D2	Intimate (50%)	6.4	1.8	7.0
	Areal (50%)	5.2	2.1	5.6
	Areal	5.1 (42%)	1.6 (56%)	5.2 (44%)
O1O2	Intimate (33%)	8.0	16.9	7.0
	Areal (33%)	7.3	9.1	7.1
	Areal	2.0 (45%)	0.5(43%)	2.1(46%)
Q1Q2	Intimate (50%)	8.5	11.3	8.1
	Areal (50%)	8.4	35.3	5.1
	Areal	6.0 (61%)	3.0 (77%)	4.5 (56%)

[a]The percentage is in volume for the intimate mixture and in area for the areal mixtures, and is relative to the first component.

measured spectrum, and not also the experimental uncertainties associated with the calculated spectrum; (*iii*) changes in the environmental conditions due to the long time necessary to perform the measurements.

I have also performed such calculation on granulometric mixtures, because for such mixture the visual agreement between measured and calculated spectra is very good; so I can use the chi-square values as a reference for the discussion of compositional mixtures. The values found are reported in Table 6.3. As it can be seen, the granulometric mixtures have values of chi-square very low if they are considered as intimate (always under ten in the whole spectral range). This is a confirmation that a chi-square of about ten can be used as a reference for the evaluation of a good agreement between two spectra. In addition, it is possible to notice that such mixtures exhibit a rather good agreement also assuming they are areal, in the whole spectral range.

Coming back to Table 6.2, the two mixtures involving olivine and dolomite, which show a good agreement and low chi-square values in the intimate approximation, show an improvement assuming they are areal. The mixtures for which there is no agreement, when they are considered as intimate, are those with quartz, as it can

be seen in Figure 5.1 and confirmed by the high chi-square value, but the agreement definitely improves, if they are considered as areal.

I have already shown, in Section 6.2, that the intimate approximation is the most appropriate way for the interpretation of the mixtures in the NIR spectral range, and such conclusion is confirmed by the chi-square values. The values obtained are, in the range $2.5 \div 5.0$ μm, almost always lower for the intimate mixtures than for the areal ones, while the opposite is occurring in the range $5.0 \div 25.0$ μm.

In spite of that, the values of the chi-square, in the NIR region, are still unacceptably high for the two mixtures involving quartz and dolomite, but, as I have explained in Section 5.4, the disagreement can be due to an inhomogeneity in the distribution; such disagreement is confirmed by the high value of chi-square, which is the highest value in this range.

In the MIR spectral range the agreement improves for all the mixtures when they are considered as areal, using the modified percentage of surface, and this confirms the discussion made in the previous section.

The main point emerging from the above discussion and the comparison between the spectra reported in Figure 5.1 and in Figure 6.10 is that the experimental spectra are almost always better fitted assuming an *intimate mixture* in the range between 2.5 and 5.0 μm and an *areal mixture* between 5.0 and 25.0 μm.

6.4 Conclusions and future works

From the above discussion it is reasonable to consider the mixtures I have analyzed as *hybrid* mixtures, i.e. intimate between 2.5 and 5.0 μm and areal between 5.0 and 25.0 μm.

As already pointed out, this behaviour is directly linked to the different values of the absorption coefficients in the restrahlen and absorption bands, in fact, as I have explained in Section 1.3, the restrahlen bands are dominated by first surface scattering, because the absorption coefficient is too high to allow the photon to survive inside a grain. An abstract of Gardiner & Salisbury (1989), quoted by Salisbury (1993), states that, due to the high value of the absorption coefficient

in the restrahlen bands, such spectral region is dominated by surface scattering and concludes that in such regime the directional-hemispherical reflectance of any mineral mixture is a linear combination of the reflectance of the single components, i.e. an areal mixture. On the contrary, in the spectral range dominated by volume scattering, such as the absorption bands region, the mixing model becomes highly nonlinear.

It is clear that my experimental findings, about the need of considering a mixture both as intimate and as areal, in order to justify the measured reflectance, fully confirm the interpretation of Salisbury (1993). In other words, the need to use areal mixtures, instead of intimate, can be interpreted in terms of the reduced penetration capability of the incident radiation. In fact, the use of areal mixtures is fully justified, if the penetration depth, due to the high value of the absorption coefficient, is limited basically to the first layer of the particulate, as I have shown.

In conclusion, in this work, I have developed and applied to laboratory samples a procedure for the analysis of particulate mixtures, which can be useful for the interpretation of the spectra of planetary surfaces.

The main point of such procedure is the comparison between the measured directional-hemispherical reflectance of a mixture and the same quantity derived, from the measured reflectance of the components, through an elaboration based on Hapke theory. The results I have achieved can be summarized as follows:

1. I have successfully extended to 5 μm the possibility to compare experimental results and theoretical predictions related to reflectance spectra, using Hapke theory of reflectance for intimate mixtures;

2. I have experimentally checked, by means of granulometric mixtures, the validity of the hypothesis of isotropic scattering, identical spherical particles and the diffraction condition, and such finding can have interesting consequences in the simplification of the analysis of the spectra of particulate mixtures;

3. I have suggested a possible explanation, for the inadequacy of the comparison between measured and calculated spectra, based on the behaviour of absorp-

tion coefficient;

4. I have solved such inadequacy by considering the same mixture either as intimate or as areal according to the penetration depth of the incident radiation, checking experimentally the consistency of such approach;

5. I have shown that the non-homogeneous distribution of the components implies some difficulties in the determination of the real portion of surface occupied by each component.

In this chapter I have considered the mixtures as areal in the MIR spectral range and, even if considering the abundance of each component produces an improvement in the agreement between the measured and the calculated spectrum, I have decided to take into account also the possibility of a non-homogeneous distribution of the particles, with the consequence that, on the surface, the percentage of each component is different from that of the whole mixture. Under such condition, determining the real surface portion occupied by each component needs a careful evaluation and poses new problems to the interpretation of planetary spectra.

Another consequence of my work is that considering a mixture as areal implies that such spectral range is not really appropriated for the determination of the composition of a planetary surface, because it is possible to associate only the result to the first layer of the surface, which could be deeply affected by atmospheric effects.

However, in this PhD thesis, I have illustrated an experimental work focused on the behaviour of particulate mixtures in the IR spectral range, even if my findings are not conclusive and much more work is necessary, to improve the theoretical fit. For example, it could be interesting to understand the behaviour of the samples with a *bad* grain size distribution. A preliminary calculation suggests that an areal distribution produces a considerable improvement in the agreement between measured and calculated spectra, with respect to the intimate hypothesis. Moreover, understanding the relation, if it exists, between the grain size and the portion of surface occupied is fundamental, before making any consideration about the behaviour of more complicated mixtures.

Conclusions

In this PhD thesis I have discussed a laboratory study about mineral mixtures. In particular such work has been thought in order to understand how to acquire information, such as abundance and grain size, about each component of a mixture, starting from the spectrum of a mixture. The main point of the procedure, followed in this work, is the comparison between the measured directional-hemispherical reflectance of a mixture and the same quantity, derived from the measured reflectance of the components.

The theory used for such work is derived by the Theory of Reflectance described by Hapke (Hapke, 1993), with some hypotheses aimed to simplify the relations. Such hypotheses are: identical spherical particles, isotropic scattering and extinction efficiencies equal to unit. These hypotheses have been applied to the theory in Chapter 2 and have been verified in Chapter 4. The most important result about such hypotheses is the fact that they are valid also for small particles, while the size parameter is comparable to the wavelength. In such case the diffraction is not negligible and the extinction efficiency should not be equal to unity. Instead, I have demonstrated that, if particles are close together, such as for laboratory sample and planetary regolith, the diffraction condition can still be applied, with the consequence that the hypothesis about the extinction efficiency is valid for all the samples, independently to their grain size.

Another important result, discussed in Chapter 4, concerns the isotropic scattering. In fact, I have experimentally checked, by means of granulometric mixtures, the validity of the hypothesis of isotropic scattering and such result can be extended to every kind of mixtures. Such finding can have interesting consequences in the

simplification of the analysis of the spectra of particulate mixtures, because the equation describing the reflectance of a mixture becomes much easier to work with.

In Chapter 5, I have successfully extended up to 5 μm, the possibility to compare experimental results and theoretical predictions related to reflectance spectra, using Hapke theory of reflectance for intimate mixtures. Such result is very important for its application to the study of planetary surface in this spectral range, since, a verification of the theory above 2.5 μm has never been made before.

In the last chapter I have experimentally tested that considering a mixture as areal, instead than intimate, above the principal Christiansen feature, produces a good agreement between the measured and the calculated spectrum. This is related to the fact that, due to the high absorption coefficient, the radiation cannot penetrate deeply into the sample. So, a good idea could be considering a mixture as *hybrid* mixtures, i.e. intimate between 2.5 and 5.0 μm and areal between 5.0 and 25.0 μm. The penetration depth of the radiation could also be a function of wavelength, since it seems to decrease with increasing wavelength both in the NIR and in the MIR spectral range. In order to assess this point it is necessary to perform some dedicated experiments, which are planned for the near future.

In addition, I have shown, both in Chapter 5 and 6, that the distribution of each component is not homogeneous. Even if the consequence of such inhomogeneity does not produce a major disagreement in the NIR range, in the MIR range such contribution is dominant. In fact, I have experimentally shown that the radiation does not penetrate into the sample, and only the first layer of surface produces the reflectance spectrum. In this scenario, an inhomogeneous distribution of particles could have major effects on the resulting spectrum. I have solved such problem using the chi-square function. However more work has to be done in order to understand the relation, if it exists, between the grain size and the distribution; after that it will be possible a full study of mixtures behaviour and its application to planetary surface.

Appendix A

The search for ancient life on Mars and the IR spectroscopy of Earth analogues

The search for ancient life on Mars is a very attractive subject in the study of the planet and it is the purpose of many studies and space missions.

One of the main aims of the next Mars space missions (e.g. Exomars, in which Lecce group has a very active role with MIMA, a spectrometer on the rover Pasteur, see Appendix B) will be to characterize biochemically the surface and the subsurface of the planet searching for elementary forms of life. To do this, it is necessary to have a correct approach to this kind of problem and laboratory analysis, carried out on Earth analogues of Martian ground, is a fundamental support for the planning of suitable instrumentation able to recognize the biological origin of a sample (Blanco et al., 2008).

Today Mars is geologically inactive and, consequently, the recycling of fundamental elements for life, such as C, N, O is very limited. However, in the early Mars, the environment was as warm and wet as in the early Earth, with a dense CO_2 atmosphere (Pollack et al., 1987), allowing the presence of liquid water. The importance of liquid water for life is well known and, in the past, Mars surface lost its water and, contemporarily, its life (Westall, 1999; Friedmann and Koriem, 1989; McKay and Stoker, 1989).

At present Mars shows evidence of transient liquid water on very small scale in

the form of gullies (Malin and Edgett, 2000), but these phenomena are sporadic and too small to permit the life formation; for this reasons the study for life detection on Mars is devoted to find fossils of bacteria and very small size organisms.

The starting point is the characterization of fossil bacteria, that occur principally by *permineralization*, so that organic material is preserved *in situ* by permeated silica in solution, which includes organic material in a matrix (Westall, 1999). Another type of fossilization is the *mineral replacement*, which consists in a replacement of organic material by minerals as aragonite and calcite. This happens mainly when the organism is bigger. These two minerals are two polymorphs of calcium carbonate ($CaCO_3$) and are particularly interesting because both of them could be formed by abiotic processes as well as by biological activity. For this reason some authors, e.g. Cabane et al. (2001, 2004), Stalport et al. (2005), Orofino et al. (2007), Blanco et al. (2008) have investigated these two minerals, in particular the comparison between the main characteristics of biotic and abiotic material and their behaviour. A result, found by Cabane et al. (2004) and Stalport et al. (2005), is that the thermal degradation of abiotic calcite starts at higher temperature than that of biologic calcite. These works are based on Differential Thermal Analysis (DTA) together with Gas-Chromatography and Mass Spectroscopy. However, Orofino et al. (2007) and Blanco et al. (2008) add the IR spectroscopy performed in transmission, but all these techniques can not be applied in remote measurements. The necessity to find an accurate technique to distinguish biotic and abiotic calcite applicable to remote sensing measurement is the starting point of this part of my work. It is clear that transmittance measurements are not adequate, and ought to be substituted with reflectance measurements, more suitable to Mars remote sensing observations.

Reflectance spectroscopy produces spectra very different from those in transmission, as already widely discussed in this PhD thesis (for example in Section 1.3).

My work is principally a characterization and a comparison of the reflectance spectra of calcite and aragonite mineral with different origins: both abiotic and biotic of different epoches.

In order to do this, the experimental apparatus must be optimized, so this work has been preceded by an accurate study of the spectrometer, discussed in

Section 3.4.1, aimed to find the best procedure for obtaining a good spectrum, capable to show also small features, with small uncertainties and good resolution. This preliminary work has shown that a measurement with a resolution of 4 cm^{-1} with 100 scans is, in most cases, sufficient to obtain a good spectrum.

The fossil samples analyzed are a *Pecten sp.* (a fossil of calcite of Middle Pleistocene, $0.8 \div 0.1$ Myr, from Salento, Italy), with grain size between 50 and 200 μm and an *Ampullinopsis crassatina* (a fossil shell of aragonite of Oligocene, $23 \div 30$ Myr, from Salento, Italy), with grain size $20 \div 50$ μm. I have also analyzed abiotic Calcite ($CaCO_3$) with two different grain sizes: $20 \div 50$ μm and $50 \div 200$ μm, both of them studied before and after being washed (for the washing procedure see Section 3.2), with the principal aim to see if there are differences with the fossil samples. The principal characteristics of each sample are listed in Table A.1.

Table A.1: Characteristics of the analyzed samples.

Material	**Size range** μm	**D[4,3]** μm	**washed or not**	**Code**
Calcite abiotic (cl1)	$20 \div 50$	39.470	not washed	$C1\_NW$
	$20 \div 50$	48.735	washed	$C1\_W$
Calcite abiotic (cl2)	$50 \div 200$	152.047	not washed	$C2\_NW$
	$50 \div 200$	157.802	washed	$C2\_W$
Pecten sp.	$50 \div 200$	112.012	not washed	$F1$
Ampullinopsis crassatina	$20 \div 50$	not avaliable	not washed	$F2$

The procedure and the instruments used have been the same of the study of mineral mixtures described in Chapter 3. For the *Ampullinopsis crassatina* it was not possible to perform a full grain size analysis because the sample was not enough for the measurement.

The resulting spectra of all the abiotic calcite samples are shown in Figure A.1, where I have shown both the sample of C1 (top panel) and C2 (bottom panel). As it can be seen in both the panels, the washed samples have always a higher spectral contrast in the first restrahlen band than that of not washed samples: this is due to the removal of fine particles from the surface of bigger grains, since surface scattering

process produces a decreasing band depth with decreasing particle size (Salisbury et al., 1992). In addition both absorption bands and transparency features increase their spectral contrast with decreasing particle size, due to the volume scattering process. This is particularly clear comparing the spectra of Figure A.1: the smaller sample (C1) has always a spectral contrast considerably higher than the bigger one (C2) excluding the first (7 μm) and the second (11.4 μm) restrahlen band, where the volume scattering, with the decreasing particle size, reduces the spectral contrast up to the total cancelation of the band if the particles are very small (Salisbury and Wald, 1991).

In Figure A.2 the spectra of *Pecten sp.* (F1), *Ampullinopsis crassatina* (F2) and abiotic calcite (C1_NW and C2_NW) are reported. I have chosen the not washed sample of both the grain sizes of abiotic calcite because the grain size distribution of the fossil is really wide (see Figure A.3).

The fact that the grain size distribution of the fossil of calcite is so wide can be noticed also in the reflectance spectrum (see Figure A.2). In fact the low spectral contrast is characteristic of big particles, while the first restrahlen band is very small and the second one is totaly absent, as for very small particles.

Looking the Figure A.2 with more attention, some differences could be noticed between the biotic (F1) and abiotic sample of calcite: for example a little band at 9.2 μm appears in the spectrum of the fossil. This band is due to either vaterite or aragonite (Farmer, 1974; Salisbury et al., 1992) (both are allotrope forms of calcite) and, in general, vaterite is the first deposit on a shell in the fossilization process. Another difference is the band at 12.1 μm, present only in the fossil; it is not clear the origin of this band, because it is not an active band in reflectance spectrum of calcite and of its allotropes and it could be caused by the biotic origin of this fossil. An EDX analysis shows that the fossil is not composed by pure calcite, but different inclusions are present, such as Na (0.27%), Mg (0.17%), Si (0.20%) and S (0.20%). In particular a stretching between Si-O-Si could explain this band (Farmer, 1974) and probably a very small quantity of Si could produce such band, excluding the possibility of a biological marker.

Finally I have measured the spectrum of an aragonite fossil (F2) and, as it can

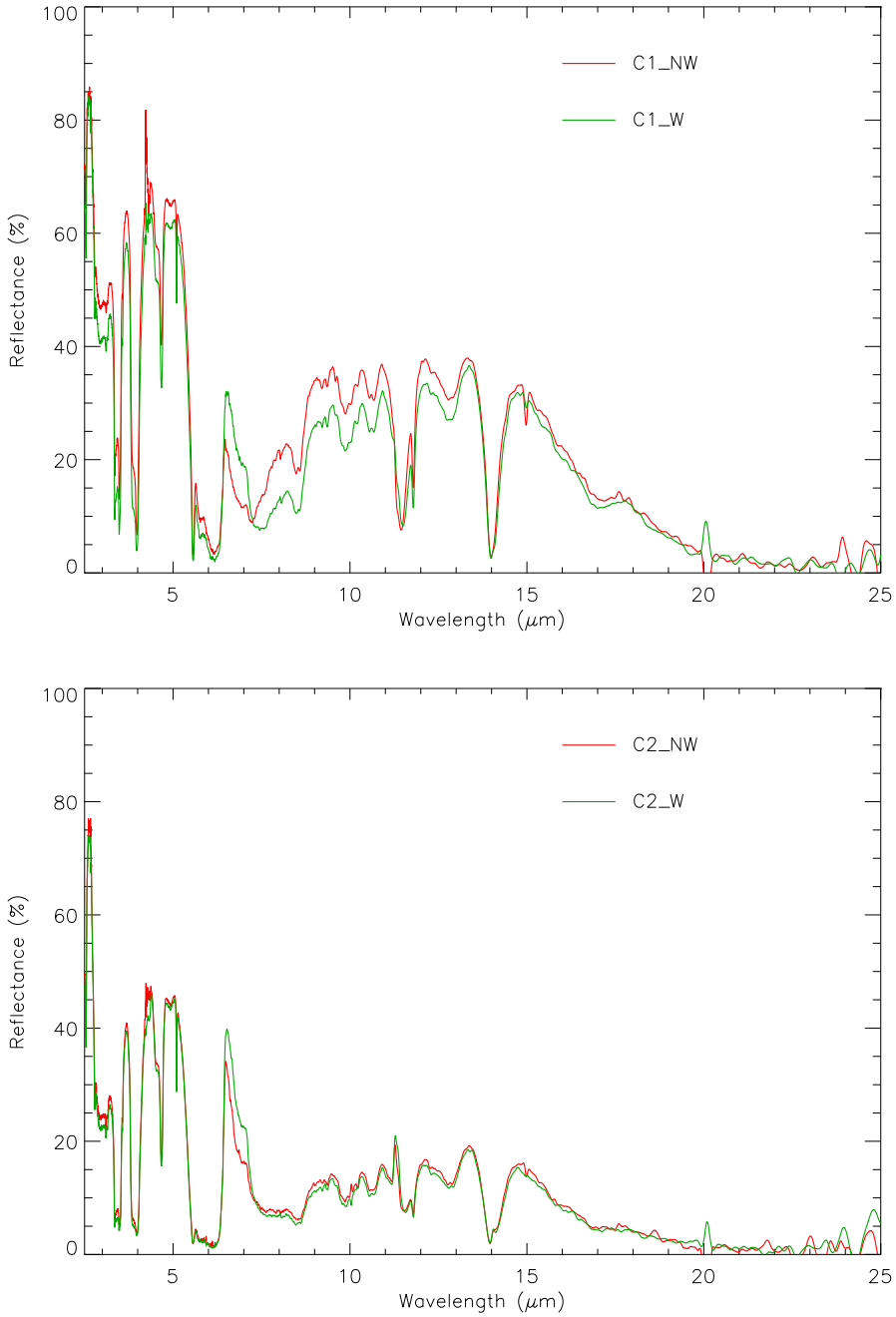

Figure A.1: Measured spectra of C1, both washed and not, in the top panel and of C2, both washed and no, in the bottom panel.

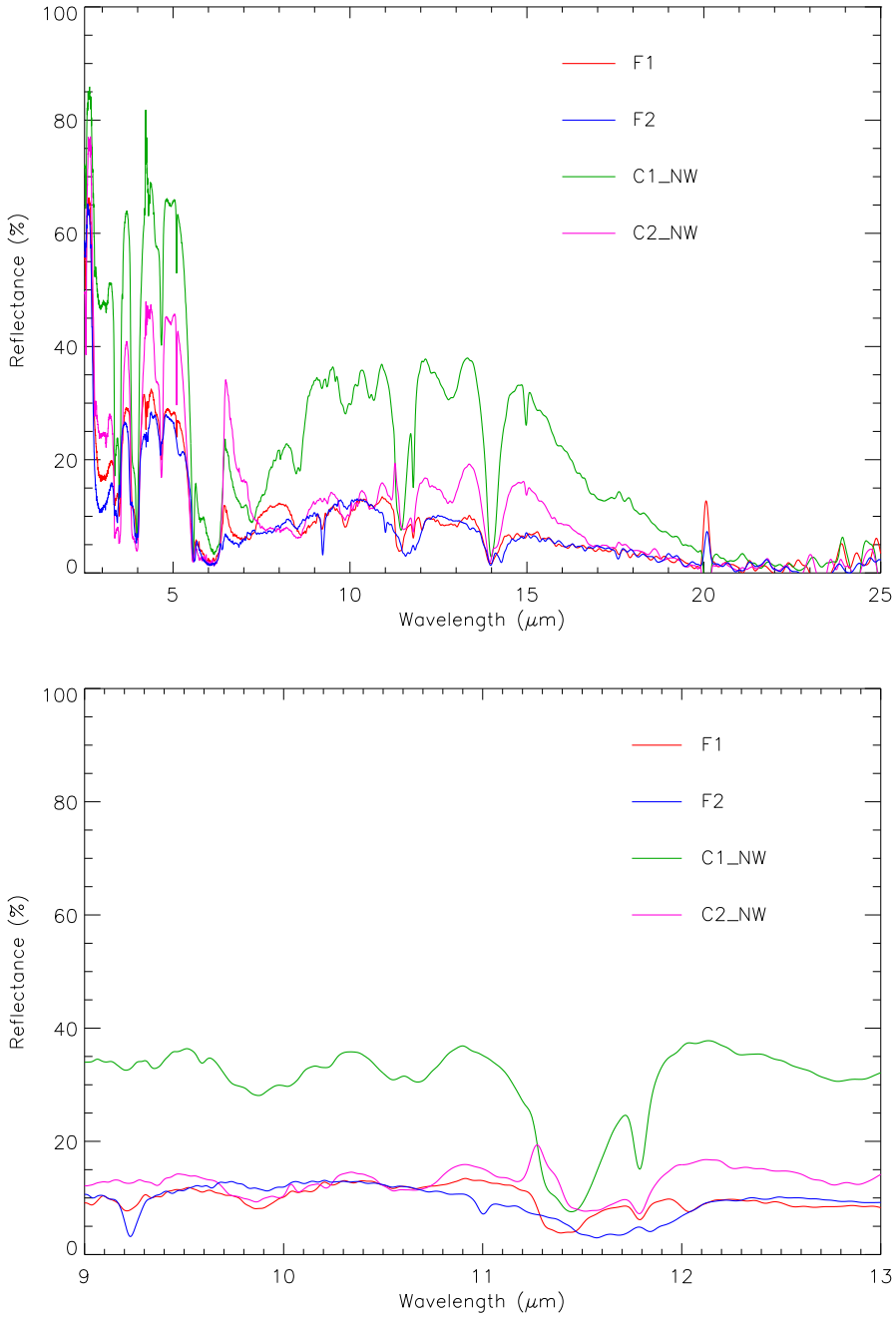

Figure A.2: In the top panel is reported the spectra of *Pecten sp.* ($F1$), *Ampullinopsis crassatina* ($F2$) and abiotic calcite ($C1\_NW$ and $C2\_NW$), while in the bottom panel the most interesting spectral region are expanded.

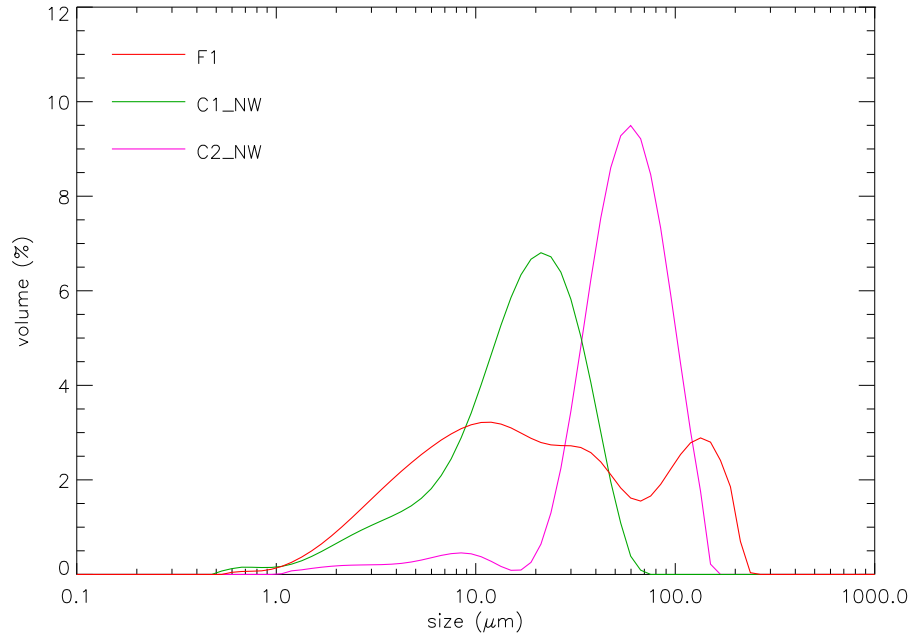

Figure A.3: Grain size distribution of *Pecten sp.* and not washed calcite fine and coarse.

be seen in Figure A.2, the two spectra are quite similar, validating the hypothesis of the origin of the band at 9.2 μm, which is also present in the spectrum of aragonite (Farmer, 1974; Salisbury et al., 1992). It is interesting to note that such feature is stronger in the spectrum of the aragonite fossil, which exhibits another band, also characteristic of aragonite, at about 11 μm. In addition the band at 12.1 μm is not present, and this could be a confirmation that this band is caused by the Si-O-Si stretching.

This first analysis, made using only reflectance spectroscopy in the NIR spectral range, is not very encouraging about the possibility of recognizing the possible biological origin of Martian samples. In fact no particularly evident features have been found and the discrimination between biotic and abiotic minerals seams to be very difficult, using only reflectance spectroscopy. Better results could be obtained, extending the study to other kinds of fossils and in other spectral regions. However my impression is that the reflectance spectroscopy alone is not an adequate technique for this kind of purpose and much effort should be applied in developing different

techniques until the most adequate research tools will be found.

Appendix B

MIMA

The *Martian Infrared MApper* (MIMA) instrument is a FT-IR spectrometer which will be mounted on the rover's mast and will be launched in 2016, on board of ExoMars, an ESA mission.

The principal objectives of such mission are:

- to search for signs of past and present life on Mars;
- to characterize the water geochemical environment as a function of depth in the shallow subsurface;
- to study the surface environment;
- to study the subsurface to understand the evolution of Mars.

In particular, the spacecraft consists of a Carrier Module and a Descendent Module, which will have on board several instruments. The Descendent Module consists of a mobile Rover and a stationary Lander. On the Rover is mounted MIMA, a drill, a sample preparation and distribution system (SPDS), and other instruments.

MIMA has been constructed for two different goals:

1. to determine the bulk mineralogical composition, target and assist in the selection of the specific rocks and soil to be investigated by means of other instrumentations;

2. to study the atmosphere to gather information about meteorological conditions at the landing site and to measure gases.

So, the scientific objectives are:

1. to reveal and record the climate;

2. to observe the atmosphere;

3. to study the mineral groups on the surface;

4. to contribute to the search for life.

Such specific goals and objectives require accurate measurements of both surface (both rocks and soils) and atmosphere spectra, so the resolution must be sufficient to reveal the characteristics features of the principal minerals, such as carbonates, sulphates, silicates, phillosilicates, organic molecules and mineral formed in water.

Such instruments perform its measurements from 2 to 25 μm, with different spectral resolutions, and two channels: the short wavelength channel (SW) from 2 to 5 μm and the long wavelength (LW) from 5 to 25 μm. In Figure B.1 I show a photo of a prototype constructed in the IFSI-INAF laboratory in Rome.

I have already said in Section 1.2, that I am involved in this project, with the characterization of the instrument. In particular I have prepared some minerals to test with the prototype. The procedure for the sample preparation is the same explained in Section 3.2, without the washing process. Such minerals are listed in the following table:

Table B.1: Characteristics of the minerals.

Material	**Size range** μm
Calcite, $CaCO_3$	$0 \div 36$
	$125 \div 250$
Olivine, Mg_2SiO_4	$20 \div 50$
	$200 \div 300$
Gypsum, $CaSO_4 * 2H_2O$	$50 \div 106$

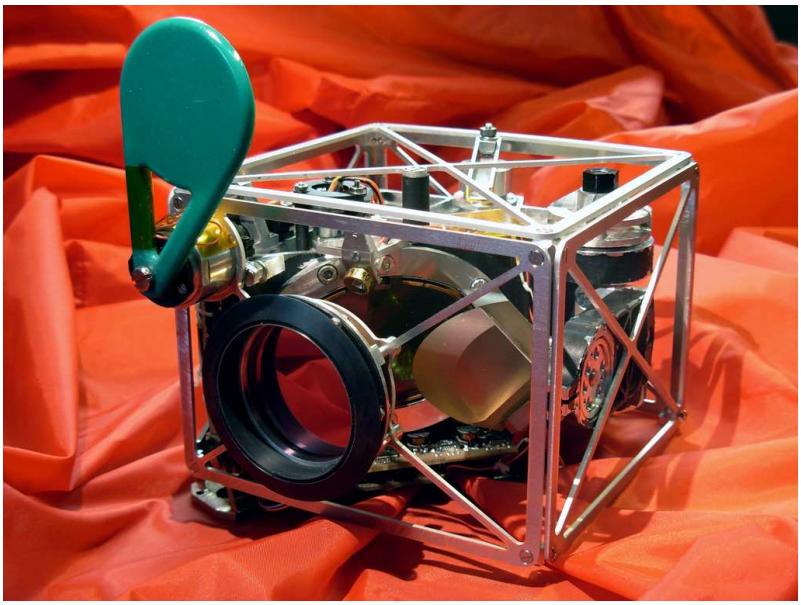

Figure B.1: A prototype of MIMA.

Such minerals have been chosen taking into account, not only their implication on Martian surface, but also their features. In fact the calcite samples of the two grain sizes have a very different behaviour: the smallest calcite has a very high absorbing bands and transparency features, while the biggest has very strong restrahlen bands. The same happens also for the two samples of olivine, even if such behaviour is less evident. However, such mineral is important because it has been found on Martian surface (Bandfield, 2002; Bibring et al., 2006). The gypsum has been chosen for its importance for the Martian climatological history (Lellouch et al., 2000; Fonti et al., 2001; Bandfield et al., 2003; Arvidson et al., 2006); in particular it is an evaporite and its formation happens in presence of liquid water.

The principal aim of such measurements is the comparison with those performed using MIMA, to see if MIMA is able to recognize the main features of such minerals. For this reason a thorough granulometric analysis is not necessary.

The directional hemispherical reflectance of all these minerals has been measured in the laboratory of the University of Salento, with the spectrometer Perkin Helmer Spectrum 2000, described in Section 3.4. In Figure B.2 I report the spectra of

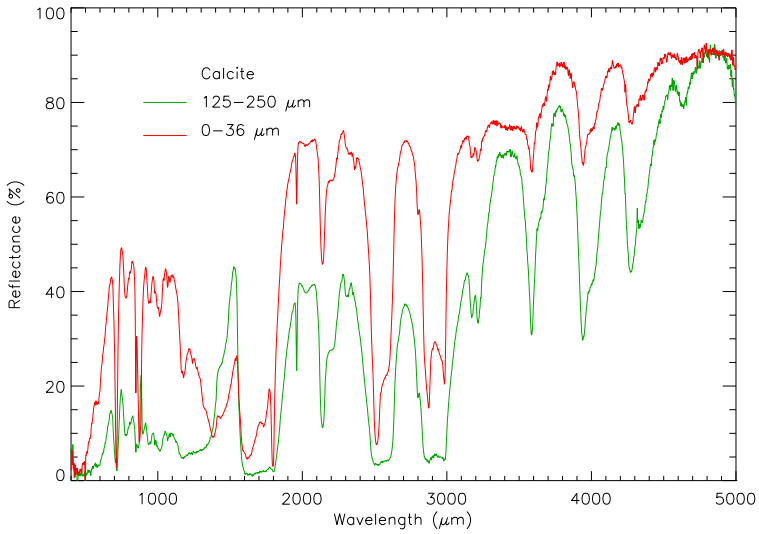

Figure B.2: Directional hemispherical reflectance of both the calcite samples.

both the calcite samples, in Figure B.3 those of both the olivine samples, and, in Figure B.4, I show the spectrum of gypsum.

The measurements with MIMA have been performed in the IFSI-INAF laboratory in Rome. In Figure B.5 I report some measurements performed with the SW channel of MIMA. In the left panel I show the spectrum of calcite with grain size $125 \div 250$ μm and in the right panel the spectrum of gypsum. The signal of the long channel is too low, probably due to a malfunctioning of the corresponding detector and shall be repeated in the near future.

As it can be seen, such measurements are rather noisy; however, it is possible to recognize the main spectral features.

In particular, looking at the calcite spectrum, performed by MIMA, it is possible to distinguish two small bands at about 2300 cm^{-1} (4.3 μm) and 2600 cm^{-1} (3.8 μm). As it can be seen such absorption bands are quite similar to the same bands of the biggest calcite, while the smallest has the same bands with higher intensity.

Also the gypsum is easy to recognize, in particular the two big absorption bands have the same behaviour of the gypsum measured in laboratory, even if their inten-

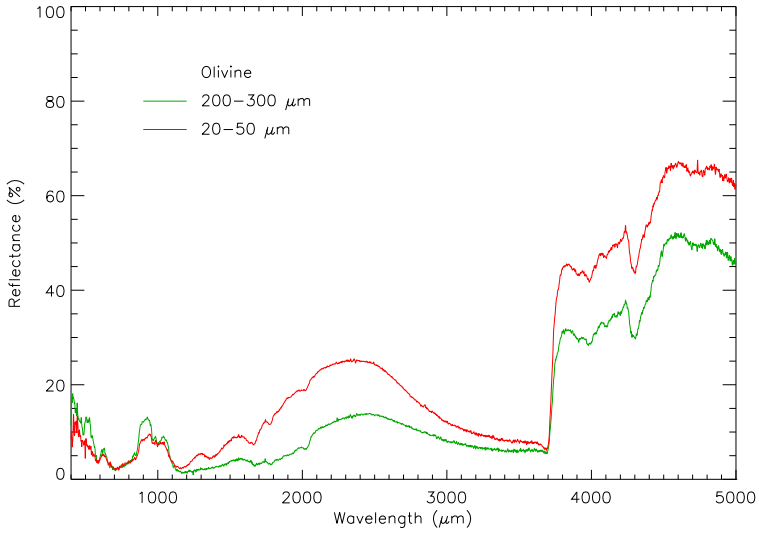

Figure B.3: Directional hemispherical reflectance of both the olivine samples.

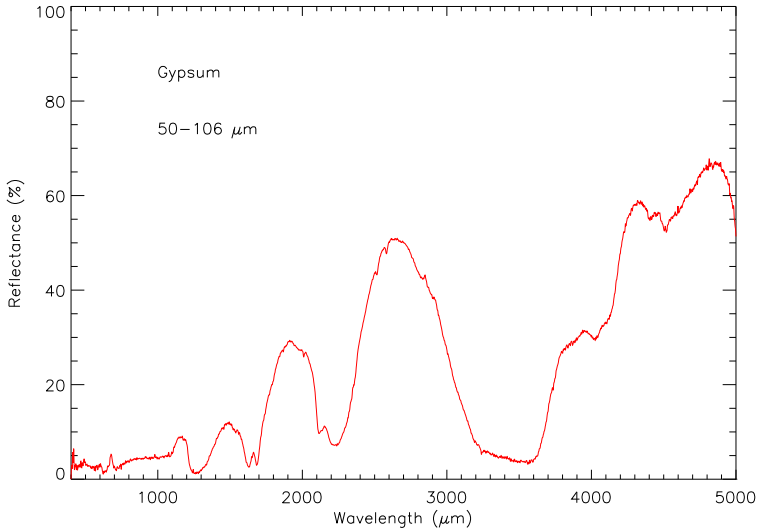

Figure B.4: Directional hemispherical reflectance of the gypsum sample.

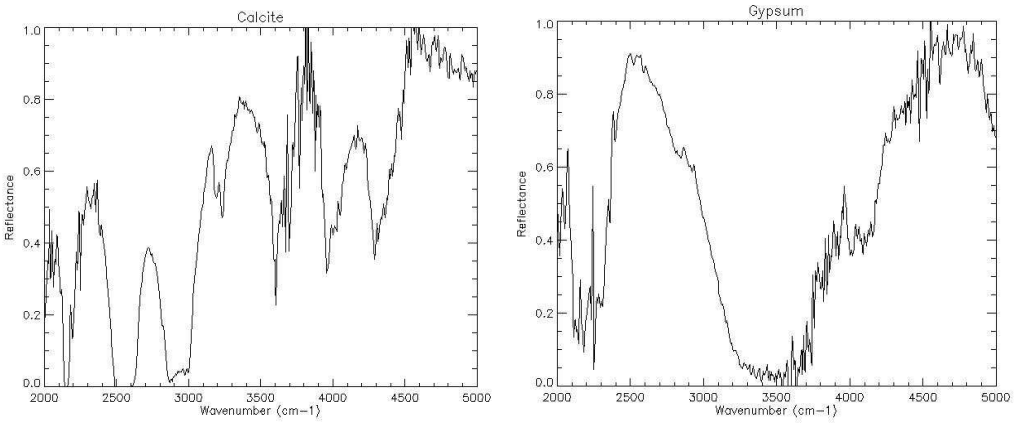

Figure B.5: MIMA reflectance measurements: of calcite 125 ÷ 250 μm in the left panel, and of gypsum 50 ÷ 106 μm in the right panel.

sity is larger in the spectrum measured with MIMA.

Since these measurements are only a first step, many problems have been found during such measurements and for the calibration of the spectra. However the obtained results must be considered as a success because the instrument works correctly, even if not at the maximum of its capabilities. Much more work must be done for a correct calibration of the spectra acquired. However the results seem to be encouraging and in the following months new measurements will be done to trace the progress of the instrument.

Appendix C

List of symbols

a	mean particle radius
A	area
B	opposition effect
d	diameter of a paritcle
D	mean particle diameter, $D = 2a$
$D[4,3]$	diameter of De Brouckere, $D[4,3] = \Sigma d^4/\Sigma d^3$
$D[3,2]$	diameter of Sauter, $D[3,2] = \Sigma d^3/\Sigma d^2$
e	zenith angle of emergence or viewing
E	volume extinction coefficient
F	volume emission coefficient
g	phase angle
G	volume angular scattering coefficient
H	Chandrasekhar function
h	penetration depth
i	$\sqrt{-1}$
i	zenith angle of incidence

I	specific intensity or radiance
I_D	radiance at the detector
J	irradiance
j	subscript denoting different types
k	imaginary part of refractive index
K	volume absorption coefficient
m	refractive index
M_I	bulk density of i-th type of particles
n	real part of refractive index
N	number of particles per unit volume or number of points in a measurement
p	particle phase function
P_E	extinguished power
P_S	scattered power
P_A	absorbed power
P_F	emitted power
Q_E	extinction efficiencies
Q_S	scattering efficiencies
Q_A	absorption efficiencies
Q_d	scattering efficiencies due only to diffraction
r	bidirectional reflectance
r_h	directional hemispherical reflectance
r_m	measured directional hemispherical reflectance
r_c	calculated directional hemispherical reflectance
R	hemispherical reflectance

s	distance, position, line element
S	volume scattering coefficient or pellet section
T	transmittance
V	volume of the material
w	particle single-scattering albedo
w	volume single-scattering albedo
x	variable
x_i	measurements
$\overline{x}$	mean of x_i measurements
X	size parameter
Z	average distance between particles, $Z = N^{-1/3}$
γ	albedo factor, $\gamma = \sqrt{1-w}$
Δ	increment
ε	emission
θ	scattering angle
ϑ	angle
λ	wavelength
μ	$\mu = cose$
μ_0	$\mu_0 = cosi$
ξ	cosine asymmetry factor
ρ	mass density
σ	particle cross-sectional area, $\sigma = \pi a^2$, or standard deviation
σ_E	particle extinction cross section
σ_S	particle scattering cross section

σ_A	particle absorption cross section
τ	optical depth
ϕ	filling factor
φ	ratio between the volume of the mixture and that of the dish
χ^2	chi square
Ω	direction
$d\omega$	solid angle
$d\Omega$	solid angle

Bibliography

Alderliesten, M. 1991. *Mean Particle Diameters, PartII: Standardization of nomenclature*. Part. Part. Syst. Charact. 8, 237-241

Allen, T., 1999. *Particle size measurement*. Chapman and Hall. London

Arvidson, R. E., Squyres, S. W., Anderson, R. C., et al., 2006. *Overview of the Spirit Mars Exploration Rover Mission to Gusev Crater: Landing site to Backstay Rock in the Columbia Hills*. J. Geophys. Res., 111, E02S01

Aumann, H. H., Kieffer, H. H., 1973. *Determination of particle sizes in Saturn's rings from their eclipse cooling and heating curves*. The Astrophysical Journal 186, 305-311

Bandfield, J. L., 2002. *Global mineral distributions on Mars*. J. Geophys. Res. 107, 9-1 - 9-20

Bandfield, J. L., Glotch, T. D., and Christensen, P. R., 2003. *Spectroscopic Identification of Carbonate Minerals in the Martian Dust*. Science 301, 1084-1086

Bibring, J. P., Langevin, Y., Gendrin, A., Gondet, B., Poulet, F., Berthé , M., Soufflot, A., Arvidson, R., Mangold, N., Mustard, J., Drossart, P., and the OMEGA team, 2005. *Mars surface diversity as revealed by the OMEGA/Mars Express observations*. Science 307, 1576-1581

Bibring J. P., Langevin, Y., Mustard, J., Poulet, F., Arvidson, R., Gendrin, A., Gondet, B., Mangold, N., Pinet, P., and Forget, F., 2006. *Global Mineralogical and Aqueous Mars History Derived from OMEGA/Mars Express Data*. Science 312, 400-404

Blanco, A., DElia, M., Licchelli, D., Orofino, V., Fonti, S., Montanaro S., 2008. *The search for ancient life on Mars and the IR spectroscopy of Earth analogues*. Mem. S.A.It. Suppl. 12, 133-137

Bohren, C.F., and Huffman, D.R., 1983. *Absorption and scattering of light by small particles*. John Wiley & Sons. New York

Cabane, M., Coll, P., Rodier, C., Israel, G., Raulin, F., Sternberg, R., Niemann, H., Mahaffy, P., Jambon, A., Rannou, P., 2001. *In situ inorganic and organic analysis (Pyr//CD-GC//MS) of the Martian soil, on the Mars 2005 mission.* Planetary and Space Science, Volume 49, Issue 5, 523-531

Cabane, M., Coll, P., Szopa, C., Isral, G., Raulin, F., Sternberg, R., Mahaffy, P., Person, A., Rodier, C., Navarro-Gonzlez, R., Niemann, H., Harpold, D., Brinckerhoff, W., 2004. *Did life exist on Mars? Search for organic and inorganic signatures, one of the goals for "SAM" (sample analysis at Mars).* Advances in Space Research, 33, 12, 2240-2245

Christensen, P. R., 1986. *The spatial distribution of rocks on Mars.* Icarus 68, 217-238

Christensen, P. R., and 25 colleagues, 2001. *Mars Global Surveyor Thermal Emission Spectrometer experiment: Investigation description and surface science results.* J. Geophys. Res. 106, 23823-23872

Clark, R. N., 1983. *Spectral properties of mixtures of montmorillonite and dark grains - Implications for remote sensing minerals containing chemically and physically adsorbed water.* J. Geophys. Res. 88, 10635-10644

Conel, J. E., 1969. *Infrared emissivities of silicates: Experimental results and a cloudy atmosphere model of spectral emission from condensed particulate mediums.* J. Geophys. Res., 74, 1614-1634

Dollfus, A., Deschamps, M., and Zimbelman, J. R., 1993. *Soil texture and granulometry at the surface of Mars.* J. Geophys. Res. 98, 3413-3429

Edgett, K. S., Christensen, P. R., 1994. *Mars aeolian sand: Region varitions among dark-hued crater floor features.* J. Geophys. Res. 99, 1997-2018

Estep-Barnes, P.A., 1977. *Infrared spectroscopy.* In: Zussman, J. (Ed.),Physical methods in determinative mineralogy (2nd edition). Academic Press. New York

Evans, J. V., Hagfors, T. , 1968. *Radar astronomy.* New York: McGraw-Hill

Farmer, V. C. (ed), 1974. *The Infrared Spectra of Minerals.* Monograph No. 4, Mineralogical Society. London

Fonti, S., Jurewicz, A., Blanco, A., Blecka, M. I., Orofino, V., 2001. *Presence and detection of carbonates on the Martian surface.* J. Geophys. Res. 106, 27815-27822

Formisano, V., Angrilli, F., Arnold, G., Atreya, S., Bianchini, G., Biondi, D., Blanco, A., Blecka, M. I., Coradini, A., Colangeli, L., and 37 coauthors, 2005. *The Planetary Fourier Spectrometer (PFS) onboard the European Mars Express mission.* Planet. Space Sci. 53, 963-974

Fridmann, S.A., 1967. *Pelleting techniques in infrared analysis: A review and evaluation.* In: Szymanski, H.A. (Ed.), Progress in Infrared Spectroscopy, 3. Plenum Press, New York

Friedmann, E. I., Koriem, A. M., 1989. *Life on Mars: How it disappeared (if it was ever there).* Adv. Space Res. 9, 6, 167-172

Gabas, N., Hiquily, N., Lagurie, C., 1994. *Response of Laser Diffraction Particle Sizer to Anisometric Particles.* Part. Part. Syst. Charact. 11, 121-126

Gardiner, J.L. and Salisbury, J.W., 1989. *Spectral reflectance of mineral mixtures an the mid-infrared ($7 \div 25$ μm).* In Abstract of the ERIM Conference on Remote Sensing and Exploration Geology, 2-3. Environmental Research Institute of Michigan, Ann Arbor

Hapke, B., 1981. *Bidirectional reflectance spectroscopy. I - Theory.* J. Geophys. Res. 86, 3039-3054

Hapke, B. and Wells, E., 1981. *Bidirectional reflectance spectroscopy. II - Experiments and observations.* J. Geophys. Res. 86, 3055-3060

Hapke, B., 1984. *Bidirectional reflectance spectroscopy. III. Corretion for macroscopic roughness.* Icarus 59, 41-59

Hapke, B., 1993. *Theory of Reflectance and Emittance Spectroscopy.* Cambridge University Press, MA.

Hapke, B., Nelson, R. M., Smythe, W., 1998. *The Opposition Effect of the Moon: Coherent Backscatter and Shadow Hiding.* Icarus 133, 89-97

Hapke, B., 2002. *Bidirectional Reflectance Spectroscopy. 5. The Coherent Backscatter Opposition Effect and Anisotropic scattering.* Icarus 157, 523-534

Hunt, G. R.; Vincent, R. K., 1968. *The behavior of spectral features in the infrared emission from particulate surfaces of various grain sizes.* J. Geophys. Res., 73, 6039-6046

Johnson, P. E., Smith, M. O., Taylor-George, S., and Adams, J. B. 1983. *A semiempirical method for analysis of the reflectance spectra of binary mineral mixtures.* J. Geophys. Res. 88, 3557-3561

Kerker, M., 1969. *The scattering of light and other electromagnetic radiation.* Academic Press. New York

Lellouch, E., Encrenaz, T., de Graauw, T., Erard, S., Morris, P., Crovisier, J., Feuchtgruber, H., Girard, T., & Burgdorf, M., 2000. *The 2.4-45μm spectrum of Mars observed with the infrared space observatory.* Planet. Space Sci. 48, 1393-1405

Malin, M. C., Edgett, K. S., 2000. *Evidence for Recent Groundwater and Surface Runoff on Mars.* Science, 288, 2330-2335

McGuire, A. F. and Hapke, B., 1995. *An experimental Study of Light Scattering by Large, Irregular Particles.* Icarus 113, 134-155

McKay, C. P., Stoker, C. R., 1989. *The Early Environment and its Evolution on Mars: Implications for Life.* Rev. Geophys. 27,189-214

Mellon, M. T., Jackosky, B. M., Kieffer, H. H., Christensen, P. R., 2000. *High-Resolution Thermal Inertia Mapping from the Mars Global Surveyor Thermal Emission Spectrometer.* Icarus 184, 437-455

Montanaro, S, Politi, R., Blanco, A., Dinoi, A., Fonti, S., Marra, A. C., Marzo, G. A., Orofino, V. 2007. *Planetary soil simulation: binary mixtures reflectance spectra.* Mem. S.A.It. Suppl. 11, 220-224

Murchie, S., Arvidson, R., Bedini, P., Beisser, K., Bibring, J.-P., Bishop, J., Boldt, J., Cavender, P., Choo, T., Clancy, R. T., Darlington, E. H., Des Marais, D., Espiritu, R., Fort, D., Green, R., Guinness, E., Hayes, J., Hash, C., Heffernan, K., Hemmler, J., Heyler, G., Humm, D., Hutcheson, J., Izenberg, N., Lee, R., Lees, J., Lohr, D., Malaret, E., Martin, T., McGovern, J. A., McGuire, P., Morris, R., Mustard, J., Pelkey, S., Rhodes, E., Robinson, M., Roush, T., Schaefer, E., Seagrave, G., Seelos, F., Silverglate, P., Slavney, S., Smith, M., Shyong, W.-J., Strohbehn, K., Taylor, H., Thompson, P., Tossman, B., Wirzburger, M., and Wolff, M., 2007. *Compact Reconnaissance Imaging Spectrometer for Mars (CRISM) on Mars Reconnaissance Orbiter (MRO).* J. Geophys. Res. 112, E05S03-E05S03

Mustard, J. F., Pieters, C. M., 1987. *Quantitative Abundance Estimates From Bidirectional Reflectance Measurements.* J. Geophys. Res. 92, E617-E626

Mustard, J. F., Pieters, C. M., 1989. *Photometric Phase Functions of Common Geologic Minerals and Applications to Quantitative Analysis of Mineral Mixture.* J. Geophys. Res. 94, E13619-13634

Mustard, J. F. and Hays, J. E., 1996. *Effects of Hyperfine Particles on Reflectance Spectra from* 0.3 *to* 25 μm. Icarus 125, 145-163

Nelson, R. M. and Hapke, B., 2000. *The opposition Effect in Simulated Planetary regoliths. Reflectance and Circular Polarization Patio Change at Small Phase Angle.* Icarus 147, 545-558

Orofino, V., Blanco, A., D'Elia, M., Licchelli, D., Fonti, S., 2007. *Infrared transmission spectroscopy of carbonate samples of biotic origin relevant to Mars exobiological studies.* Icarus 187, 2, 457-463

Pollack, J. B., Kasting, J. F., Richardson, S. M., Poliakoff, K.,1987. *The case for a wet, warm climate on early Mars.* Icarus 71, 203-224

Ran, D., 1998. *Laser diffraction measurement.* Proc. SPIE, vol. 3558 pp.201-208. Automated Optical Inspection for Industry: Theory, Technology, and Applications II. Shenghua Ye, Editors

Salisbury, J. W., Wald, A., 1991. *The Role of Volume Scattering in Reducing Spectral Contrast of Reststrahlen Bands in Spectra of Powdered Minerals.* Icarus 96, 121-128

Salisbury, J. W., Walter, L. S., Vergo, N., D'aria, D. M., 1992. *Infrared (2.1-25 μm) Spectra of Minerals.* The Johns Hopkins University Press. Baltimore and London

Salisbury, J.W., 1993. *Mid-infrared spectroscopy: Laboratory data.* In: Pieters, C.M., Englert, P.A. (Eds.), Remote Geochemical Analysis: Elemental and Mineralogical Composition. Cambridge University Press. Cambridge

Salisbury, J.W., Wald, A., D'Aria, D.M., 1994. *Thermal-infrared remote sensing and Kirchhoff's law 1. Laboratory measurements.* J. Geophys. Res. 99, 11897-11911

Singer, R.B. and McCord, T.B., 1979. *Mars: Large scale mixing of bright and dark surface materials and implications for analysis of spectral reflectance.* Proc. Lunar and Planetary Science Conference, 10th, 1835-1848

Spencer, B. G., 1990. *A rough-surface thermophysical model for airless planets.* Icarus 83, 27-38

Spitzer, W.G. and Kleinman, D.A., 1961. *Infrared lattice bands of quartz.* Phys. Rev. 121, 1324-1335

Stalport, F., Coll, P., Cabane, M., Person, A., Gonzlez, R.N., Raulin, F., Vaulay, M.J., Ausset, P., McKay, C.P., Szopa, C., Zarnecki, J., 2005. *Search for past life on Mars: Physical and chemical characterization of minerals of biotic and abiotic origin: part 1 - Calcite.* Geophysical Research Letters, 32, 23, L23205

Taylor, J.R., 1982. *An introduction to error analysis: the study of uncertainties in physical measurements*. University Science Books, Mill Valley.

Van de Hulst, H.C., 1957. *Light scattering by small particles*. John Wiley & Sons. New York

Walter, L. S., Salisbury, J. W., 1989. *Spectral characterization of igneous rocks in the 8- to 12-micron region*. J. Geophys. Res. 94, 9203-9213

Wenrich, M. L. and Christensen, P. R., 1996. *Optical constants of minerals derived from emission spectroscopy: Application to quartz*. J. Geophys. Res. 101, 15921-15931

Westall, F., 1999. *The nature of fossil bacteria: A guide to the search for extraterrestrial life*. J. Geophys. Res. 104, 16437-16451

Author Bibliography

Publications in International Journals

S. Montanaro, S. Fonti, R. Politi, A. Blanco, A.C. Marra, G.A. Marzo, V. Orofino, *Mid-Infrared Reflectance Spectra of Particulate Mixtures* in preparation

Conference Presentations and Proceedings

S. Montanaro, R. Politi, A. Blanco, A. Dinoi, S. Fonti, A. C. Marra, G. A. Marzo, V. Orofino, *Simulazione del suolo planetario: spettri in riflessione di misture binarie*, VII Convegno Nazionale di Scienze Planetarie , 5-9 Sept. 2006, San Felice Circeo (LT), Italy

S. Montanaro, R. Politi, A. Blanco, A.C. Marra, G.A. Marzo, V. Orofino, S. Fonti *Deconvolution of intimate mixtures spectra for comparison with Martian observations*, 2 International Workshop Exploring Mars and its Earth Analogues, 19-23 June 2007, Trento, Italy

S. Montanaro, R. Politi, A. Blanco, A. Dinoi, S. Fonti, A. C. Marra, G. A. Marzo, V. Orofino, 2007. *Planetary soil simulation: binary mixtures reflectance spectra.* Mem. S.A.It. Suppl. 11, 220-224

S. Montanaro, R. Politi, A. Blanco, S. Fonti, A.C. Marra, G.A. Marzo, V. Orofino, *Spectra of particulate mixtures in the near and medium IR*, VIII Convegno Nazionale di Scienze Planetarie, 21-25 Gen. 2008, Bormio (SO), Italy

A. Blanco, M. D'Elia, D. Licchelli, V. Orofino, S. Fonti, S. Montanaro, *The search for ancient life on Mars and the IR spectroscopy of Earth analogues*, VIII Convegno Nazionale di Scienze Planetarie, 21-25 Gen. 2008, Bormio (SO), Italy

S. Montanaro, S. Fonti, R. Politi, A. Blanco, A.C. Marra, G.A. Marzo, V. Orofino, *Reflectance spectra of particulate mixtures in the near and medium infra-red*

spectral range: part I, European Geoscience Union, General Assembly 2008, 14-19 April 2008, Vienna, Austria

S. Fonti, S. Montanaro, R. Politi, A. Blanco, A.C. Marra, G.A. Marzo, V. Orofino, *Reflectance spectra of particulate mixtures in the near and medium infra-red spectral range: part II*, European Geoscience Union, General Assembly 2008, 14-19 April 2008, Vienna, Austria

A. Blanco, M. D'Elia, D. Licchelli, V. Orofino, S. Fonti, and S. Montanaro, 2008. *The search for ancient life on Mars and the IR spectroscopy of Earth analogues*, Mem. S.A.It. Suppl. Vol. 12, 133-137